UNIVERSIDADE DE LISBOA

FACULDADE DE CIÊNCIAS

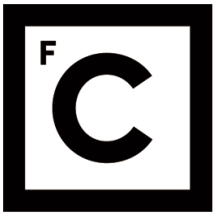

Ciências
ULisboa

Anoctamin 1 - A Member of a Novel Family of Ion Channels with Extended Functions and Significance in Disease

Doutoramento em Biologia

Especialidade: Biologia de Sistemas

Joana Ramos Rapaz Lérias

Tese orientada por:

Prof. Dr. Karl Kunzelmann e Prof. Dr. Margarida D. Amaral

Documento especialmente elaborado para a obtenção do grau de doutor

2018

UNIVERSIDADE DE LISBOA

FACULDADE DE CIÊNCIAS

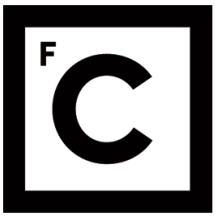

Ciências
ULisboa

Anoctamin 1 - A Member of a Novel Family of Ion Channels with Extended Functions and Significance in Disease

Doutoramento em Biologia

Especialidade: Biologia de Sistemas

Joana Ramos Rapaz Lérias

Tese orientada por:

Prof. Dr. Karl Kunzelmann e Prof. Dr. Margarida D. Amaral

Júri:

Presidente:

- Doutor Rui Manuel dos Santos Malhó, Professor Catedrático da Faculdade de Ciências da Universidade de Lisboa

Vogais:

- Doutor Karl Kunzelmann, Kunzelmann, Professor, Faculty of Biology and Pre-Clinical Medicine da University of Regensburg, Alemanha (orientador);
- Doutor Ana Colette Pereira de Castro Osório Maurício, Professora Associada com Agregação, Instituto de Ciências Biomédicas Abel Salazar (ICBAS) da Universidade do Porto;
- Doutor Peter Jordan, Investigador Principal, Departamento de Genética Humana do Instituto Nacional de Saúde Doutor Ricardo Jorge;
- Doutora Maria da Graça Tavares Rebelo de Soveral Rodrigues, Professora Associada com Agregação, Faculdade de Farmácia da Universidade de Lisboa.

Documento especialmente elaborado para a obtenção do grau de doutor

Fundação para a Ciência e Tecnologia do Ministério da Educação e Ciência (FCT/ SFRH / BD / 52489 / 2014)

2018

De acordo com o disposto no artigo 24º do Regulamento de Estudos de Pós-Graduação da Universidade de Lisboa, Despacho nº 7024/2017, publicado no Diário da República – 2ª Série – nº 155 – 11 de Agosto de 2017, foram utilizados nesta dissertação resultados incluídos nos seguintes artigos:

1. **Lérias JR***, Pinto MC*, Botelho HM, Awatade NT, Quaresma MC, Silva IAL, Wanitchakool P, Schreiber R, Pepperkok R, Kunzelmann K, Amaral MD (2018). A novel microscopy-based assay identifies extended synaptotagmin-1 (ESYT1) as a positive regulator of anoctamin 1 traffic. *Biochim Biophys Acta* **1865**: 421-431. [*Shared first authorship]

2. **Lérias J***, Pinto M*, Benedetto R, Schreiber R, Amaral MD, Aureli M, Kunzelmann K (2018). Compartmentalized Crosstalk of CFTR and ANO1 (ANO1) Through EPAC and ADCY1. *Cell Signal* **44**:10-19. [*Shared first authorship]

No cumprimento do disposto da referida deliberação, a autora esclarece serem da sua responsabilidade, exceto quando referido o contrário, a execução das experiências que permitiram a elaboração dos resultados apresentados, assim como da interpretação e discussão dos mesmos. Os resultados obtidos por outros autores foram incluídos com a autorização dos mesmos para facilitar a compreensão dos trabalhos e estão assinalados nas respetivas figuras e metodologias.

.

Index

Acknowledgments

A special acknowledgement to my supervisor Prof. Dr. Karl Kunzelmann, who hosted me in his lab for one year and a half and started my journey in the amazing human physiology field. His support was not only crucial for this work, but also to allow me to have a more “scientific thinking”.

I would like to express my gratitude for my co-supervisor Prof. Dr. Margarida Amaral for all the support, help, and guidance and for the opportunity to work on her lab during my PhD project. Her knowledge and experience were essential to improve my work.

The development of this PhD project would not have been possible without my BioSys 1st edition colleges, especially Sara, Nikhil, Hugo, Paulo, Cibelle and Ana. All the discussions, worries (and dinners) helped me to grow as a person and as a scientist.

To all my colleges at FCUL, a word of gratitude for all the help and support through all these years, especially to Verónica, Sara, João and Nikhil.

To all my Portuguese-German-Thai-Italian family at Regensburg, Inês, Filipa, Ana, Kip, Robi, Karina, Catarina and Sara, for all the friendship and support amid the “madness”; to Ji for teaching me the patch-clamp technique; to Rainer for all the help in PCRs and cloning; to Brigitte, Susi and Silvia for showing me the German “bright side of life”; to Tini and Patricia for all the help in lab.

I would also like to thank to all my friends outside the “lab life”, who helped me throughout this PhD with their calmness whenever I needed.

To my family, especially to my mum and dad, to my sisters Muriel and Sofia, to Quim and to my brothers-in-law João Gil and João Cambeiro, you were the ones supporting me every step of the way and viewing my strength even when I would not see it.

Abbreviations

007-AM	8-pCPT-2-O-Me-cAMP
1-EBIO	1-ethyl-2-benzimidazolinone
ATP	Adenosine triphosphate
ADCY	Adenylyl cyclase
BFA	Brefeldin A
bp	Base pair
Ca^{2+}	Calcium ion
CaCC	Calcium dependent chloride channel
Cal-33	Head and neck squamous carcinoma cells
cAMP	Cyclic adenosine monophosphate
CCH	Carbachol
CF	Cystic Fibrosis
CFBE	Cystic fibrosis bronchial epithelial
CFTR	Cystic fibrosis transmembrane conductance regulator
CIP	CFTR interactor protein
Cl^-	Chloride ion
CLCA1	Calcium-activated chloride channel regulator 1
CK2	Casein kinase 2
DIDS	4,4’-diisothiocyanatostilbene-2,2’-disulphonic acid
DMSO	Dimethyl sulfoxide
DNA	Deoxyribonucleic acid
Dox	Doxycycline
EB	Efflux buffer
eGFP	Enhanced green fluorescent protein
ENaC	Epithelial sodium channel
EPAC1	Exchange protein directly activated by cAMP 1
ER	Endoplasmic reticulum
ERQC	Endoplasmic reticulum quality control
ESI09	α-[(2-(3-Chlorophenyl)hydrazinylidene]-5-(1,1-dimethylethyl)-β-oxo-3-isoxazolepropanenitrile
ESYT	Extended synaptotagmin
GOI	Gene of interest

GPCR	G-protein coupled receptor
HA	Hemagglutinin
HCO_3^-	Bicarbonate ion
HBE	Human bronchial epithelial
HEK	Human embryonic kidney
I^-	Iodide ion
I/F	IBMX/Forskolin
IL	Interleukin
IONO	Ionomycin
Ist2	Increased sodium tolerance protein 2
IP_3	Inositol 1,4,5-triphosphate
IP_3R	Inositol 1,4,5-triphosphate receptor
I/V	Current/voltage
K^+	Potassium ion
KD	Knock-down
M3R	Muscarinic receptor 3
MUC5AC	Mucin 5AC
mRNA	Messenger ribonucleic acid
Na^+	Sodium ion
NFM	Non-fat milk
nhANO	*Nectria haematococca* anoctamin
ORAI	Calcium Release-Activated Calcium Channel Protein
ORP	Oxysterol-binding protein
$P2RY_2$	Purinergic receptor $P2Y_2$
PDE	Phosphodiesterase
PFA	Paraformaldehyde
PGLYRP3	Peptidoglycan recognition protein 3
PGRP	Peptidoglycan recognition protein family
PIP_2	Phosphatidylinositol 4,5-biphosphate
PLC	Phospholipase C
PM	Plasma membrane
RNA	Ribonucleic acid
SEM	Standard error of mean

SERCA	Sarco/endoplasmatic reticulum Ca^{2+}-ATPase
siRNA	Small interfering ribonucleic acid
SOcAMP	Store operated cAMP
ST034307	6-Chloro-2-(trichloromethyl)-4*H*-1-benzopyran-4-one
STIM1	Stromal interaction molecule 1
TBB	4,5,6,7-Tetrabromo-2-azabenzimidazole, 4,5,6,7-Tetrabromobenzotriazole
TMAO	Trimethylamine-N-oxide
UTP	Uridine triphosphate
% v/v	Percentage expressed in volume per volume
WT	Wild-type
% w/v	Percentage expressed in weight per volume

Summary

Cystic fibrosis (CF), the most common life-shortening autosomal recessive disorder in Caucasians, is caused by >2,000 different mutations in the gene encoding the CF Transmembrane Conductance Regulator (CFTR). CFTR is a Cl^- and HCO_3^- permeant channel expressed in the epithelial apical membrane. Clinically, the majority of CF patients suffer mostly from severe lung disease.

A possible approach to treat CF is through the stimulation of alternative channels, such as anoctamins, that could compensate for absence of CFTR mediated Cl^- secretion, thus being called “bypass” approach.

The prime objective of this PhD project focusses on identifying novel anoctamin regulators as possible drug targets for CF.

The **first chapter** describes the generation of CFBE-3HA-ANO1-eGFP cells and their use in a siRNA traffic screen. As a result, nine hits were selected for functional validation: Extended Synaptotagmin Member 1 (ESYT1) and Casein Kinase 2 (CSNK2) as negative modulators and Peptidoglycan Recognition Protein 3 (PGLYRP3) and Coat Protein Complex I subunit β1 (COPβ1) as positive hits.

These screen data also showed a positive regulation of ANO1 by GPCRs, which were further characterized in **chapter two.** Our data illustrate an overlap between Ca^{2+}- and cAMP- induced currents, which prevent a clear distinction between their respective Cl^- currents.

Our data in the **third chapter** describes the relationship between ANO1 and mucus and show that IL4 treatment (an inducer of ANO1 expression) does not affect MUC5AC levels, in contrast to other studies which proposed a causative role for ANO1 in mucus production.

In the **fourth chapter**, the relationship between ANO1, ANO6 and CFTR was further investigated and our data suggest that CFTR activation requires at least one anoctamin member trafficking to the PM, to probably modulate cellular Ca^{2+} signalling and activate CFTR by SOcAMPs and Ca^{2+}-sensitive adenylyl cyclases.

Key-words: anoctamins, CFTR, traffic regulators, GPCRs, cystic fibrosis.

Resumo

A fibrose quística (FQ), a mais frequente doença autossómica letal em Caucasianos, afecta 1:2,500-6,000 nados-vivos e é causada por mutações no gene que codifica o ***C****ystic* ***F****ibrosis* ***T****ransmembrane Conductance* ***R****egulator* (CFTR).

A proteína CFTR é um canal permeável aos iões Cl^- e HCO_3^-, expressa na membrana apical do epitélio de tipo pulmonar e parcialmente responsável pelo transporte de sais e água. Clinicamente, apesar de esta doença poder afetar vários órgãos, a maioria dos pacientes com FQ tem como principal órgão-alvo o pulmão, afeção que frequentemente apenas é solucionada através de um transplante pulmonar. A principal característica da FQ é o muco extremamente viscoso, que provoca transporte mucociliar ineficiente, obstrução pancreática com consequente malnutrição, atraso no crescimento e possivelmente *Diabetes mellitus* (~40% dos pacientes adultos com FQ).

As mutações da CFTR podem ser divididas em 7 classes, de acordo com o seu defeito funcional, existindo tratamentos específicos para as mutações em algumas classes (*e.g.* VX-809 e VX-770 são, em conjunto, benéficos para doentes homozigóticos para F508del). No entanto, não existe um tratamento único que possa ser usado em todos os tipos de mutações. Assim sendo, um importante passo para a terapêutica da FQ seria a estimulação de canais alternativos que poderiam compensar a falta de secreção de Cl^- resultante das mutações na CFTR. De entre, estes salientam-se os canais de Cl^- ativados pelo Ca^{2+} (CaCCs), nomeadamente os membros da família das anoctaminas. A estimulação destes canais, chamada terapêutica de "*bypass*", seria não só vantajosa para todos os doentes independentemente da classe de mutação, tal como, *e.g.*, a terapia génica, mas (ao contrário desta) seria baseada em canais iónicos endógenos já presentes nos doentes com FQ, sendo portanto, de mais fácil execução.

A família das anoctaminas é constituída por 10 membros (ANO1-10) dos quais 4 (ANO1, ANO2, ANO6 e ANO7) possuem a capacidade de produzir correntes de Cl^-. A ANO1 localiza-se na membrana apical das células e é ativada pelo aumento da concentração intracelular de Ca^{2+} originando uma corrente *outwardly rectifying*. Através da ativação dos GPCRs (do inglês ***G*-*p****rotein* ***c****oupled* ***r****eceptors*) por agonistas dos recetores purinérgicos, PIP_2 (do inglês *Phosphatidylinositol 4,5-bisphosphate*) é hidrolisado pela fosfolipase C, produzindo dois mensageiros

secundários, diacilglicerol e IP_3 (do inglês *inositol triphosphate*). A ligação do IP_3 aos seus recetores no retículo endoplasmático estimula um aumento do ião Ca^{2+}, que se liga directamente à ANO1, levando à sua ativação, que resulta no efluxo de ião Cl^-.

Recentemente, a estrutura da ANO1 de ratos (*Mus musculus*) foi descrita, demonstrando que a ANO1 tem dois poros, pertencentes a cada subunidade individual desta proteína dimérica. Além disso, este modelo demonstrou que os poros estão separados da membrana plasmática, contrariamente ao modelo anterior proposto do poro proteolípidico, que considerava que os canais de ANO1 eram parcialmente compostos por lípidos.

Os canais ANO1 são parcialmente controlados pela CFTR devido à intensa sobreposição de sinais de ativação de ambos os canais, o que impede uma total divisão entre as correntes formadas por cada ANO1 e a CFTR. Além disso, o canal ANO1 é expresso em vários dos tecidos afetados pela FQ, pode transportar os iões Cl^- e HCO_3^- e é expresso em tecidos epiteliais em pacientes com FQ ou *wild-type*. Assim sendo, alguns dos membros da família das anoctaminas, com especial ênfase na ANO1, são possíveis canais alternativos na terapêutica de "*bypass*" que, teoricamente, poderá ser aplicada em todos os pacientes com FQ qualquer que seja a classe de mutação a que pertencem.

De acordo com a importância das terapêuticas de "*bypass*", os principais objetivos deste projeto doutoral foram a descoberta de novos reguladores dos canais ANO1 e a sua relação com a CFTR para posterior desenvolvimento de fármacos e terapias inovadoras para os doentes com FQ.

Na primeira parte desta tese doutoral (**Capítulo 1**), três novas linhas celulares foram criadas expressando ANO1 mutada com dois tipos de marcadores (*tags*): proteína verde fluorescente melhorada (eGFP, do inglês ***e****nhanced* ***g****reen* ***f****luorescent* ***p****rotein*) que permite medir a expressão total de ANO1, e uma marcação no 1º *loop* extracelular da ANO1 com tripla hemaglutinina que permite medir a porção de ANO1 presente na membrana plasmática usando um anticorpo anti-HA, sem permeabilizar as células. Este sistema pode ser usado em diversas funções, nomeadamente (1) identificação de reguladores da ANO1 como possíveis alvos terapêuticos; (2) identificação de novos compostos/fármacos moduladores do tráfego da ANO1 e (3) perceção dos mecanismos envolventes no tráfego da proteína ANO1. Células CFBE a sobreexpressar 3HA-ANO1-eGFP foram usadas num *screen* de tráfego com siRNAs (do inglês ***s****mall* ***i****nterfering* ***r****ibo****n****ucleic* ***a****cid*) usando *hits* de 3 bibliotecas: (1)

screen de tráfego de WT-CFTR em células A549 a sobreexpressar WT-CFTR; (2) moduladores positivos obtidos num *screen* de tráfego de F508del-CFTR em células CFBE a sobreexpressar mCherry-flag-F508del-CFTR e (3) *screen* em células HEK a expressar WT- ou F508del-CFTR de proteínas que interajam com a CFTR. Nos resultados do *screen* primário, obteve-se 94 *hits* (41 siRNAs que reduziam e 53 que aumentavam o tráfego da ANO1) e, após um segundo *screen*, 14 *hits* em comum entre ambos os *screens* foram identificados. Desses 14 *hits*, 9 siRNAs foram escolhidos para serem validados com a técnica de *whole-cell patch-clamp*: siRNAs ***E**xtended **Sy**napt**t**otagmin Member* **1** (ESYT1) e **C**a**s**ei**n** **K**inase **2** (CSNK2) foram identificados como moduladores negativos de tráfego e função e os siRNAs ***P**eptido**gly**can **R**ecognition **P**rotein **3*** (PGLYRP3) e ***C**oat **P**rotein **C**omplex I* subunidade **β1** (COPβ1) como moduladores positivos de tráfego e função da ANO1.

Após a análise dos resultados obtidos neste *screen*, observou-se uma regulação negativa da ANO1 aquando do KD de GPCRs. Assim sendo, a segunda parte desta tese (**capítulo 2**), focou-se no estudo mais aprofundado da relação entre ANO1, GPCRs e CFTR. Os resultados obtidos nos ensaios efetuados confirmaram a existência de alguma co-regulação entre os canais ANO1 e CFTR, o que impede uma separação total entre ambas as correntes de Cl^-. De facto, estes dados revelaram duas proteínas essenciais para essa relação: ***1***) a EPAC1 (do inglês ***E**xchange **P**rotein Directly **A**ctivated by **c**AMP)*; e ***2***) a ADCY1 (do inglês ***Ad**enylyl **Cy**clase* sensível ao ião Ca^{2+}, ambas fundamentais para a interação entre as correntes induzidas por cAMP e Ca^{2+}. A EPAC1 é ativada pelo cAMP e aumenta os níveis celulares de Ca^{2+} através da fosfolipase C ativando, assim, os canais ANO1. Contrariamente, a ADCY1 produz cAMP ativando a CFTR. Além disso, inibidores considerados específicos de cada uma destas proteínas (CFTR inh_{172} e CaCC AO1 para CFTR e ANO1, respetivamente), inibiram correntes produzidas por ambas as proteínas. Uma vez que a CFTR também pode ser ativada pelo aumento de Ca^{2+}, existe uma sobreposição adicional entre as correntes induzidas por cAMP e Ca^{2+}. Considerando os dados obtidos, colocamos a hipótese dos GPCRs transferirem as proteínas ADCY1 e EPAC1 para microdomínios específicos da membrana plasmática (*lipid rafts*) que contêm GPCRs, CFTR e ANO1, permitindo a co-regulação entre as correntes induzidas quer por cAMP quer por Ca^{2+}.

Tendo em consideração as várias aplicações desta linha celular, a terceira parte desta tese (**capítulo 3**) abordou a relação entre ANO1 e a produção de muco. A

literatura dedicada a este tema é controversa, uma vez que os inibidores da ANO1 reduzem a produção de muco. Como este canal também transporta HCO_3^-, um ião essencial para a expansão dos grânulos de mucinas, a ativação da ANO1 poderá, concomitantemente, auxiliar a secreção do muco. Outro fator que deve ser considerado nesta relação complexa diz respeito às diferentes ações entre a ANO1 endógena e ANO1 sobreexpressa, uma vez que foi sugerido que níveis mais altos de expressão desta proteína reduzem a produção de citocinas e, assim, diminuem a inflamação associada à produção de muco. De acordo com os dados obtidos, as células CFBE com sobreexpressão de ANO1 modularam a expressão de mucina 5AC (MUC5AC), uma vez que se observou o mesmo nível de MUC5AC com ou sem incubação de interleucina 4 (IL4) em células induzidas. Este resultado deveu-se provavelmente a alguma produção basal de citocinas antes do tratamento com IL4.

Por fim, e como a proteína ANO6 também é considerada como um possível canal alternativo de ião Cl^-, a quarta parte desta tese (**capítulo 4**) analisou a relação entre os canais ANO6, ANO1 e CFTR. Os resultados obtidos demonstraram uma forte correlação entre a expressão e função da CFTR com a ANO6, mas não com a ANO1 em células Calu-3. Estes dados sugeriram que a CFTR requer pelo menos um membro da família das anoctaminas para um tráfego correto para a membrana plasmática. Além disso, provavelmente os membros da família das anoctaminas modulam os sinais de Ca^{2+} e ativam a CFTR através de sinalização por SOcAMP (do inglês ***S**tore **O**perated **cAMP***) e ADCYs sensíveis a Ca^{2+}. Além disso, os dados obtidos em ensaios em células HEK demonstraram o papel fundamental da ANO6 na função da ANO1 como canal de Cl^-. De facto, a expressão de ambas as proteínas (ANO1 e ANO6) aumentou significativamente as correntes induzidas por ATP, quando comparada com células a expressarem apenas ANO1, o que sugere que o ANO6 aumenta o Ca^{2+} disponível nas células.

Palavras-chave: ANO1, CFTR, reguladores de tráfego, GPCRs, fibrose quística.

I. Introduction

1. Cystic Fibrosis

1.1. General introduction

Cystic fibrosis (CF) is the most common life-limiting autosomal recessive disorder in Caucasians, affecting 1:2,500-6,000 newborns (Quinton, 1983). This disease is found in Caucasian individuals, although it also affects people from other ethnicities (O'Sullivan and Freedman, 2009). The first medical reports of CF symptoms were described in 17th century, though CF disorder was only reported in the 1930s by pathologist Dr. Dorothy Andersen (Andersen, 1938). Finally, the cystic fibrosis transmembrane conductance regulator (CFTR) gene, whose mutations are responsible for this disease, was cloned and the protein encoded in 1989 (Riordan *et al.*, 1989; Kerem *et al.*, 1989; Rommens *et al.*, 1989). Until now, over 2,000 different CFTR mutations have been identified, from which deletion of Phe508 in the first nucleotide binding domain (NBD1) of CFTR is the most frequent mutation, occurring in >85% of CF alleles worldwide (Cystic Fibrosis Mutations Database; available at http://www.genet.sickkids.on.ca/cftr/; access on January 2018).

1.2. Pathophysiology

Clinically, lung disease is the most critical feature for the majority of CF patients. Thick mucus and inflammation cause failure to clear microorganisms and generate a toxic pro-inflammatory local microenvironment (De Boeck and Amaral, 2016) (Fig. 1). Other affected organs include sweat glands, biliary ducts, the male reproductive system and the gastrointestinal system. Most patients with severe phenotype also suffer from pancreatic insufficiency (PI). Indeed, pH values are reduced (more acidic fluid) in the pancreatic ducts leading to activation of digestive enzymes before they reach the small intestine, thus gradually destroying the pancreas (O'Sullivan and Freedman, 2009; Kongsuphol *et al.*, 2010). The loss of pancreatic exocrine function results in malnutrition and failure to grow. CF patients may also develop CF-related *Diabetes mellitus*, caused by loss of islet cell function, which occurs in ~40% of CF adult patients (Plant *et al.*, 2013).

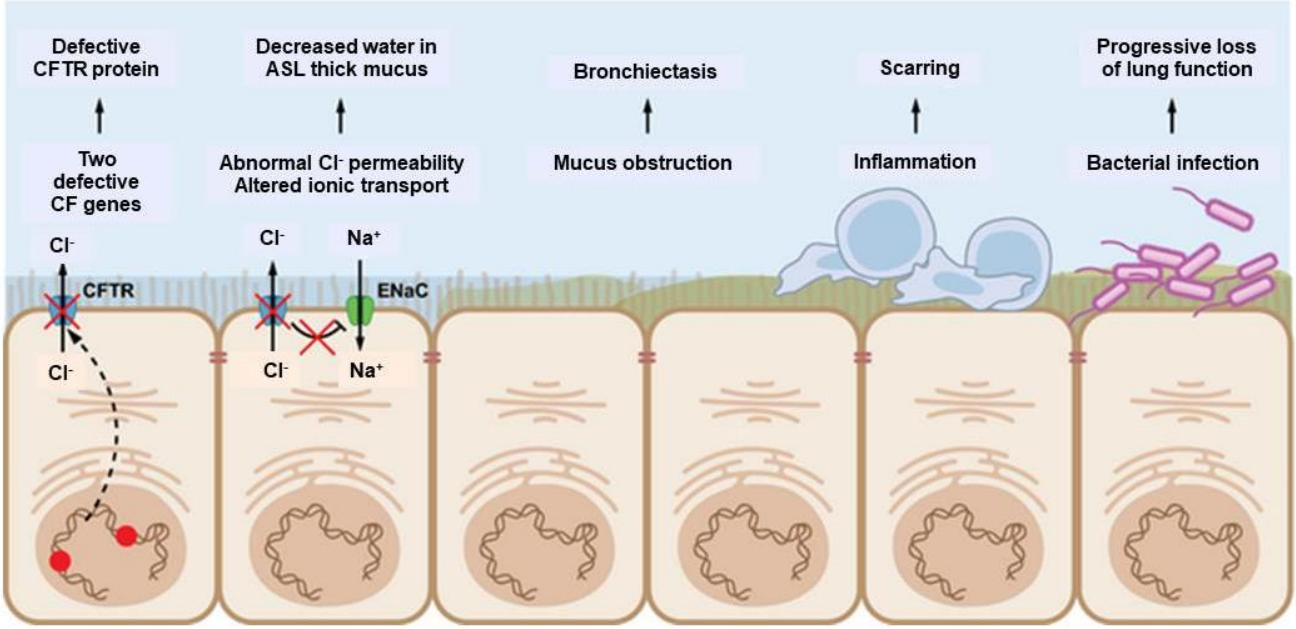

Fig. 1 Pathophysiology of CF in the lung. Primary CFTR gene defect leads to thick mucus, resulting in bronchiectasis, mucus obstruction, progressive inflammation, bacterial infection and ultimately loss of lung function. [Amaral (2015)].

1.3. Molecular basis of disease and mutation-specific therapies

CF pathophysiology is characterised by atypically high electrical potential differences and reduced Cl^- efflux through apical membrane of epithelial cells from CF patients (Knowles *et al.*, 1983). CF is caused by mutations in the CFTR gene, encoding a cAMP-regulated Cl^- ion channel. CFTR channel dysfunction affects ionic and water homeostasis at the surface epithelia, which causes elevated mucus viscosity in affected organs. CFTR is also responsible for regulating other ion conductances, such as downregulating Na^+ absorption through ENaC. Thus, reduction of Cl^- flow and increment of Na^+ absorption are the main features that lead to a variety of CF typical symptoms (Riordan *et al.*, 1989; Verkman *et al.*, 2003).

CFTR mutations were originally grouped into four functional classes, as proposed by Welsh and Smith (1993), then updated to 5 by Tsui (1992), and to 6 by Lukacs *et al.* (1999) and more recently revised to 7 classes, as these evolved into theratypes by De Boeck and Amaral (2016). Class I mutations produce premature termination of CFTR mRNA translation, with reduced or absent CFTR protein production. These mutations, such as G542X or R1162X, can be due to splice site alterations, frameshifts caused by insertions or deletions, or nonsense mutations. Class II mutations fail to traffic to the cell surface with protein retention by the endoplasmic

reticulum (ER) quality control (ERQC) and premature proteasome degradation. The most common CF-causing mutation, F508del, is included in this class. Class III corresponds to CFTR mutations (*e.g.* G551D or S549R) that, although correctly located at the plasma membrane (PM), fail to function as a Cl^- channel, due to a defect in channel gating. Class IV mutations, such as R334W or P205S, are also adequately located at PM, but have altered conductance, resulting in reduced Cl^- efflux rate through CFTR channel. Class V mutations (*e.g.* 3272-26A>G and G576A) cause reduction in functional CFTR protein levels, most commonly due to alternative splicing that allows production of normal CFTR protein, but in much lower levels. Class VI mutations, such as 120del23, are associated with reduced CFTR stability at PM by an increased endocytosis or reduced recycling. Lastly, in class VII mutations, considered unrescuable, there is usually no CFTR mRNA, due for example to extensive deletions, such as dele2,3(21kb) mutation.

Regarding approaches to correct mutations in each of these classes/theratypes, for the class I aminoglycoside antibiotics, such as G418, gentamycin or tobramycin, can suppress premature termination codons, responsible for mRNA transcripts degradation by the nonsense-mediated decay system, and fail to produce CFTR protein (De Boeck and Amaral, 2016). For management of class II mutations, compounds that promote proper folding and allow ERQC escape can be used. These include unspecific molecules that improve general protein folding, named chemical chaperones, (*e.g.* glycerol or TMAO) (Pedemonte *et al.*, 2005) but these can only be used *in vitro*. For the F508del mutation, a class of molecules, named correctors, have been used successfully in the clinic to rescue and correct F508del trafficking defect, such as VX-809 (Lumacaftor) (Van Goor *et al.*, 2011), VX-660 (tezacaftor) or next generation correctors (VX-440; VX-152) (Vertex Pharmaceuticals Incorporated; available at http://clinicaltrials.gov/ct2/show/NCT02951182; access on January 2018) in combination with a potentiator. For class III and IV mutations, CFTR potentiators, *i.e.*, molecules that increase defective CFTR activity at cell PM, such as genistein or VX-770 (Ivacaftor), can be used (Van Goor *et al.*, 2009). For class V mutations, antisense oligonucleotides that correct aberrant splicing habe been successfully used *in vitro* (Igreja *et al.*, 2016), but both correctors and potentiators can be also beneficial to patients bearing these mutations by increasing CFTR trafficking and channel activity (De Boeck and Amaral, 2016). For class VI, molecules that stabilise CFTR, such as hepatocyte growth factor, acting via Rac1 signalling and the actin

cytoskeleton may be of use (Moniz *et al.*, 2013). Finally, for class VII, rescue of CFTR in not possible, thus potential treatments require either gene therapy/editing or activation of alternative Cl^- channels, such as ANO1 (De Boeck and Amaral, 2016).

2. Alternative (non-CFTR) chloride channels as potential targets for CF therapy: the anoctamin family

2.1. The Anoctamin family: an overview

The anoctamin family comprises ten members (ANO1-10) which are expressed in several tissues and have essential roles in cellular functions, such as epithelial secretion, smooth muscle regulation, neuronal and cardiac excitability control, sensory transduction, nociception, among others (Duran and Hartzell, 2011; Kunzelmann *et al.*, 2011). This family is well conserved amid eukaryotes and a Cl^- channel activity was positively established for ANO1, 2 and ANO4-10 (Kunzelmann *et al.*, 2011; Tian *et al.*, 2012). ANO1 is significantly upregulated by the pro-inflammatory cytokines IL13 and IL4 (Caputo *et al.*, 2008) and its overexpression has been associated in a causative manner with Goblet cell metaplasia and airway hyperreactivity (Huang *et al.*, 2012; Scudieri *et al.*, 2012a). Furthermore, one study showed that ANO1 inhibitors reduced both mucus secretion and airway hyperreactivity (Huang *et al.*, 2012).

2.2. ANO1 structure and function

Brunner *et al.* (2014) reported the crystal structure of *Nectria haematococca* anoctamin (nhANO), whose structural properties can be well translated to structure/function of ANO1. According to the structure of this ortholog, ANO1 should have ten (and not eight) transmembrane helices and a highly conserved hydrophilic membrane-traversing cavity embedded in the lipid bilayer, which includes a conserved Ca^{2+}-binding site and mediates ANO1 Ca^{2+}-activation. Recently, Paulino *et al.* (2017)b characterized mouse ANO1 (mANO1) structure, with similar organization to nhANO, with each subunit containing a cytosolic N- and C-terminal domains, a transmembrane unit consisting of ten membrane-spanning α-helices and an extracellular component (Fig. 2). The authors described that mANO1 has two pores, each contained within a single subunit of the dimeric protein. Furthermore, the

model of mANO1 shows that the conductive pore is largely shielded from the membrane, contrarily to the proposed model of proteolipidic pore hypothesis, which considered that ANO1 channels are partly composed of lipids (Whitlock and Hartzell, 2016).

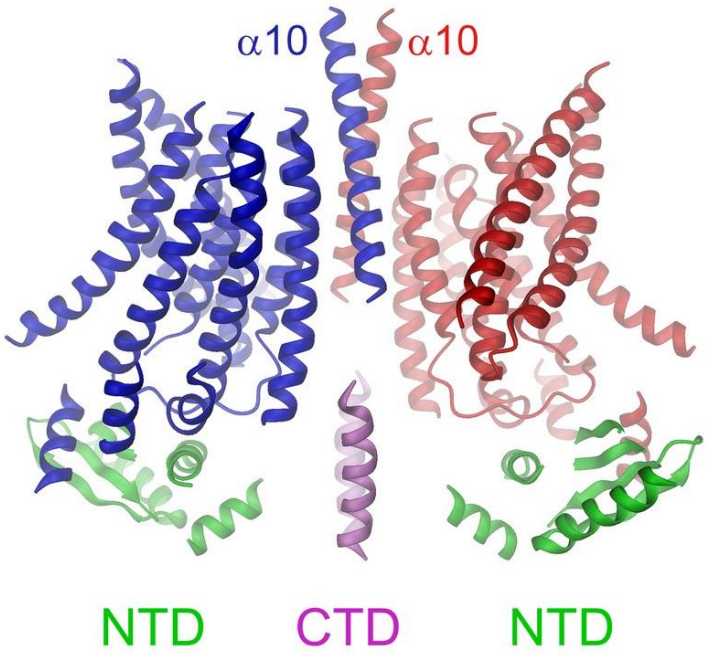

Fig. 2 Mouse ANO1 structure. Ribbon representation of the mANO1 dimer. The transmembrane domains of individual subunits are colored in blue and red, respectively; N-terminal domains (NTD) in green and the C-terminal domains (CTD) in violet. [Paulino *et al.* (2017)b].

Regarding ANO1 pore conformation, though considered a Cl^- channel, ANO1 has poor cation/anion selectivity (PNa/PCl ratio 0.14), being permeable to most monovalent anions (Yang *et al.*, 2012). ANO1 permeability sequence is $SCN^->I^->Br^->Cl^->F^-$, with the particularity of more permeable ions (SCN^-, I^- and Br^-) being the more easily dehydrated (Schroeder *et al.*, 2008). Finally, a proposed hypothesis is that permeant anion occupation in the pore stabilises an open state, regulating the channel gating (Xiao *et al.*, 2011).

Concerning Ca^{2+} binding sites, mANO1 has two Ca^{2+} ions residing at similar locations to those in nhANO1. Moreover, five acidic residues form a Ca^{2+} cage that harbours two Ca^{2+} ions, but specifically for mANO1, three polar residues (N650, N651 and N730) at α6 interact with Ca^{2+} ions (Brunner *et al.*, 2014; Paulino *et al.*, 2017a).

Interestingly, Paulino *et al.* (2017a) data suggest that Ca^{2+} interferes with mANO1 gating mechanism. During activation, Ca^{2+} binding in the transmembrane domains α7 and α8 alters the electrostatic properties of ion conduction and provokes a rearrangement of ANO1. Thereby, an α-helix comes into contact with the bound ligand, directly coupling Ca^{2+} binding and pore opening. Ca^{2+} activated Cl^- secretion may be triggered by purinergic receptor agonists, such as ATP and UTP, or Ca^{2+} ionophores (*e.g.* ionomycin). Via activation of Gq/11 GPCRs by purinergic receptor agonists, PIP_2 is hydrolysed by PLC, producing two secondary messengers, diacylglycerol and IP_3. IP_3 gating to its receptors at ER provoke a Ca^{2+} increment, which directly binds to ANO1, leading to its activation, which results in Cl^- efflux (Duran and Hartzell, 2011).

2.3. ANO1 function in different organs

The human airway system has several mechanisms for pathogenic defense, one of them involving the presence of periciliary liquid provided by active anion transport in airway epithelium (Kunzelmann *et al.*, 2012; Kunzelmann and Schreiber, 2014) (Fig. 3).

ANO1 expression in airway epithelial cells is localised at the apical PM and in intestinal epithelial cells at basolateral PM. Nevertheless, it is also suggested to be localised at the ER membrane, where it facilitates Ca^{2+} release by IP_3R gating, operating as a counter ion for Ca^{2+}. At the basolateral PM, ANO1-mediated Cl^- absorption causes a driving force that promotes Cl^- secretion by CFTR through the apical membrane. Furthermore, ANO1 acts as a tethering protein, therefore facilitating activation of basolateral Ca^{2+}-activated KCNN4 K^+ channels, which also supply a driving force for Cl^- exit by CFTR (Schreiber *et al.*, 2014) (Fig. 3).

In the endocrine pancreas, both CFTR and ANO1 are essential for exocytosis and insulin secretion by β-cells. Edlund *et al.* (2014) reported that CFTR regulates Cl^- influx through ANO1, enhancing granular priming. This process involves the link of the granule to the PM, preceding its fusion to PM. Moreover, some CF patients fail to correctly produce insulin, both due to severe exocrine tissue damage, destroying β-cells, but also by the direct effect of lack of CFTR in β-cells function (Edlund *et al.*, 2014). ANO1 is highly expressed in the epithelium of the proximal tubule in human

kidney and is essential for proton secretion and protein reabsorption (Faria *et al.*, 2014).

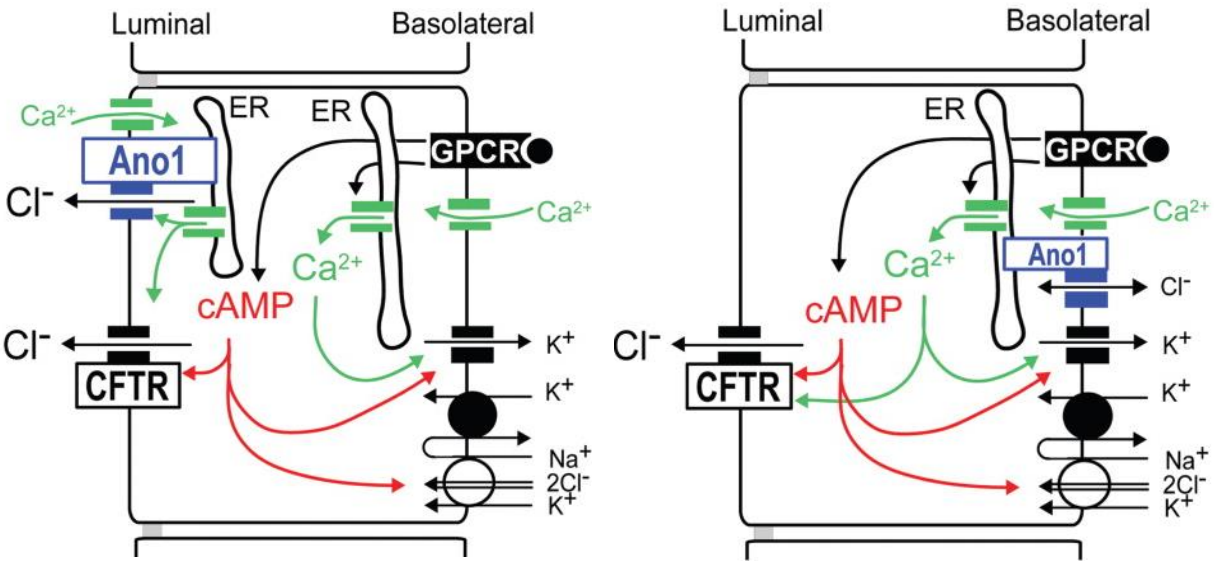

Fig. 3 Cellular models for Cl^- secretion in airway and intestinal epithelial cells. Models for the roles of ANO1 in airway (left) and intestinal (right) epithelium. CFTR is activated through intracellular cAMP and Ca^{2+} dependent second messenger pathways. In airway epithelial cells, ANO1 is located in, or close to the apical membrane. There it may operate as a Cl^- exit channel independent of CFTR, or may control apical Ca^{2+} signaling. In intestinal epithelial cells, ANO1 may support Ca^{2+} dependent Cl^- secretion by facilitating basolateral Ca^{2+} signaling. [Kunzelmann and Schreiber (2014)].

2.4. ANO1 and CFTR

The relationship between CaCCs and CFTR has been studied for a long time in the CF field. Enhanced Ca^{2+}-activated Cl^- conductance was reported in airway cells from CF patients (Paradiso *et al.*, 2001; Martins *et al.*, 2011b), though other studies demonstrated an inhibitory effect of CFTR on ANO1 (Kunzelmann *et al.*, 1997; Wei *et al.*, 1999). Martins *et al.* (2011)b suggested that F508del-CFTR may act as an ER Cl^- counter ion channel for Ca^{2+} exit, thus leading to the accumulation of Ca^{2+} in the ER, therefore increasing Ca^{2+}-activated Cl^- conductance. Recently, Benedetto *et al.* (2017) reported that epithelial cells from ANO1-knockout mice had absence of Ca^{2+}-induced Cl^- currents as expected, but also absence of cAMP-induced Cl^- currents. These data show that ANO1 provides a mechanism for enhanced ER Ca^{2+} store release, possibly engaging SOcAMPs and activating Ca^{2+}-regulated adenylyl cyclases (ADCYs) (Benedetto *et al.*, 2017). In line with these data, Namkung *et al.*

(2010) reported that primary cultures of HBE cells elicited a CFTR-mediated Cl^- current by Ca^{2+} activation of ADCY1. Additionally, it is known that intracellular Ca^{2+} affects the activity of enzymes that control cAMP levels, as ADCYs and phosphodiesterases (Namkung *et al.*, 2010; Kunzelmann *et al.*, 2012). Likewise, cAMP affects several proteins that control intracellular Ca^{2+}, such as SERCA or IP_3 receptors (Bruce *et al.*, 2003; Kunzelmann *et al.*, 2012). Overall, these studies demonstrate a crosstalk between cAMP- and Ca^{2+}-dependent Cl^- secretion and so between the activities of CFTR and ANO1.

2.5. "Bypass" therapies for Cystic Fibrosis

In CF lung disease, two of the main features related to CFTR dysfunction are an impaired cAMP-dependent Cl^- secretion and an enhanced Na^+ absorption. Both processes lead to fluid hyperabsorption in surface epithelium resulting in a reduction of airway surface liquid volume (Amaral and Kunzelmann, 2007). CFTR is also involved in HCO_3^- secretion, which is vital for fluid secretion, mucus hydration and pH regulation (Verkman *et al.*, 2003). These data show that CFTR functions not only as a Cl^- channel but also as a central regulator for several epithelial channels, hence modulation of other channels/transporters can be used to compensate for the loss of functional CFTR.

One such strategy that may benefit for CF patients involves the activation of basolateral K^+ channels, to indirectly activate CFTR by increasing secretory driving force for Cl^-. Therefore, CFTR activation occurs as a result of cell membrane hyperpolarisation, which electrically drives Cl^- through the luminal side of the epithelium (Kunzelmann and Mall, 2003; Amaral and Kunzelmann, 2007). Some compounds activate these channels, such as 1-EBIO, which stimulates Ca^{2+}-activated K^+ channel KCNN4 (Roth *et al.*, 2011) or, for cAMP-regulated K^+ channels, compounds that are agonists of the cAMP pathway, such as β-adrenergic compounds or phosphodiesterases blockers (amrinone or milrinone) (Kunzelmann and Mall, 2001).

In CF epithelia, ENaC channel function is hyperactive, and can be blocked by already existing drugs, such as amiloride, benzamil, phenamil or loperamide (Kunzelmann and Mall, 2003). Interestingly, stimulating purinergic receptors by ATP not only activates ANO1 but also reduces Na^+ absorption, mimicking CFTR Cl^-

secretion and regulation of Na^+ absorption functions (Kunzelmann and Mall, 2003). Moreover, *in vitro* studies showed that ATP and UTP could restore liquid transport in CF culture, enhance tracheal mucus clearance, and increase ciliary beat frequency, among other effects (Kunzelmann *et al.*, 2004; Moss, 2013). To activate ANO1, synthetic nucleotides more stable than ATP, such as INS37217 (Denufosol), were used in clinical trials, though it failed to demonstrate any benefit in phase 3 trial (Moss, 2013). Therefore, development of different drugs with an effect on ANO1 activation has an essential future role in CF therapies.

II. Objectives of the present work

Objectives

The present doctoral work aimed to gain insight into ANO1 regulation and its relationship to CFTR. The ultimate goal of such expected results is to contribute to the development of new therapies for CF patients, namely those based in alternative (non-CFTR) Cl^- channels, also termed “bypass” therapies to compensate for the absence of functional CFTR. To this goal, the following tasks/specific goals were envisaged:

1. To establish an assay for assessment of PM traffic of ANO1 by fluorescent microscopy;

2. To identify genes that affect ANO1 traffic through a siRNA microscopy screen using a double-tagged ANO1;

3. To functionally validate the effects of the top screen hits from the siRNA screen;

4. To study the role of ANO6 in CFTR and ANO1 expression and function.

III. Materials and Methods

1. Production of double-tagged 3HA-ANO1-eGFP

ANO1 a,b,c isoform (NCBI Reference Sequence: XP_011543427.1) was used for cloning of a double-tagged 3HA-ANO1-eGFP. The expressing plasmid with eGFP tag linked to ANO1 C-terminal via a small linker (LEFLNCCPGCCMEPSTT) was kindly provided by Prof. Dr. Rainer Schreiber (University of Regensburg, Germany). Hemagglutinin tag (YPYDVPDYA) was inserted by mutagenesis (ANO1-3HA-FW/RV primers, table 1) in triplicate (3HA) between His396 and Asn397, *i.e.*, in the first extracellular loop of ANO1. The double-tagged construct was cloned using In Fusion HD Cloning Kit (Clontech #121416) into the Lenti-X Tet-On 3G Inducible Expression System (Clontech #631187) that include a pLVX-TRE3G plasmid to express the GOI and a pLVX-Tet3G plasmid for inducibility features. Briefly, small extensions were introduced in the 3HA-ANO1-eGFP fragment (pLVX-ANO1-FW/RV primers, table 1) and were digested by restriction enzymes MluI (NEB #R0198S) and BamHI (NEB #R0136S) in addition to pLVX-TRE3G empty plasmid. This produced matching ends between empty plasmid and 3HA-ANO1-eGFP fragment. Both pLVX-TRE3G empty plasmid and 3HA-ANO1-eGFP fragment were purified from the agarose gel (NZYtech #MB01101) and the In Fusion HD Cloning Kit (Clontech #121416) was followed according to manufacturer's conditions to insert the 3HA-ANO1-eGFP fragment into the pLVX-TRE3G plasmid.

After assessment of correct sequencing, pLVX-TRE3G-3HA-ANO1-eGFP and pLVX-Tet3G constructs were transfected into HEK293T cells to produce lentiviral particles using Lipofectamine 2000 Transfection reagent (Invitrogen #11668027). Briefly, HEK293T cells were seeded in a 6 well-dish and, after 24h, cells were transfected with lentiviral plasmids pMD2G (Addgene plasmid #12259), psPAX2 (Addgene #12260) and pRSV-Rev (Addgene #12253) and either pLVX-TRE3G-3HA-ANO1-eGFP or pLVX-Tet3G constructs in a specific ratio (pLVX : pMD2G : psPAX2 : pREV; 2:2:1:0.1). After 18h, media from these cells were changed and lentiviral particles collected after 30h (total of 48h after transfection). These lentiviral particles were then used to transduce target cells seeded in 6-well dishes (CFBE parental or CFBE expressing mCherry-flag-WT-/F508del-CFTR), by changing their media for 1.5mL of enriched pLVX-TRE3G-3HA-ANO1-eGFP lentiviral particles media, 1.5mL of enriched pLVX-Tet3G lentiviral particles media and polybrene (8 µg/mL) (Sigma-Aldrich #107689). Then, the 6-well plates were centrifuged 1h at 220 rpm and 25ºC

and 48h after, selective antibiotics were used in the media. In this case, puromycin (2 µg/mL) (Sigma-Aldrich #P8833) and G418 (400 µg/mL) (Invitrogen #108321-42-2) were used.

Cells were kept in selective media to maintain the expression and sorted by flow cytometry in a BC MoFlo Cell Sorter (Beckman Coulter, Inc, Indianapolis IN, USA) to select for high eGFP fluorescence.

Table 1 Primers used to generate pLVX-TRE3G-3HA-ANO1-eGFP construct.

Name of the primer	Sequence 5' -> 3'
ANO1-3HA-FW (forward primer)	CCCAGCATGGAGATGTGTGACCAGAGACACTACCCATACGAT GTTCCAGATTACGCTTACCCATACGATGTTCCAGATTACGCTT ACCCATACGATGTTCCAGATTACGCTAATATTACCATGTGCCC GCTTTGCGACAAGACC
ANO1-3HA-RV (reverse primer)	GGTCTTGTCGCAAAGCGGGCACATGGTAATATTAGCGTAATCT GGAACATCGTATGGGTAAGCGTAATCTGGAACATCGTATGGG TAAGCGTAATCTGGAACATCGTATGGGTAGTGTCTCTGGTCAC ACATCTCCATGCTGGG
pLVX- ANO1-FW (forward primer)	TCTTATACTTGGATCCATGAGGGTCAACGAGAAGTACTCG
pLVX- ANO1-RV (reverse primer)	GGCATGGACGAGCTGTACAAGTAAACGCGTCATATGGAAT

1.1. Cells and Culture conditions

During this PhD work, four cell lines were used: cystic fibrosis bronchial epithelial (CFBE) cells, human embryonic kidney 293T (HEK293T) cells, Calu-3 cells and human colon adenocarcinoma (HT-29) cells.

CFBE cells are an immortalised cell line produced from primary cells of a CF patient. Nonetheless, CFTR protein expression at this moment is null due to cells' passages (Zeitlin *et al.*, 1991; Kunzelmann *et al.*, 1993). CFBE cells stably expressing 3HA-ANO1-eGFP were cultured in EMEM with 2 mM L-Glutamine (Lonza #BE12-611F) supplemented with 10% (v/v) heat-inactivated fetal calf serum (Gibco #10106), 400 µg/ml G418 (Sigma-Aldrich #A1720) and 2 µg/ml puromycin (Invitrogen #ant-pr-1), at 37°C and 5% CO_2.

CFBE cells overexpressing double-tagged ANO1 and mCherry-flag-WT-/F508del-CFTR were cultured in DMEM high glucose (Gibco #41965) with 2 mM L-Glutamine (Lonza #BE12-611F) supplemented with 10% (v/v) heat-inactivated fetal calf serum (Gibco #10106), 400 µg/ml G418 (Sigma-Aldrich #A1720), 2 µg/ml puromycin (Invitrogen #ant-pr-1) and 10 µg/ml Blasticidin (Sigma-Aldrich #15205), at 37°C and 5% CO_2. CFBE expressing mCherry-flag-WT-/F508del-CFTR were cultured in the same conditions, but with different selective antibiotics (2 µg/ml puromycin and 10 µg/ml Blasticidin). Finally, CFBE expressing WT-/F508del-CFTR were also cultured in the same conditions, but only with 2 µg/ml puromycin as the selective antibiotic.

HEK293T cells were cultured in DMEM (Gibco #11885-084), supplemented with 10% (v/v) heat-inactivated fetal calf serum (Gibco #10106) at 37°C and 5% CO_2.

Calu-3 cells were cultured in DMEM F12 (Gibco #11320-033), supplemented with 2 mM L-glutamine (Lonza #BE12-611F), 10mM HEPES (Thermofisher Scientific #15630106) and 10% (v/v) heat inactivated fetal calf serum (Gibco #10106) at 37°C and 5% CO_2.

HT-29 cells were cultured in McCoy's 5A (modified) media (Gibco #16600082), supplemented with 10% (v/v) heat-inactivated fetal calf serum (Gibco #10106) at 37°C and 5% CO_2.

2. Biochemical and Cell Biology Techniques

2.1. cDNA and siRNAs transfection

Cells were transfected with different cDNAs for 48h or 72h using Lipofectamine™ 3000 transfection reagent (Invitrogen #L3000075), according to manufacturer's conditions.

2.2. Semiquantitative Reverse-transcriptase PCR

Total RNA was isolated from cells using NucleoSpin RNA II columns (Macherey-Nagel #740955.50). Total RNA (1 µg/50 µl reaction) was reverse-transcribed using random primers and M-MLV reverse transcriptase (Promega #9PIM170). Each RT-PCR reaction contained sense and antisense primers for the respective gene (0.5 µM) or GAPDH (0.5 µM), 0.5 µl cDNA and GoTaq Polymerase (Promega #9PIM300). After 2 min at 95°C, cDNA was amplified during 30 cycles for 30s at 95°C, 30s at

56°C and 1 min at 72°C. PCR products were visualised by loading on agarose gels containing peqGREEN DNA/RNA Dye (Peqlab Biotech #732-3196) and analysed using Meta Morph Vers. 6.2 (Molecular Devices, USA).

2.3. Western-blot

CFBE cells were collected and lysed in 0.5% (v/v) NP40 lysis buffer. Proteins were separated by 7% (w/v) SDS-PAGE gels and transferred into PVDF membranes. The membranes were blocked with 5% (w/v) non-fat milk (NFM) powder in Tris buffer saline (Sigma-Aldrich #T5912) with Tween 20 (Sigma-Aldrich #P9416) (TBS-T) for 1h at room temperature and incubated overnight at 4°C with rabbit DOG1 antibody (Novus Biologicals #NP060513) (1:500 in 1% (w/v) NFM/TBS-T) and rabbit anti β-Actin (Sigma-Aldrich #A2066) (1:10000 in 1% (w/v) NFM/TBS-T) or rabbit α-tubulin (Sigma-Aldrich #SAB3501072) (1:10000 in 1% (w/v) NFM/TBS-T). The membranes were incubated with Goat-anti-rabbit IgG (H+L)-HRP conjugate (Bio-Rad #1706515) (1:3000 in 1% (w/v) NFM/TBS-T) for 1h at room temperature. Signals were detected using a SuperSignal West Pico chemiluminescence substrate (Thermo Fisher Scientific #34577).

2.4. cAMP immunoassay

cAMP Direct Immunoassay Kit (Abcam #ab138880) was used following the manufacturer's protocol. This assay is based on the competition between HRP-labeled cAMP and free cAMP present in the sample for cAMP antibody binding sites. Briefly, WT-/F508del-CFTR expressing CFBE cells were treated either with IBMX (100 µM) (Sigma-Aldrich #I5879) and forskolin (2 µM) (Abcam #ab120058) or ATP (100 µM) (Sigma-Aldrich #A1852) and then lysated and centrifuged to obtain the cAMP containing supernatant. The supernatant was incubated in the cAMP antibody coated 96-well plate for 10 min and, after incubation, cAMP-HRP conjugated was added. The amount of cAMP-HRP bound to the plate was determined by reading HRP activity at OD 450 nm using a NOVOstar Microplate Reader (BMG LABTECH GmbH, Ortenberg, Germany). The intensity of OD 450 nm is inversely proportional to the concentration of cAMP in samples and cAMP concentration was obtained using a standard curve with known cAMP-HRP concentrations.

2.5. Immunocytochemistry

2.5.1. 3HA tag

Cells were washed three times with ice cold PBS (Gibco #10010023) and incubated 2h at 4˚C with monoclonal anti-HA antibody (Biolegend # 901502) diluted 1:100 in PBS supplemented with 1% (w/v) bovine serum albumin (BSA) (Sigma-Aldrich #A9056). Then, cells were washed three times with ice cold PBS and incubated 10 min with 4% (v/v) PFA (Merck Millipore #104005) at room temperature. Cells were then washed three times with PBS and incubated 1h with anti-mouse Alexa Fluor 647-conjugated secondary antibody (Invitrogen #A31571) diluted 1:500 in PBS supplemented with 1% (w/v) BSA. Afterwards, cells were washed three times with PBS and incubated with a Hoechst 33342 solution (Sigma-Aldrich #B2261) for 1h. Finally, cells were washed three times with PBS, immersed in PBS and incubated overnight before imaging. All solutions were prepared in PBS freshly supplemented with 0.7 mM $CaCl_2$ and 1.1 mM $MgCl_2$.

Immunofluorescence was detected acquired with Leica DMI 6000B (objective 63x, water) and analysed with the profile measurement tool Image J/Fiji.

2.5.2. ANO1

Cells were washed three times with PBS (Gibco #10010023) and fixed for 10 min with methanol (Roth #8388.1) and acetone (Roth #T906.1) (4:1) at -20ºC. Cells were washed three times with PBS and afterwards incubated for 30 min at 37ºC with PBS supplemented with 1% (w/v) BSA (Roth #3737.2) and 0.04% (v/v) Triton X-100 (Sigma-Aldrich #9002-93-1) to block and permeabilize the cells, respectively. Cells were incubated for 1h at room temperature with primary rabbit DOG1 antibody (Novus Biologicals #NP060513) diluted to 1:100 in PBS supplemented with 1% (w/v) BSA. Cells were washed three times with PBS and incubated with the secondary antibody Alexa Fluor 488-conjugated donkey anti-rabbit IgG (Invitrogen #A-11008) diluted 1:300 in PBS supplemented with 1% (w/v) BSA and Hoechst 33342 (Aplichem #A0741) (1:200) for 1h at room temperature. Coverslips were mounted with fluorescence mounting medium (Dako #S3023). Immunofluorescence was detected with an Axiovert 200 microscope equipped with an ApoTome and analysed with the profile measurement tool of AxioVision software (AxioVs40; V 4.8.2.0; Zeiss).

2.5.3. ANO6

Cells were washed three times with PBS (Gibco #10010023) and fixed for 10 min with PFA 4% (v/v) (Merck Millipore #104005) at room temperature. Cells were washed three times with PBS and afterwards incubated for 30 min at 37ºC with PBS supplemented with 1% (w/v) BSA (Roth #3737.2) and 0.04% (v/v) Triton X-100 (Sigma-Aldrich #9002-93-1) to block and permeabilize the cells, respectively. Cells were incubated for 1h at room temperature with primary rabbit ANO6 antibody (Thermo Fisher Scientific #PA5-35240) diluted to 1:200 in PBS supplemented with 1% (w/v) BSA. Afterwards, cells were washed three times with PBS and incubated with the secondary antibody Alexa Fluor 546–conjugated donkey anti-rabbit IgG (Invitrogen # A-11030) diluted 1:300 in PBS supplemented with 1% (w/v) and Hoechst 33342 (Aplichem #A0741) (1:200) for 1h at room temperature. Coverslips were mounted with fluorescence mounting medium (Dako #S3023). Immunofluorescence was detected with an Axiovert 200 microscope equipped with an ApoTome and analyzed with the profile measurement tool of AxioVision software (AxioVs40; V 4.8.2.0; Zeiss).

2.5.4. CFTR

Cells were washed three times with PBS (Gibco #10010023) and fixed for 10 min with PFA 4% (v/v) (Merck Millipore #104005) at room temperature. Cells were washed three times with PBS and afterwards incubated for 30 min at 37ºC with PBS supplemented with 1% (w/v) BSA (Roth #3737.2) and 0.04% (v/v) Triton X-100 (Sigma-Aldrich #9002-93-1) to block and permeabilize the cells, respectively. Cells were incubated for 1h at room temperature with primary mouse CFTR 570 antibody (CFF #A2) diluted to 1:200 in PBS supplemented with 1% (w/v) BSA. Afterwards, cells were washed 3 times with PBS and incubated with the secondary antibody Alexa Fluor 546–conjugated donkey anti-mouse IgG (Invitrogen # A-11030) diluted 1:300 in PBS supplemented with 1% (w/v) and Hoechst 33342 (Aplichem #A0741) (1:200) for 1h at room temperature. Coverslips were mounted with fluorescence mounting medium (Dako #S3023). Immunofluorescence was detected with an Axiovert 200 microscope equipped with an ApoTome and analyzed with the profile measurement tool of AxioVision software (AxioVs40; V 4.8.2.0; Zeiss).

2.5.5. EPAC

Cells were washed three times with PBS (Gibco #10010023) and fixed for 10 min with PFA 4% (v/v) (Merck Millipore #104005) at room temperature. Cells were washed three times with PBS and afterwards incubated for 30 min at 37ºC with PBS supplemented with 1% (w/v) BSA (Roth #3737.2) and 0.04% (v/v) Triton X-100 (Sigma-Aldrich #9002-93-1) to block and permeabilize the cells, respectively. Cells were incubated overnight at 4ºC with primary mouse EPAC antibody (Santa-Cruz #sc_28366) diluted to 1:50 in PBS supplemented with 1% (w/v) BSA. Cells were washed three times with PBS and incubated with the secondary antibody Alexa Fluor 546–conjugated donkey anti-mouse IgG (Invitrogen #A-11030) diluted 1:300 in PBS supplemented with 1% (w/v) BSA and Hoechst 33342 (Aplichem #A0741) (1:200) for 1h at room temperature. Coverslips were mounted with fluorescence mounting medium (Dako #S3023). Immunofluorescence was detected with an Axiovert 200 microscope equipped with an ApoTome and analyzed with the profile measurement tool of AxioVision software (AxioVs40; V 4.8.2.0; Zeiss).

2.5.6. Mucin 5AC

Cells were washed three times with PBS (Gibco #10010023) and fixed for 10 min with PFA 4% (v/v) (Merck Millipore #104005) at room temperature. Cells were washed three times with PBS and afterwards incubated for 5 min at room temperature with PBS supplemented with 0.1% (v/v) Triton X-100 (Sigma-Aldrich #9002-93-1) to permeabilize the cells. Cells were incubated 1 hour at room temperature with primary mouse MUC5AC antibody (Abcam #77576) diluted to 1:100 in PBS supplemented with 1% (w/v) BSA (Roth #3737.2). Cells were washed three times with PBS and incubated with the secondary antibody Alexa Fluor 546–conjugated donkey anti-mouse IgG (Invitrogen #A-11030) diluted 1:300 in PBS supplemented with 1% (w/v) BSA and Hoechst 33342 (Aplichem #A0741) (1:200) for 1h at room temperature. Coverslips were mounted with fluorescence mounting medium (Dako #S3023).

Immunofluorescence was detected acquired with Leica DMI 6000B (objective 63x, water) and analyzed with the profile measurement tool Image J/Fiji.

2.6. Chemiluminescence

2.6.1. ANO1

CFBE parental cells were seeded on coated black 96-well plates (Corning #3631) at a density of $7.5x10^3$ cells/well. On the following day, cells were transfected with cDNAs/siRNAs targeting the genes of interest (72h transfection) and in the day after with pLVX-3HA-ANO1 and its regulator plasmid (pLVX-Tet) (48h transfection) and induced with 1 µg/ml doxycycline (dox) (Sigma-Aldrich #D9891). 48h after, cells were washed once with ice cold PBS (Gibco #10010023). Then cells were incubated for 1h at 4˚C with monoclonal anti-HA (Biolegend #901501) diluted to 1:500 in PBS supplemented with 1% (w/v) BSA (Roth #3737.2). Afterwards, cells were washed three times with ice cold PBS, incubated 10 min with PFA 4% (v/v) (Merck Millipore #104005) at 4°C and transferred to room temperature for the remaining procedure. Cells were then washed three times with PBS and incubated 1h at room temperature with a goat anti-mouse HRP-conjugated secondary antibody (BioRad #1706516) diluted to 1:5000 in PBS supplemented with 1% (w/v) BSA. Signals were detected using a SuperSignal West Pico chemiluminescence substrate (Thermo Fisher Scientific #34577) using a NOVOstar Microplate Reader (BMG LABTECH GmbH). All solutions were prepared in PBS freshly supplemented with 0.7 mM $CaCl_2$ and 1.1 mM $MgCl_2$.

2.6.2. CFTR

CFBE-mCherry-flag-WT-/F508del-CFTR cells were seeded on coated black 96-well plates (Corning #3631) at a density of $8x10^3$ cells/well. On the following day, cells were induced with 1 µg/ml dox (Sigma-Aldrich #D9891) and transfected with the cDNAs/siRNAs targeting the genes of interest. 48h after the transfection, cells were washed once with ice cold PBS (Gibco #10010023). Then cells were incubated for 1h at 4˚C with mouse anti-flag-HRP conjugated (Sigma-Aldrich #A8592) diluted 1:1000 in PBS supplemented with 1% (w/v) BSA (Roth #3737.2) and then washed three times with PBS. Afterwards, cells were washed 3 times with ice cold PBS, incubated 10 min with PFA 4% (v/v) (Merck Millipore #104005) at 4°C. Signals were detected using a SuperSignal West Pico chemiluminescence substrate (Thermo Fisher Scientific #34577) using a NOVOstar Microplate Reader (BMG LABTECH GmbH). All

solutions were prepared in PBS freshly supplemented with 0.7 mM $CaCl_2$ and 1.1 mM $MgCl_2$.

2.7. ANO1 Traffic Assay

2.7.1. Preparation of siRNA coated multi-well plates

Multi-well plates (BD Falcon #353962) were coated with customised siRNAs for solid-phase reverse transfection adapted from a previously reported protocol (Erfle *et al.*, 2007) with adjustments also described before (Botelho *et al.*, 2015). All tested siRNAs were Ambion Silencer Select.

CFBE-3HA-ANO1-eGFP cells were grown to confluence and split (50%). 24h later, cells were trypsinised to antibiotic-free medium and seeded in siRNA coated 384-well plates (50 µl/well, $3x10^3$ cells/well) using a Multidrop™ Combi peristaltic dispenser (Thermo Scientific #5840300). ANO1 expression was induced for 48h (24h after seeding) with antibiotic-free medium supplemented with 1 µg/ml dox (Sigma-Aldrich #9891).

2.7.2. Liquid siRNA transfection

Liquid siRNA transfection of CFBE-3HA-ANO1-eGFP cells was carried out using siRNAs. The expression of 3HA-ANO1-eGFP was induced by addition of 1 µg/mL dox (Sigma-Aldrich #9891) 24h after transfection. Experiments were performed 72h after transfection (48h of Dox induction).

2.7.3. Immunocytochemistry

Extracellular HA-tag was immunostained in non-permeabilized cells 72h after seeding. After culture medium removal, cells were washed once with ice cold PBS (Gibco #10010023) and incubated 1h at 4˚C with monoclonal anti-HA antibody (Biolegend # 901502).

Then, cells were washed three times with ice cold PBS, incubated 20 min with 3% (v/v) PFA (Merck Millipore #104005) at 4°C and transferred to room temperature for the remaining procedure. Cells were then washed three times with PBS and incubated 1h with an anti-mouse Alexa Fluor 647-conjugated secondary antibody (Invitrogen #A31571). Cells were then washed three times with PBS and incubated

with a Hoechst 33342 solution (Sigma-Aldrich #B2261) for 1h. Finally, cells were washed three times with PBS, immersed in PBS and incubated overnight before imaging.

All solutions were prepared in PBS freshly supplemented with 0.7 mM $CaCl_2$ and 1.1 mM $MgCl_2$. Antibody solutions additionally contained 1% (w/v) BSA (Sigma-Aldrich #A9056). All liquid handling was performed with a manual 96 channel pipette liquidator (Liquidator™ 96, Mettler Toledo #17010335).

2.7.4. Image acquisition of fixed samples and time-lapse microscopy

Cell imaging was performed with (automated) widefield epifluorescence microscope with a Scan^R software (Olympus Biosystems) equipped with a motorized stage and a metal halide light source (MT20), a 12-bit 1344 x 1024 pixel resolution C8484 CCD camera (Hamamatsu OrcaFlash4) and a 10x UPlanApo objectives (Olympus) and 0.4 numerical aperture. Exposure times at maximum light brightness were for Hoechst, eGFP and Alexa Fluor 647 of (ms) 10-20, 500 and 2000, respectively. The Hoechst channel was used for contrast-based autofocus (fixed samples) and hardware autofocus for time-lapse imaging. Fixed samples were imaged at room temperature and filter settings (Excitation wavelengths/excitation band (nm) – Ex, Emission wavelengths/emission band (nm) – Em): Hoechst – Ex 347/50, Em 460/50; eGFP – Ex 470/40, Em 525/50; Alexa 647 – Ex 640/30, Em 690/50.

2.7.5. Analysis of time-lapse microscopy images

Time-lapse microscopy images were processed and quantified in Image J/Fiji. Briefly, a cell-free region was used for baseline correction. Then, representative cells were selected - *i.e.* cells which remain viable and within the field of view during the whole time-lapse - and their average fluorescence intensity was determined and plotted as a function of time. Finally, the grayscale lookup table was adjusted for optimal contrast.

2.7.6. Automatic Image Analysis Pipeline

Automatic image analysis was performed with open source software tools (CellProfiler, R), using pipelines tailored to the specific application as described

before for CFTR (Botelho *et al.*, 2015). Initially, overall transfection efficiency was assessed by observing if cells transfected with siRNAs compromising chromosome segregation exhibited mitotic phenotypes (Simpson *et al.*, 2012). Failure to observe these phenotypes in more than 75% of images implied the rejection of the corresponding plate from the analysis. The algorithm for background subtraction was also described before (Botelho *et al.*, 2015). Briefly, it comprised: 1) the computation of illumination correction functions for each fluorescence channel, which defines the pixel-by-pixel fluorescence baseline for each channel as produced by image illumination and background fluorescence; 2) subtraction of the corresponding illumination correction function from each image. The pipeline includes quality control (QC) steps excluding cells which do not significantly express ANO1, have abnormal morphology (*e.g.* apoptotic cells) or contain a significant amount of saturated pixels. This fluorescence quantification data allowed determining ANO1 traffic in each cell according to the following formula:

$$\text{ANO1 Traffic Efficiency} = \frac{PM\ ANO1}{Total\ ANO1} = \frac{Alexa\ Fluor\ 647\ Integrated\ Fluorescence}{eGFP\ Integrated\ Fluorescence}$$

(Formula 1)

For each image, the ANO1 Traffic Efficiency was considered to be the median for all cells in the image, as previously described (Botelho *et al.*, 2015). After averaging the ANO1 Traffic Efficiency for all images relating to the same siRNA, the effect of each siRNAs was compared with the one measured under the effect "Scrbld" non-targeting siRNA treatment (*Traffic Efficiency*$_{Neg\_control}$) using the following formula:

$$\text{Deviation Score} = \frac{Traffic\ Efficiency_{Test} - Traffic\ Efficiency_{Neg\_control}}{2 \times SEM_{Neg\_control}}$$ (Formula 2)

Where $SEM_{Neg\_control}$ is the standard error of the mean for the Traffic Efficiency recorded upon "Scrbld" siRNA. We consider significant ANO1 Traffic Efficiency effects those whose magnitude is larger than twice the negative control. Thus, ANO1 traffic enhancer has a Deviation Score above +1 and ANO1 traffic inhibitor a Deviation Score below -1. Additionally, two-tailed Student's t-tests were performed to quantify statistical significance versus the corresponding negative control.

2.8. CLCA1 enriched media production

CLCA1 enriched media was produced accordingly to the procedure described in Sala-Rabanal *et al.* (2015). Briefly, HEK293T cells were seeded in T75 flasks and, after 24h, were transfected with CLCA1 expressing plasmid or mock plasmid. 6 hours after, transfection media was removed and fresh medium applied; following overnight incubation, the medium of these cells was harvested and centrifuged (1500 x g, 5 min) to remove possible contamination with HEK293T cells. CFBE expressing double-tagged ANO1 and mCherry-flag-WT-CFTR seeded in 24-well plate were incubated for 24 hours with 1.5mL of CLCA1 or mock enriched media.

3. Functional assays

3.1. Iodide effluxes

ANO1 function as a channel was assessed for the 3HA-ANO1-eGFP construct by iodide efflux as previously described (Long and Walsh, 1997; Moniz *et al.*, 2013). Briefly, HEK293T cells were seeded in 6-well dishes coated with poly-L-lysin (Sigma-Aldrich #A-005-C) and transfected with pLVX-3HA-ANO1-eGFP and pLVX-Tet3G for 48h with Lipofectamine 2000 Transfection reagent (Invitrogen #11668027) and either induced with dox (1 µg/ml) (Sigma-Aldrich #9891) or non-induced. Cells were incubated 30 min at 37ºC with pre-warmed loading buffer (mM: 136 NaI, 3 KNO_3, 2 $Ca(NO_3)_2$, 2 $MgSO_4$, 10 D-Glucose, 20 HEPES, pH 7.5). Then washed four times with efflux buffer (EB) (136 mM $NaNO_3$ replacing NaI in the loading buffer) and equilibrated for 10 min at 37ºC with EB. Next, cells were stimulated with either ATP (100 µM) (Sigma-Aldrich #A1852) or DMSO (Sigma-Aldrich #D8418) for 5 min at 37ºC to stimulate ANO1. Cells were quickly washed with EB, lysed with 1 mL of EB plus 0.5% (v/v) Triton X-100 (Sigma-Aldrich #X100), scraped and centrifuged at 16000 x g for 5 min. Aliquots from each sample were used to quantify total protein using Quick StartTM Bradford Protein Assay (Bio-Rad #5000201), according to manufacturer's conditions. Iodide concentration in lysates was determined using an Iodide-selective electrode (MP225, Thermo Electron Corp., Waltham, MA, USA) and normalised to the amount of protein in the sample.

3.2. Ussing Chamber assay

For open circuit measurements CFBE-3HA-ANO1-eGFP cells were seeded at approximately 3.5 x 10^5 cells/ml onto Costar Transwell permeable supports of pore size 0.4 µm and 1.13 cm^2 area (Corning #3801). Transepithelial electrical resistances (TEER) of CFBE-3HA-ANO1-eGFP monolayers were measured with a chopstick electrode (STX2, WPI, Sarasota, FL, USA) and electrophysiological analyses were carried out in monolayers with resistance values above 600 Ω x cm^2. Transepithelial resistance (R_{te}) was determined by applying 1 s current pulses of 0.5 µA (5 s-period). For Ussing Chamber measurements, Snapwells were mounted in the Chamber device and continuously perfused with Ringer containing (mM): 145 NaCl, 1.6 K_2HPO_4, 1 $MgCl_2$, 0.4 KH_2PO_4, 1.3 Ca^{2+}-gluconate, 5 Glucose, pH 7.4. ANO1 was activated by ATP (100 µM) (Sigma-Aldrich #A1852) added to the luminal as well as to the basal side and inhibited by the CaCCinh-AO1 (30 µM) (Tocris #4877) (Namkung *et al.*, 2011). Values for the transepithelial voltage (V_{te}) were referenced to the basal epithelial surface. Equivalent short-circuit current (I_{eq-sc}) were calculated according to Ohm's law from V_{te} and R_{te} ($I_{eq-sc}=V_{te}/R_{te}$), with appropriate correction for fluid resistance.

3.3. Whole-cell patch-clamp

2 or 3 days after transfection, transfected cells were identified by incubating the cells for 1-2 minutes with Dynabeads CD8 (Invitrogen #11147D). Coverslips were mounted on the stage of an inverted microscope (IM35; Carl Zeiss, Jena, Germany) and kept at 37ºC. Patch pipettes were filled with a cytosolic-like solution (mM: 30 KCl, 95 K^+-gluconate, 1.2 NaH_2PO_4, 4.8 Na_2HPO_4, 1 EGTA, 0.758 Ca^{2+}-gluconate, 1.03 $MgCl_2$, 5 D-glucose, 3 ATP, pH 7.2). The intracellular (pipette) Ca^{2+} activity was 0.1 µM. Fast whole-cell current recordings were performed as previously described (Martins *et al.*, 2011a). The bath was perfused continuously with Ringer solution (mM: 145 NaCl; 0.4 KH_2PO_4; 1.6 K_2HPO_4; 5 Glucose; 1 $MgCl_2$; 1.3 Ca^{2+}-Gluconate, pH 7.4) containing 50 nM TRAM34 (Abcam #ab141885) at a rate of 8 ml/min. Patch pipettes had an input resistance of 2–6 MΩ and whole-cell currents were corrected for serial resistance. Currents were recorded using a patch clamp amplifier (EPC 7, List Medical Electronics, Darmstadt, Germany), the LIH1600 interface and PULSE software (HEKA, Lambrecht, Germany) as well as Chart software (AD Instruments,

Spechbach, Germany). In regular intervals, membrane voltage (Vm) was clamped in steps of 20 mV from -100 to +100 mV from a holding voltage of -100 mV. The current density was calculated by dividing whole-cell currents by cell capacitance.

For these assays, several reagents were used diluted either in Ringer (extracellular solution) or in the pipette filling solution, as described in Table 2.

Table 2 Reagents used in whole-cell patch-clamp assays.

Reagent	Solution for dilution	Cells' pre-incubation
DMSO (Sigma-Aldrich #D8418)	Same as the comparison reagent	Same as the comparison reagent
ATP (100 µM) (Sigma-Aldrich #A1852)	Extracellular solution	-
IBMX (100 µM) (Sigma-Aldrich #I5879)	Extracellular solution	-
Forskolin (2 µM) (Abcam #ab120058)	Extracellular solution	-
BAPTA-AM (50 µM) (Merck #196419)	Extracellular solution	15 min
Ionomycin (0.1 or 1 µM) (Abcam #ab120116)	Extracellular solution	-
8-Br-cAMP (25µM) (Sigma-Aldrich #B7880)	Extracellular solution	-
CFTR inhibitor 172 (20 µM) (Tocris #3430)	Extracellular solution	-
CaCC inhibitor AO1 (30 µM) (Tocris #4877)	Extracellular solution	-
8-pCPT-2-O-Me-cAMP (007-AM) (30 µM) (Biolog #C041)	Pipette filling solution	-
Brefeldin A (BFA) (10 µM) (Sigma-Aldrich #20350-15-6)	-	24h
ESI09 (10 µM) (Tocris #4773)	Pipette filling solution	Overnight
ST034307 (30 µM) (Tocris #6271)	Pipette filling solution	3h
Carbachol (100 µM) (Sigma-Aldrich #C4382)	Extracellular solution	-
Tram34 (50 nM) (Abacam #ab141885)	Extracellular solution	-
Histamine dihydrochloride (50 µM) (Abcam #ab120734)	Extracellular solution	-

3.4. Ca^{2+} measurements

3.4.1. Ca^{2+} measurements with G-CAMP6

CFBE cells were transfected on coated glass coverslips with pcDNA3.1-Pl-G-CAMP6 fused to the C-terminus of CFTR and were mounted in a perfusion Chamber 72 h after transfection. Cells were perfused with Ringer solution (mM: 145 NaCl; 0.4 KH_2PO_4; 1.6 K_2HPO_4; 5 Glucose; 1 $MgCl_2$; 1.3 Ca^{2+}-Gluconate, pH 7.4) at a rate of 8 ml/min at 37°C. Cells' fluorescence was measured continuously with an inverted microscope Axiovert S100 (Zeiss) with a 40x objective (Fluar 340/1.3 oil; Zeiss) and a high-speed polychromator system (VisiChrome; Visitron, Puchheim, Germany). Pl-GCaMP6 was excited at 485 and 405 nm. Emission was recorded between 520 and 550 nm with a CCD-camera (CoolSnap HQ; Visitron, Hauppauge, NY, USA).

3.4.2. Ca^{2+} measurements with Fura-2

CFBE cells were seeded on glass coverslips and loaded with 2 mM Fura-2/AM (Biotium #50033-1) and 0.02% (v/v) Pluronic F-127 (Thermo Fischer Scientific #P3000MP) in Ringer solution (mM: 145 NaCl; 0.4 KH_2PO_4; 1.6 K_2HPO_4; 5 Glucose; 1 $MgCl_2$; 1.3 Ca^{2+}-Gluconate, pH 7.4) for 1 h at room temperature. Fluorescence was detected in cells perfused with Ringer solution at 37ºC using an inverted microscope (Axiovert S100, Zeiss, Germany) with a 20x objective and a highspeed polychromator system (VisiChrome, Germany). Fura-2 was excited at 340/380 nm, and emission was recorded between 470 and 550 nm using a CoolSnap camera (CoolSnap HQ, Visitron). Control of experiments, imaging acquisition, and data analysis was performed with the software package Meta-Fluor (Universal Imaging, New York, NY, USA).

IV. Results and Discussion

CHAPTER 1

A novel cell-based traffic assay to identify potential ANO1 traffic regulators by high-throughput microscopy.

Data included in this chapter was partially published in:

Lérias JR*, Pinto MC*, Botelho HM, Awatade NT, Quaresma MC, Silva IAL, Wanitchakool P, Schreiber R, Pepperkok R, Kunzelmann K, Amaral MD (2018). A novel microscopy-based assay identifies extended synaptotagmin-1 (ESYT1) as a positive regulator of anoctamin 1 traffic. Biochim Biophys Acta **1865**(2):421-431 [*Shared first authorship].

1. Production of stable inducible 3HA-ANO1-eGFP expressing cell lines

For the assessment of ANO1 PM traffic by fluorescent microscopy, a 3HA-ANO1-eGFP expressing vector was produced. This double-tagged ANO1 has an enhanced green fluorescent protein (eGFP) tag in C-terminal and a 3HA tag present in the first extracellular loop. The eGFP allows the measurement of total ANO1 expression, and a 3HA tag allows the measuring of ANO1 present at PM without cell permeabilisation (Fig. 4, Fig. 5). As previously described for CFTR (Botelho *et al.*, 2015), this double-tagged ANO1 allows the ratiometric readout of traffic efficiency on a single cell basis, constituting a reliable cellular model to study ANO1 traffic. Finally, the double-tagged ANO1 expression is inducible (Tet-ON inducible), allowing the assessment of the effect of genes KD in early stages of secretory traffic.

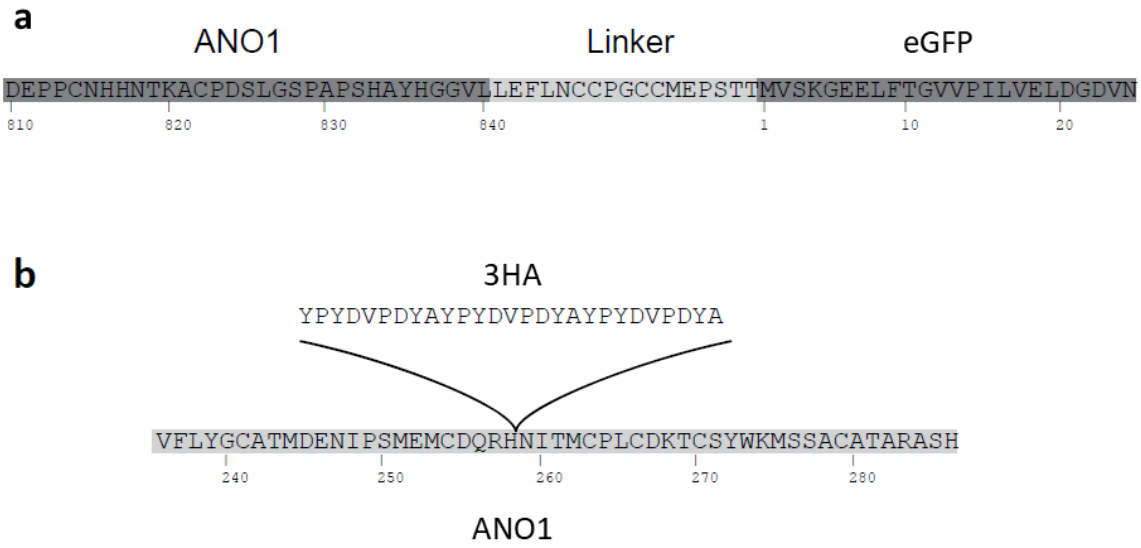

Fig. 4 Amino acid sequence of 3HA-ANO1-eGFP construct. (a) Amino acid sequence showing the linker (light grey shadow) connecting eGFP and ANO1 (dark grey shadows); **(b)** ANO1 amino acid sequences showing the insertion of 3HA peptide between His^{396} and Asn^{397}. The numbering corresponds to ANO1 isoform X5 (NCBI Reference Sequence: XP_011543427.1). [Images by Hugo Botelho, included with permission].

A total of three different cell lines were produced expressing the double-tagged ANO1: CFBE parental and CFBE-mCherry-flag-WT-/F508del-CFTR.

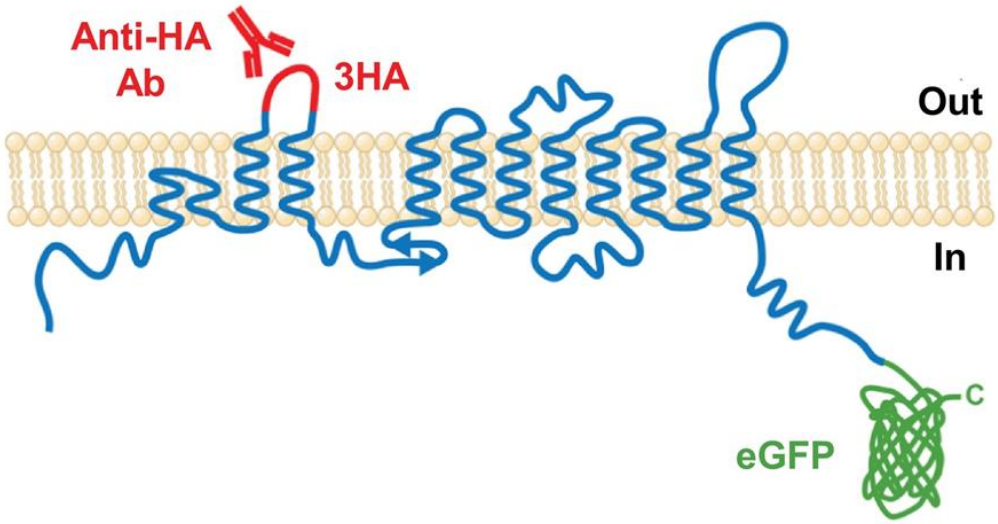

Fig. 5 The 3HA-ANO1-eGFP traffic reporter construct. Topology of ANO1 protein showing the ten transmembrane domains, with eGFP in C-terminal and 3HA tag in the first extracellular loop. [Images by Hugo Botelho, included with permission].

2. Characterization of 3HA-ANO1-eGFP stably expressing cells lines

2.1. Double-tagged ANO1 in HEK293T cells

Firstly, inducibility of pLVX-TRE3G-3HA-ANO1-eGFP was evaluated by transfecting this plasmid with its regulator plasmid (pLVX-Tet3G) in easy transfectable HEK293T cells. Then, these cells were induced with 1 µg/ml dox or incubated with DMSO (non-induced). After 48h, eGFP fluorescence was assessed using live-cell imaging, revealing a remarkable difference between induced and non-induced cells (Fig. 6). Moreover, ANO1 was mostly located at the PM, as previously reported by other authors (Schreiber *et al.*, 2010; Scudieri *et al.*, 2012a). The same system was used with HEK293T cells to assess pLVX-TRE3G-3HA-ANO1-eGFP functionality, by both iodide effluxes and whole cell patch-clamp techniques (Fig. 7). Considering the first technique, lower iodoide (I^-) concentrations would be expected after ATP stimulation, with more significant differences for induced cells, compared to non-induced.

Nevertheless, the results were variable, with some assays reporting the expected response, and others showing almost no differences (Fig. 7, c). The lack of homogeneity of results was probably due to differences in plasmid transfection rates

within the same assay and between assays. For whole-cell patch-clamp data, these results firmly proved pLVX-3HA-ANO1-eGFP plasmid inducibility and functionality, as there was a significant difference in ATP response between non-induced and induced cells and ATP-induced currents were large and outwardly rectifying (Fig. 7, a, b), as is typical for ANO1 (Kunzelmann, 2015).

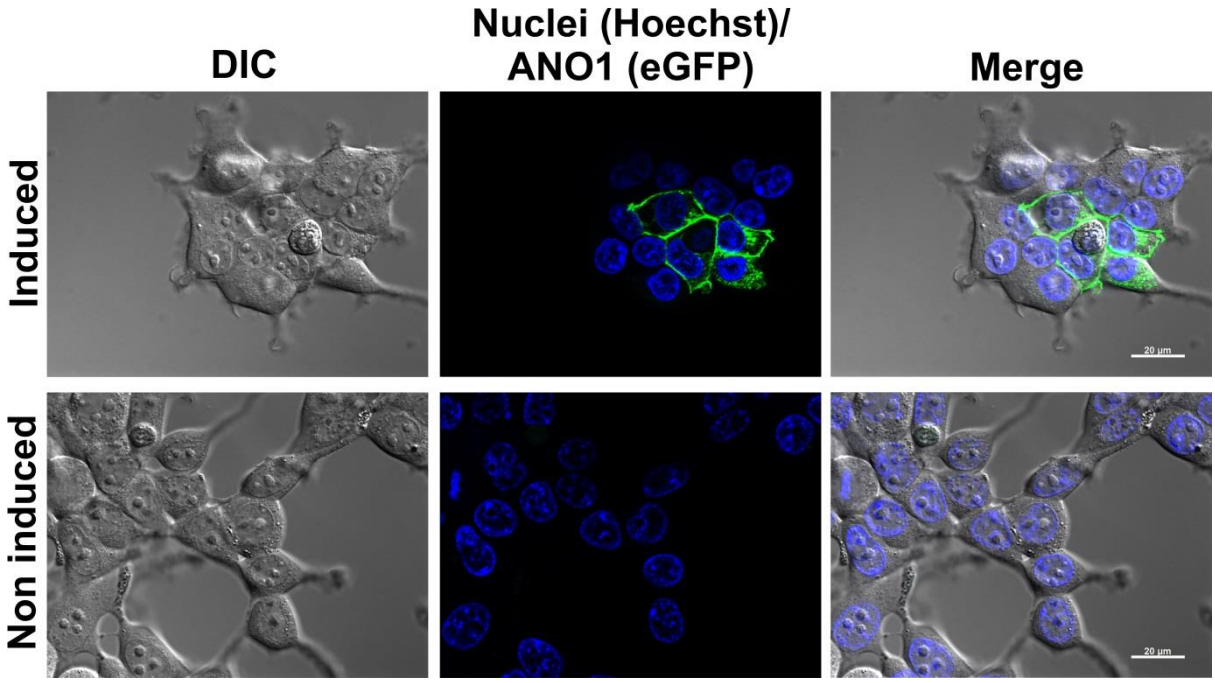

Fig. 6 3HA-ANO1-eGFP construct expression in HEK293T cells. Total amount of expressed 3HA-ANO1-eGFP, represented by eGFP fluorescence, in non-induced or induced cells. Images were acquired in Axiovert 200 microscope equipped with an ApoTome (objective 63x, oil); scale bar = 20 µM.

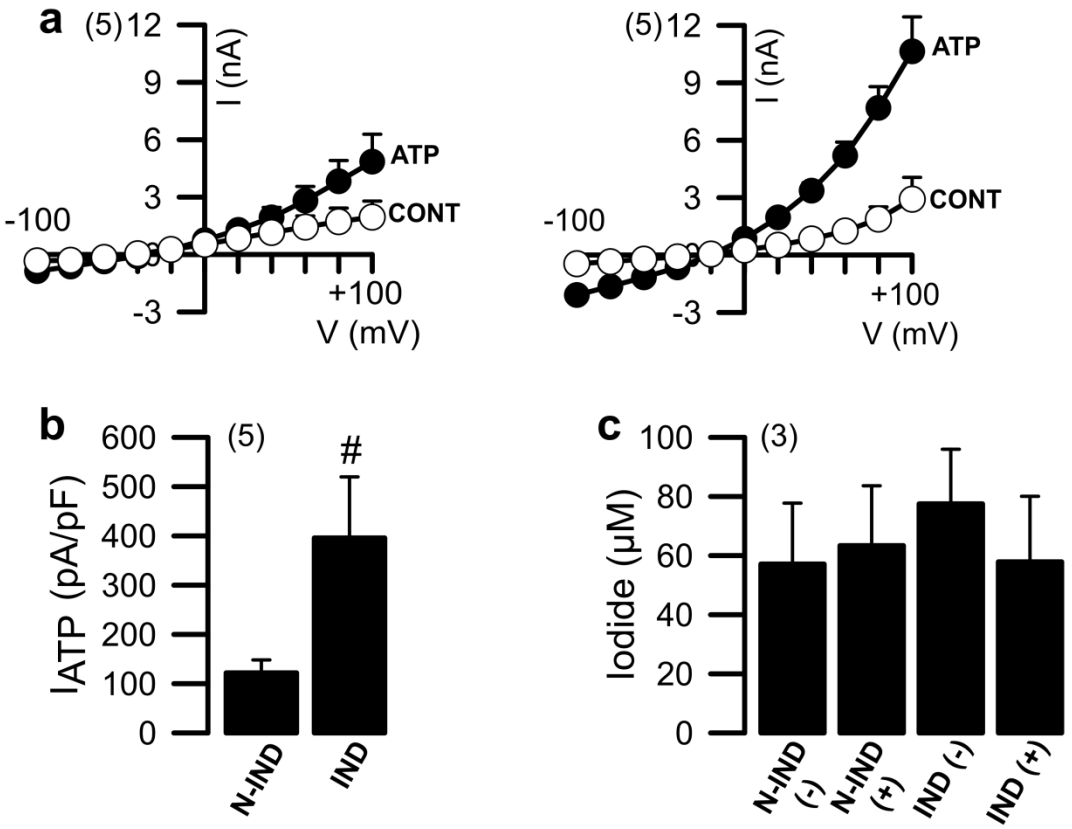

Fig. 7 3HA-ANO1-eGFP construct function in HEK293T cells. (a) Whole-cell patch-clamp data, shown as I/V curves -100mV to +100mV for non-induced (left) or induced (right) cells, as a control in ringer (CONT) or after stimulation by ATP (100 µM); **(b)** Delta of ATP current densities for non-induced (N-IND) or induced (IND); **(c)** Intracellular I^- concentration without (-) or with (+) ATP (100 µM) stimulation, in non-induced (N-IND) or induced (IND) cells. '#' indicates significant differences between non-induced vs induced ($p \leq 0.05$ in unpaired T-student test); number of experiments between brackets.

2.2. Double-tagged ANO1 in three novel cell lines: protein expression, tags fluorescence and channel functionality

After confirming the plasmid inducibility and functionality in HEK293T cells, three original cell lines were created and characterised for protein expression (Western-Blot), fluorescence (live-cell imaging/immunostaining) and functionality (Ussing Chamber and whole-cell patch-clamp). Regarding the Western-blot results, there was a higher ANO1 expression in induced cells, compared with non-induced, for the three cell lines, confirming the cells' inducibility (Fig. 8).

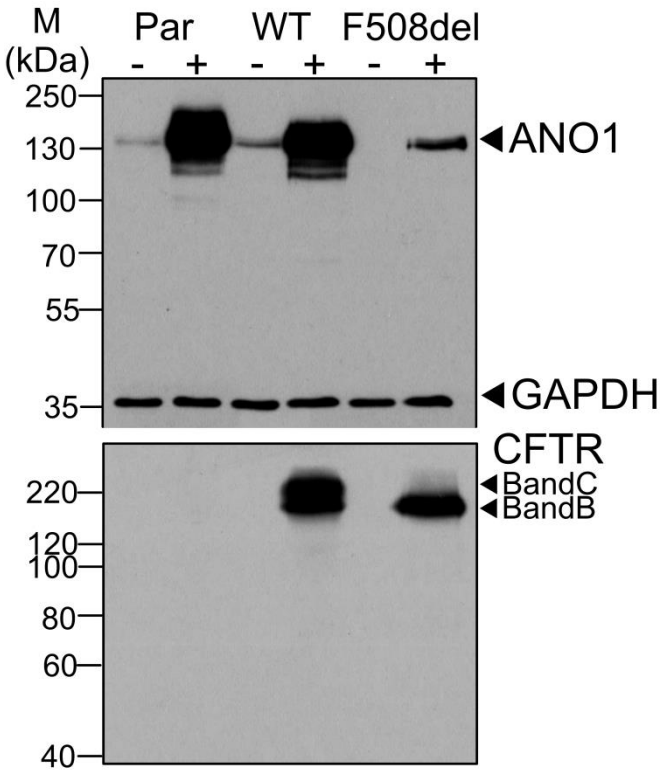

Fig. 8 Western-Blot for 3HA-ANO1-eGFP expressing CFBE cell lines. ANO1 and CFTR protein expression were tested in CFBE overexpressing only 3HA-ANO1-eGFP (parental) or also mCherry-flag-WT-CFTR (WT) or mCherry-flag-F508del-CFTR (F508del). All cell types show the inducibility feature, characterised by higher ANO1 protein expression (~130kDa) in non-induced (-) compared with induced (+) cells. Endogenous ANO1 (~110kDa) is not detected since it is expressed at much lower levels. Relative to CFTR protein expression, in WT-CFTR overexpressing cells, band B and C were detected and, for F508del-CFTR overexpressing cells, only band B was detected. GAPDH was used as a loading control and molecular mass markers are shown on the left. [Data obtained jointly with Podchanart Wanitchakool and included with permission].

Western-blots from the three cell lines indicated marked differences in CFTR expression, with bands b and c for CFBE expressing WT-CFTR, only band b for CFBE expressing F508del-CFTR and no CFTR detection in CFBE only overexpressing 3HA-ANO1-eGFP. Rather unexpectedly, there were also differences in ANO1 expression, with the lowest rate for cells expressing F508del-CFTR. These findings may be due to the sorting to which these cell lines were subjected, this resulting in different 3HA-ANO1-eGFP expression levels. Indeed, sorting by flow cytometry was used to increase double-tagged ANO1 expression by enhancing overall eGFP fluorescence in these populations. Additionally, Ruffin *et al.* (2013) described a reduced ANO1 expression in CFBE41o- (CF, F508del/F508del) compared to non-CF cells (non CF, 16HBE14o-), similar to our data. Martins *et al.* (2011)b also denoted a reduced ANO1 expression in CFBE expressing F508del-

CFTR compared to CFBE expressing WT-CFTR. Finally, these differences may also be due to a clonal drift in F508del-CFTR overexpressing cells.

Regarding fluorescence features of these cells, immunostainings were performed to confirm eGFP fluorescence (total ANO1) and also the ability to detect ANO1 PM fraction using an anti-HA antibody.

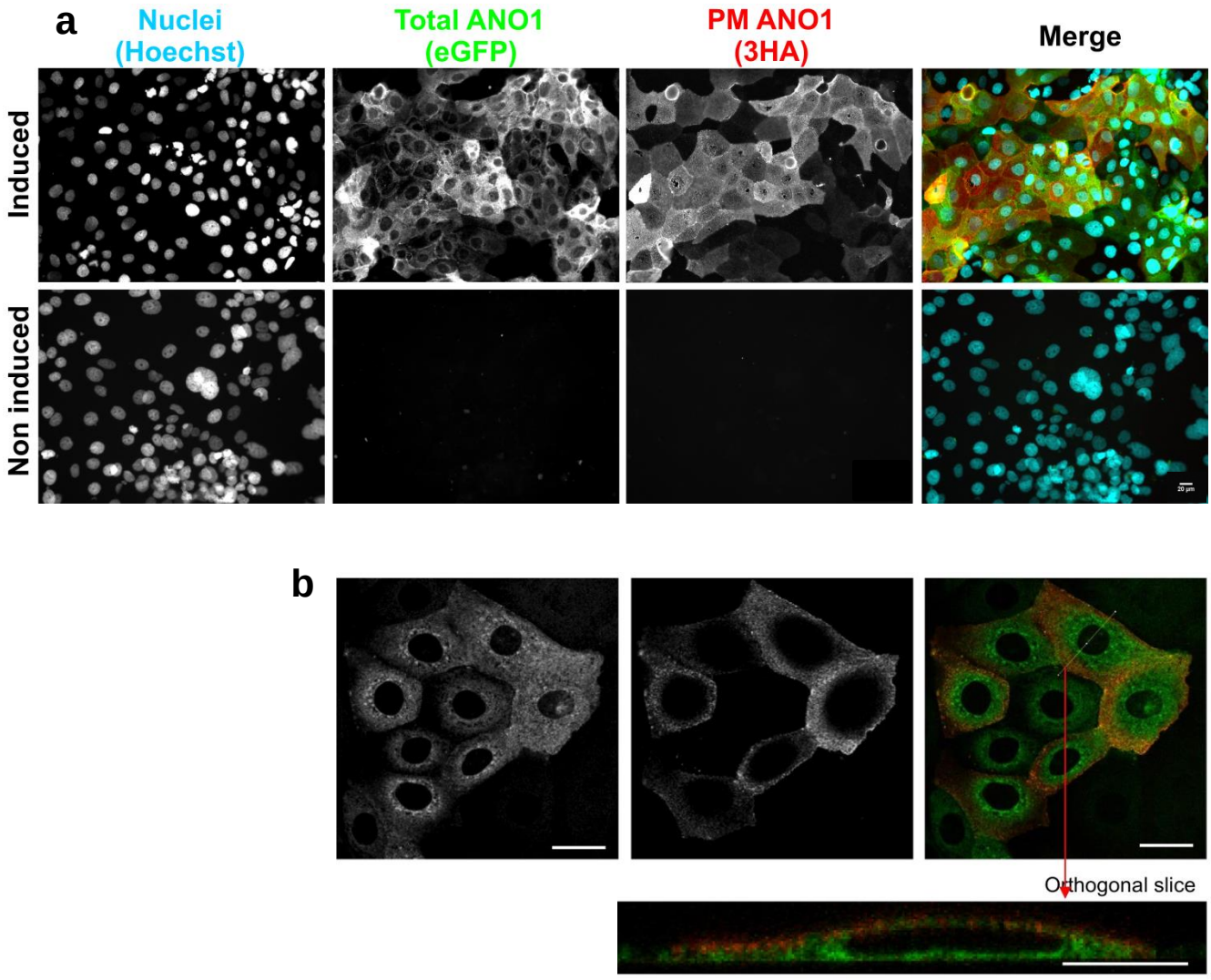

Fig. 9 CFBE-3HA-ANO1-eGFP fluorescence features. (a) CFBE-3HA-ANO1-eGFP cells were induced for 48h or non-induced. Total ANO1 measured by eGFP fluorescence and PM ANO1 measured by Alexa Fluor 647 of anti-HA antibody. Images were acquired with Leica DMI 6000B (objective 63x, water); scale bar = 20 µM; **(b)** Confocal images of induced cells showing total ANO1 (eGFP) or PM portion of ANO1 (3HA). Images were acquired in Olympus FV1200 confocal microscope (objective 60x, water); scale bar = 15 µM. [Confocal images acquired by Madalena Pinto and included with permission].

The data obtained from these cellular systems can only be used in CF biomedical research if the double-tagged ANO1 holds the main features that characterise endogenous ANO1, such as traffic to the PM and function as a Cl^- channel. Previous

reports described that ANO1 traffics to the PM (Schreiber *et al.*, 2010; Scudieri *et al.*, 2012b), which is also accomplished by part of 3HA-ANO1-eGFP protein, as observed in the immunostaining images (Fig. 9, Fig. 10).

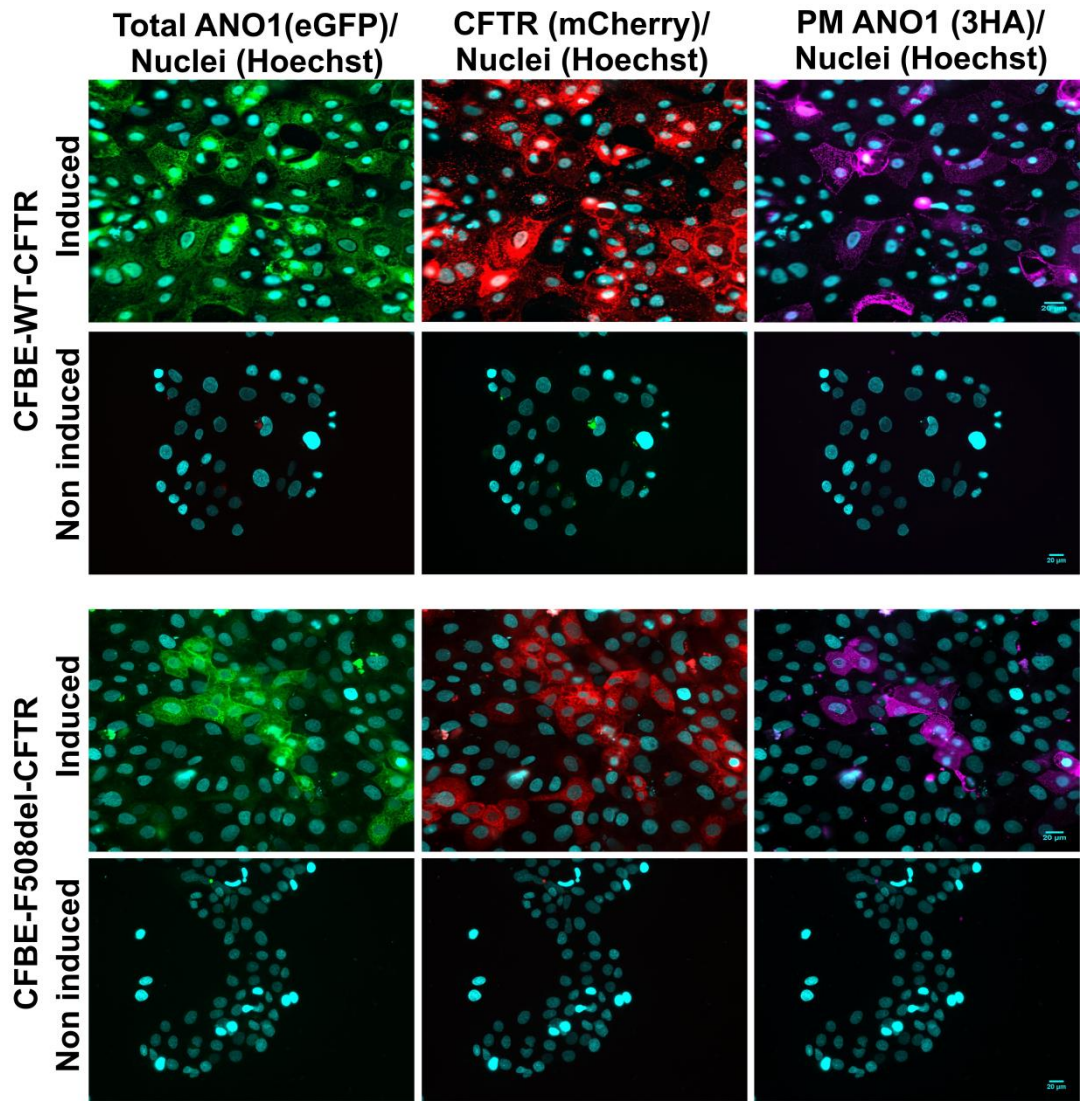

Fig. 10 CFBE overexpressing 3HA-ANO1-eGFP and CFTR fluorescence features. CFBE overexpressing 3HA-ANO1-eGFP and either mCherry-flag-WT-CFTR (WT-CFTR) or mCherry-flag-F508del-CFTR (F508del-CFTR) cells were induced for 48h or non-induced. Total ANO1 measured by eGFP fluorescence, CFTR by mCherry fluorescence and PM ANO1 by anti-HA antibody. Images were acquired with Leica DMI 6000B (objective 63x, water); scale bar = 20 µM.

Furthermore, the immunostainings results showed cells' inducibility with eGFP fluorescence almost absent in non-induced cells and a robust eGFP signalling after 48h of dox. Regarding the extracellular 3HA tag detection, it is also absent for non-induced cells, and well detected by the anti-HA antibody in induced cells.

Nevertheless, these populations exhibit heterogeneity regarding their fluorescence levels, *i.e.*, cells have different eGFP/3HA signals. This heterogeneity is particularly high for cells overexpressing WT-/F508del-CFTR. The heterogeneity observed in these new cell lines can be considered an advantage, since human cells' populations are also heterogeneous (Altschuler and Wu, 2010). Nonetheless, particularly for screening purposes, homogeneity is an essential factor for data reproducibility between assays and throughout time. Moreover, in this study, only cells expressing eGFP/3HA tags can be used for the microscopy trafficking screen.

The highest heterogeneity in eGFP/3HA signals occurs in CFBE overexpressing 3HA-ANO1-eGFP and F508del-CFTR. Indeed, the immunostaining images reveal that a large number of cells presented low or absent 3HA-ANO1-eGFP expression. This result in is line with a reduced ANO1 protein expression in this cell line, compared to the other two, observed in the Western-blot results (Fig. 8). Furthermore, as mentioned above, Ruffin *et al.* (2013) reported reduced ANO1 expression in CF cells vs non-CF. Possibly, the expression of F508del-CFTR in these cells is reducing 3HA-ANO1-eGFP levels, mimicking the effect of endogenous ANO1. Regarding the other two cell lines, CFBE-3HA-ANO1-eGFP showed the highest eGFP/3HA signal and the highest homogeneity level.

The three cell lines overexpressing 3HA-ANO1-eGFP were functionally characterised by whole-cell patch-clamp for ANO1 and CFTR currents. Surprisingly, CFBE overexpressing double-tagged ANO1 and F508del-CFTR showed no differences between induced and non-induced cells for ATP- and I/F-activated currents (Fig. 11, c, d). Indeed, one would expect higher ATP-activated currents in induced cells, due to the higher ANO1 expression. Regarding I/F-activated current, this was almost absent in both induced and non-induced cells as expected, since these cells express a defective CFTR protein. The absence of differences of ATP-activated currents in induced cells is due to the low overall expression of 3HA-ANO1-eGFP and the high heterogeneity level in this population, as previously described. Therefore, to use this cell line in screening proposes, it is crucial to enhance 3HA-ANO1-eGFP expression and reduce population heterogeneity. Nevertheless, this cell line can be used for other types of assays where homogeneity is not essential or where cells are selected for their 3HA-ANO1-eGFP expression.

Whole-cell patch-clamp data results from CFBE cells overexpressing 3HA-ANO1-eGFP and WT-CFTR showed differences between induced and non-induced cells for both ATP- and I/F-activated currents, as expected (Fig. 11, a, b).

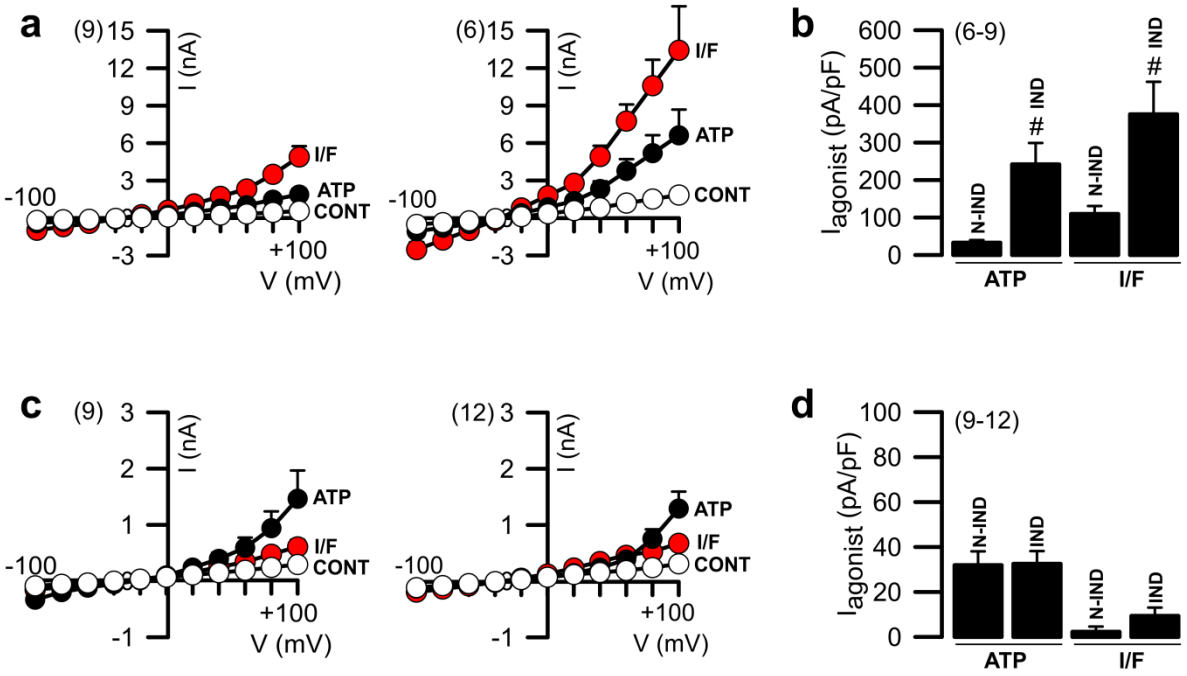

Fig. 11 Functional characterisation of CFBE cells overexpressing 3HA-ANO1-eGFP and CFTR. (a) I/V curves -100mV to +100mV for CFBE overexpressing 3HA-ANO1-eGFP and mCherry-flag-WT-CFTR non- induced (left) or induced (right) as a control in Ringer (CONT) or after stimulation by ATP (100 μM) or IBMX/Forskolin (I/F; 2 μM/100 μM); **(b)** Correspondent deltas of ATP and I/F current densities for non-induced (N-IND) or induced (IND) cells; **(c)** I/V curves -100mV to +100mV for CFBE overexpressing 3HA-ANO1-eGFP and mCherry-flag-F508del-CFTR non-induced (left) or induced (right) as a control in Ringer (CONT) or after stimulation by ATP (100 μM) or IBMX/Forskolin (I/F; 2 μM/100 μM); **(d)** Correspondent deltas of ATP and I/F current densities for non-induced (N-IND) or induced (IND) cells. '#' indicates significant differences between non-induced vs induced ($p \leq 0.05$ in unpaired T-student test); number of experiments between brackets.

Finally, since CFBE-3HA-ANO1-eGFP cells are the most homogeneous and prone to be used for the first traffic screen, whole-cell patch-clamp and Ussing Chamber techniques were used. The results displayed differences between induced and non-induced cells and a robust inhibition of ATP response by CaCC inhibitor AO1 (Fig. 12). It is important to emphasise that ATP-activated currents are produced by both endogenous and exogenous 3HA-ANO1-eGFP and inhibited by AO1.

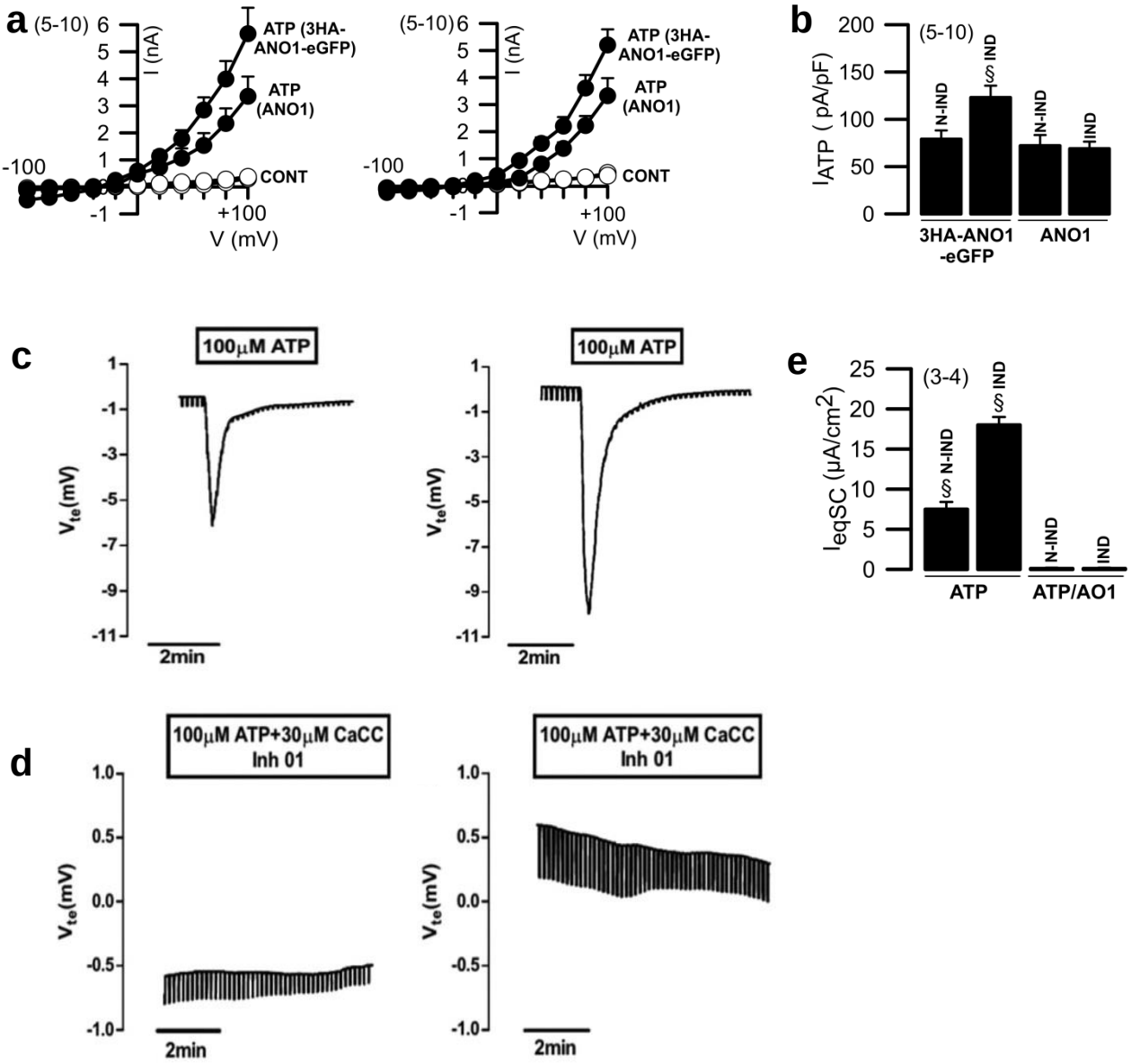

Fig. 12 Functional characterisation of CFBE cells overexpressing 3HA-ANO1-eGFP. (a) I/V curves -100mV to +100mV for CFBE-3HA-ANO1-eGFP (3HA-ANO1-eGFP) and CFBE parental cells (ANO1) non-induced (left) or induced (right) as a control in Ringer (CONT) or after stimulation by ATP (100 μM); **(b)** Correspondent deltas of ATP current densities; **(c)** Original Ussing chamber tracings obtained after ATP (100 μM) stimulation for CFBE-3HA-ANO1-eGFP non-induced (left) or after induced (right); **(d)** Original Ussing Chamber tracings obtained after ATP (100 μM) stimulation in the presence of AO1 (30 μM) for CFBE-3HA-ANO1-eGFP non-induced (left) or induced (right); **(e)** Correspondent I_{SC-eq} summaries. '§' indicates significant differences to all ($p \leq 0.05$ in unpaired T-student test); number of experiments between brackets. [Ussing chamber data obtained jointly with Nikhil Awatade, Iris Silva and Madalena Pinto and included with permission].

Therefore, CFBE parental cells (express only endogenous ANO1) were used to evaluate the current fraction composed solely of endogenous ANO1 and also to validate an indirect effect by dox (Fig. 12).

Comparing the ATP-induced currents in CFBE parental and CFBE-3HA-ANO1-eGFP, it was concluded that (1) dox molecule does not have any effect on endogenous ANO1 currents and (2) exogenous ANO1 is responsible only for approximately 50% of total ATP-activated currents. Judging by the Western-blot results, where no endogenous ANO1 and only a band of exogenous protein are detected, 20-fold or higher ATP-activated currents in induced cells would be expected. Nevertheless, the eGFP signal in 3HA-ANO1-eGFP is mostly cytoplasmic, revealing that a large percentage of this protein is not trafficking to PM. This may occur due to (1) overload of the traffic system; (2) absence of specific proteins to stabilize ANO1 at the PM; (3) negative feedback due to the high level of ANO1 expression and (4) interference of 3HA/eGFP tags in ANO1 traffic/stabilization at PM. Nonetheless, the 3HA-ANO1-eGFP that reaches PM is enough to increase ATP-activated currents and to detect 3HA tag. Additionally, a reduced size of induced cells compared to non-induced cells was observed (Suppl. Fig. 1). This is probably due to the positive ANO1 modulation in cell proliferation, as proliferating cells are smaller than differentiating cells (Su and O'Farrell, 1998).

Finally, CFBE-3HA-ANO1-eGFP is the most promising cell line for a first traffic screen approach due to its high eGFP/3HA homogeneity and distinct differences in protein expression and function within induced and non-induced cells. In addition, this cell line enables the evaluation of the impact of genes on ANO1 traffic without the influence of CFTR expression in the same cell.

2.3. Pilot screen and identification of hits

A siRNA traffic screen with CFBE-3HA-ANO1-eGFP was performed by Madalena Pinto at EMBL (Heidelberg, Germany). As these cells have an eGFP tag in ANO1 C-terminal and a 3HA tag in the 1st extracellular loop, it is possible to obtain the ratio between total ANO1 (eGFP) and the PM portion (3HA), similar to the description in Botelho *et al.* (2015). The screen comprised of previous hits of 490 genes (980 siRNAs) from 3 screens: (1) WT-CFTR traffic screen assay in A549-WT-CFTR cells; (2) F508del-CFTR traffic enhancers in CFBE-mCherry-flag-F508del-CFTR cells and (3) CFTR interactome (CIP) screen in HEK overexpressing WT- or F508del-CFTR (performed by Stagljar group in University of Toronto, Canada). The 3HA-ANO1-eGFP traffic screen resulted in 94 siRNA hits (41 siRNAs decreasing and 53

enhancing ANO1 traffic). To increase the credibility of the list of hits, a second screen with the same library was performed using FLIPR membrane potential assay in Cal-33 cells (work by Madalena Pinto). A total of 67 hits were identified, with 14 hits in common between both screens. Finally, from these 14 hits, nine were chosen for further functional validation by whole-cell patch-clamp (Table 3). The score values presented in Table 3 are related to ANO1 traffic efficiency compared to negative control (scores above +1 or below -1 correspond to traffic enhancers or inhibitors, respectively), as further explained in Material and Methods section.

Table 3 Hit siRNAs from the traffic screen.

Gene	Score (primary screen)	Name of gene	Library
ESYT1	-1.67	Extended synaptotagmin-like protein 1	WT-CFTR in A549
CK2A2	-1.06	Casein Kinase 2 subunit alpha	CIP in F508del-CFTR in HEK
CASP10	1.45	Caspase 10	Traffic enhancer of WT-CFTR in A549
IPPK	1.50	Inositol-pentakisphosphate 2-kinase	WT-CFTR in A549
ISG20	1.73	Interferon-stimulated gene 20 kDa protein	Traffic enhancer F508del-CFTR in CFBE
PGLYRP3	1.04	Peptidoglycan recognition protein 3	Traffic enhancer of WT-CFTR in A549
RGS19	1.02	Regulator of G-protein signalling 19	Traffic enhancer of WT-CFTR in A549
TANK	1.06	TRAF family member-associated NF-kappa-B activator	CIP in WT-/F508del-CFTR in HEK
COPβ1	3.81	Coatomer protein complex, subunit beta 1	Traffic enhancer of WT-CFTR in A549

2.4. Validation of ESYTs and COPβ1 as ANO1 traffic regulators

The ANO1 traffic screen identified siRNA COPβ1 as a significant 3HA-ANO1-eGFP traffic enhancer (Score = +3.81) (Fig. 13), without increasing total ANO1 protein expression, assessed by Western-Blotting (Suppl. Fig. 2). siRNA COPβ1 was also reported for WT-CFTR screen as a protein traffic enhancer (Botelho *et al.*, 2015). ESYT1, a member of the extended synaptotagmin protein family, was identified as a traffic inhibitor (Score = -1.67) (Fig. 13). Since the ESYT family has two other members, ESYT2 and ESYT3, their KD effect was also assessed for 3HA-ANO1-eGFP PM expression. siRNA ESYT2 reduced double-tagged ANO1 traffic to the PM compared to scrambled transfected cells. Contrariwise, siRNA ESYT3 did not affect 3HA-ANO1-eGFP membrane expression (Fig. 13), which is caused by reduced ESYT3 levels in CFBE cells (Suppl. Fig. 3). Therefore it is expected that its KD has a reduced effect on ANO1 traffic.

During this traffic screen, a siRNA against ANO1 was used with two proposes: (1) to assess siRNA transfection levels and (2) to verify that this traffic screen can detect different ANO1 levels. Indeed, siANO1 decreased fluorescence signal compared to scrambled transfected cells (Fig. 13).

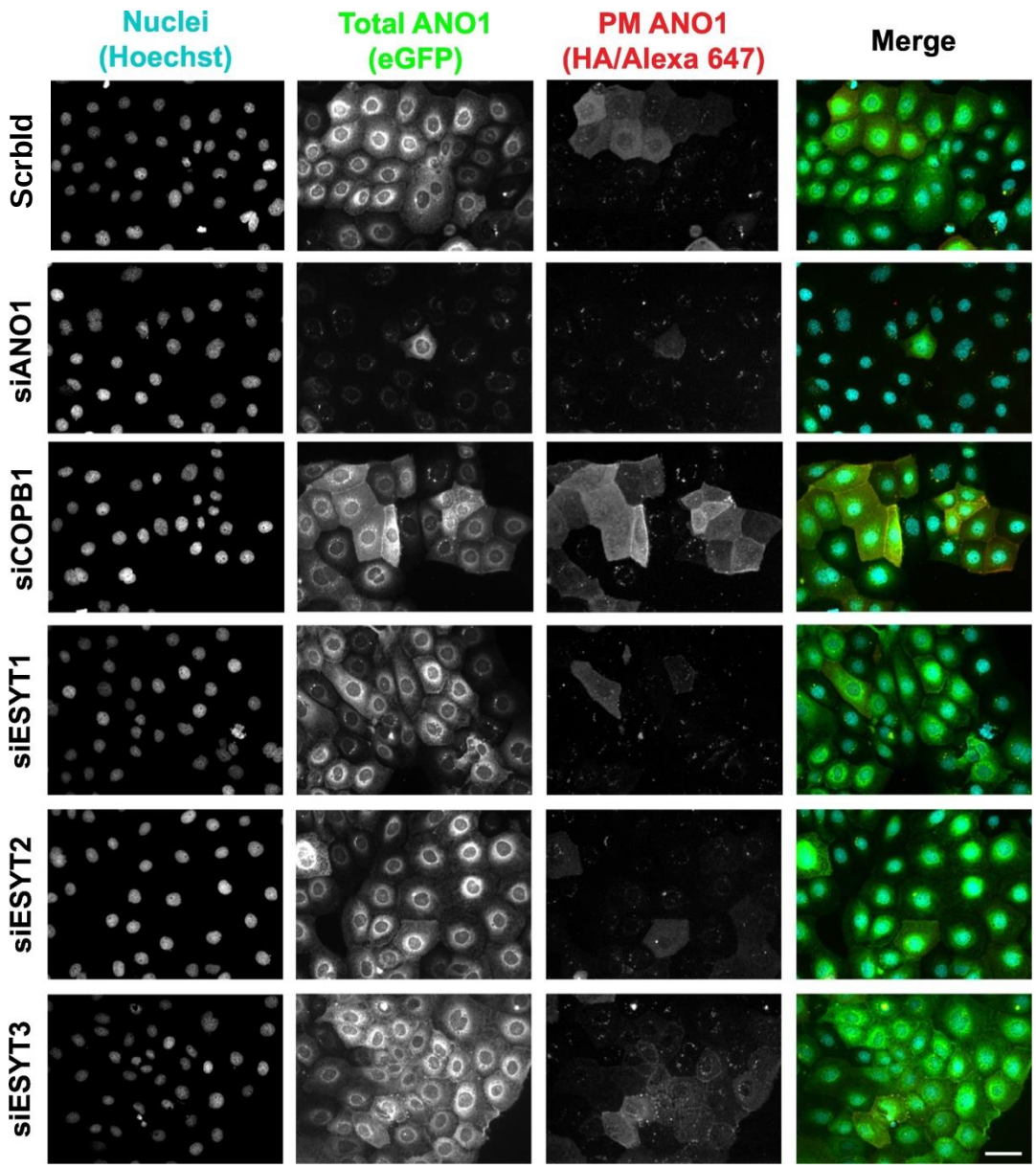

Fig. 13 Representative widefield epifluorescence microscopy images obtained for the ANO1 traffic screen. CFBE-3HA-ANO1-eGFP cells were treated with distinct siRNAs: scrambled (scrbld), or siRNA against COPβ1 (siCOPβ1), ANO1 (siANO1) or against the 3 ESYTs members (siESYT1, siESYT2 and siESYT3) and stained with anti-HA antibody. Images were acquired with Olympus Scan R microscope (objective 20x); scale bar = 50 µM. [Images acquired by Madalena Pinto and included with permission].

ESYT family members are ER-PM tethering proteins, *i.e.*, these proteins reduce the distance between both membranes, a feature also proposed for ANO1 (Kunzelmann and Schreiber, 2014b; Yu *et al.*, 2016; Herdman and Moss, 2016). Additionally, ESYT1 was reported as an ANO1 interactor in a proteomic study (Perez-Cornejo *et al.*, 2012).

The whole-cell patch-clamp data with siRNAs against ESYT1-3 and COPβ1 was in line with the correspondent traffic results. Indeed, ATP-induced currents were higher in cells transfected with siCOPβ1 and lowered for all siRNA against ESYTs members compared to scrambled (Fig. 14).

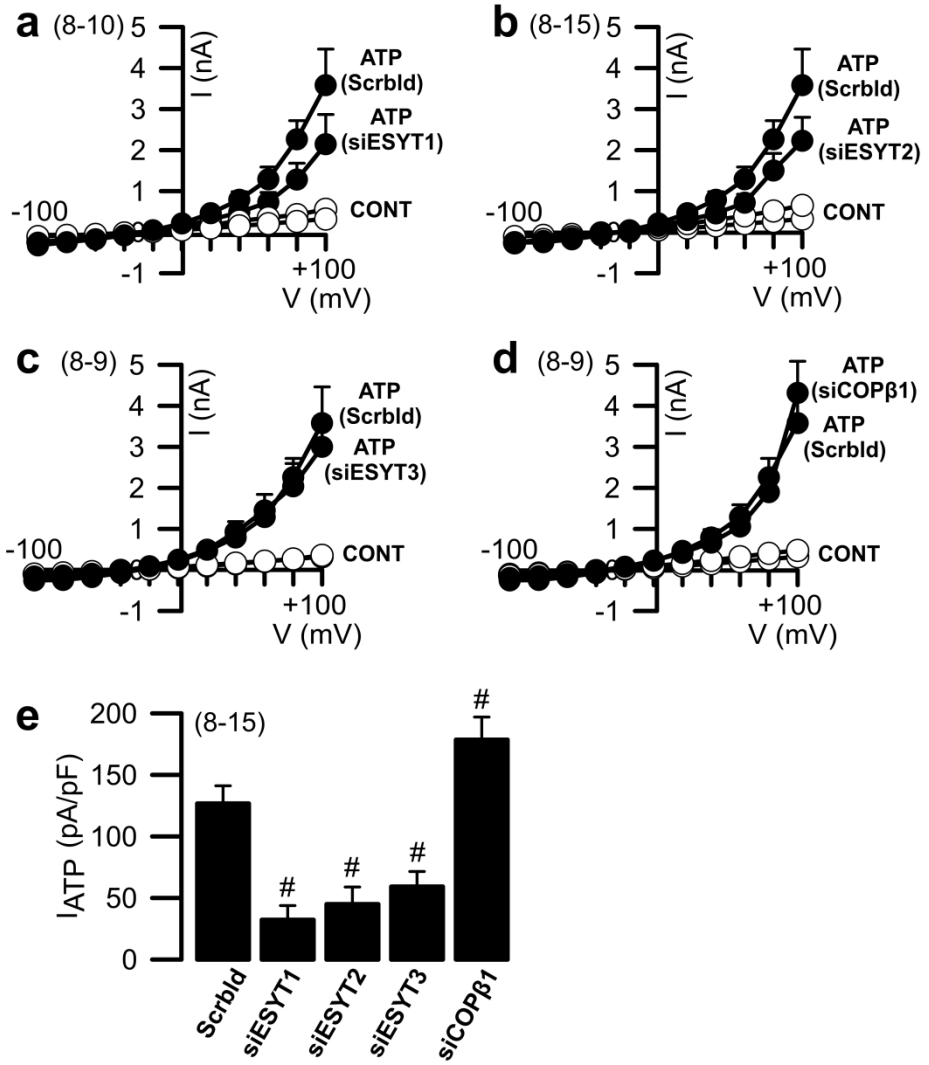

Fig. 14 Impact of screen hits COPβ1 and ESYT1-3 on 3HA-ANO1-eGFP function. **(a-d)** Whole-cell patch-clamp data, shown as I/V curves -100mV to +100mV, obtained for CFBE-3HA-ANO1-eGFP cells transfected with siRNAs targeting screen hits ESYT1 (siESYT1), ESYT2 (siESYT2), ESYT3 (siESYT3) or COPβ1 (siCOPβ1), as well as scrambled (Scrbld) as a control in Ringer (CONT) or after stimulation by ATP (100 µM); **(e)** Delta of the average of ATP-induced current densities. '#' indicates significant differences between Scrambled vs siRNA transfected cells ($p \leq 0.05$ in unpaired T-student test); number of experiments between brackets.

To confirm that this effect was definitely caused by KD of ESYTs or COPβ1 genes, mRNA level of these genes after transfection with siRNAs was also tested. The data showed a substantial decrease of mRNA levels (70 to 100% of gene KD) (Suppl. Fig. 3), enabling the confirmation of these siRNAs KD efficiencies.

Nevertheless, it was essential to determine whether these hits would have the same effect in endogenous ANO1, *i.e.*, if the regulatory mechanisms for double-tagged and endogenous ANO1 are the same. In line with that, a positive (siCOPβ1) and a negative hit (siESYT1) with the most extensive ANO1 expression/function differences to scrambled were used in CFBE parental cells. The data acquired showed that KD of ESYT1 reduced and KD of COPβ1 increased ATP-induced currents. These data assume that 3HA-ANO1-eGFP traffic regulatory mechanisms are similar to the endogenous ANO1, as determined by KD of COPβ1 and ESYT1 results, thus being physiologically relevant (Fig. 15).

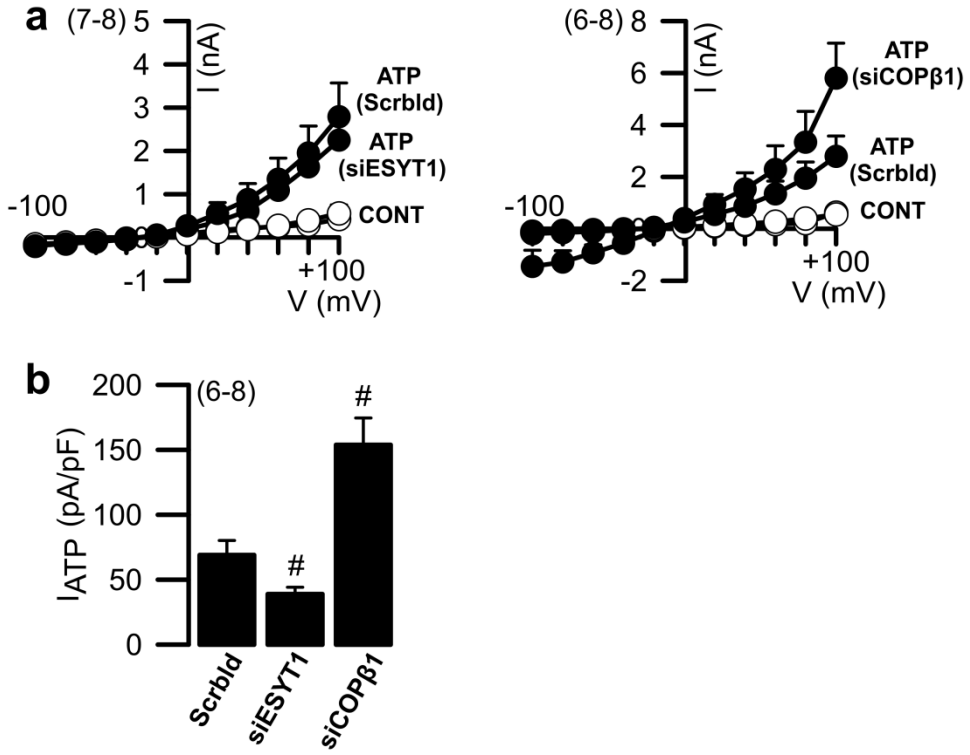

Fig. 15 Impact of screen hits siCOPβ1 and siESYT1 on endogenous ANO1 function. (a) Whole-cell patch-clamp data, shown as I/V curves -100mV to +100mV, obtained for CFBE parental cells transfected with siRNAs targeting screen hits ESYT1 (siESYT1) or COPβ1 (siCOPβ1) as well as scrambled (Scrbld) as a control in Ringer (CONT) or after stimulation by ATP (100 µM); **(b)** Delta of the average of ATP-induced current densities. '#' indicates significant differences between Scrambled vs siRNA transfected cells ($p \leq 0.05$ in unpaired T-student test); number of experiments between brackets.

Due to the intricate relationship between ANO1 and CFTR proteins, the effect of siRNA ESYT1 in WT-CFTR currents by whole-cell patch-clamp was also evaluated. CFBE expressing WT-CFTR had reduced ATP-activated currents, but unexpectedly, also reduced I/F-induced currents. Indeed, I/F-induced currents reduced

approximately to one third compared with the same currents in control cells (transfected with Scrambled siRNA) (Fig. 16).

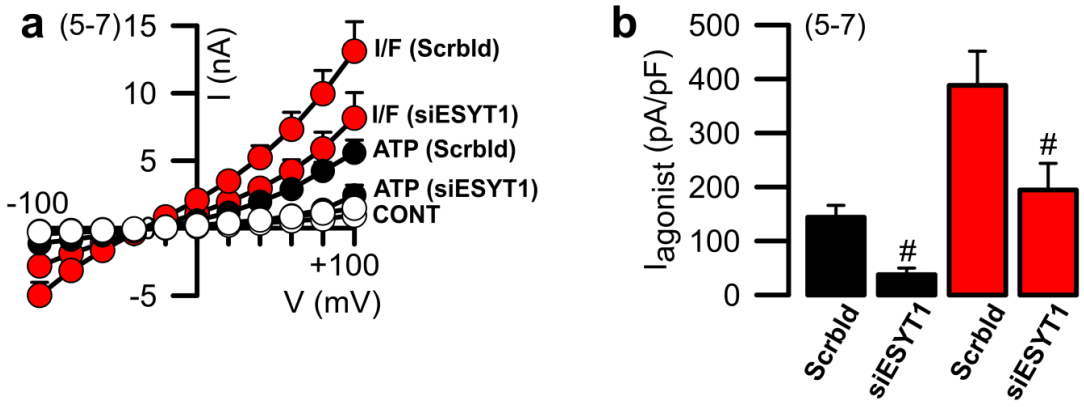

Fig. 16 Impact of screen hit siESYT1 on endogenous ANO1 and WT-CFTR function. (a) Whole-cell patch-clamp data, shown as I/V curves -100mV to +100mV, obtained for WT-CFTR/CFBE transfected with siRNA targeting screen hit ESYT1 (siESYT1) as well as scrambled (Scrbld) as a control in ringer (CONT) or after stimulation with ATP (100 µM) or IBMX/Forskolin (I/F; 2 µM/100 µM); **(b)** Delta of the average of ATP- or I/F-induced currents densities, in black or red, respectively. '#' indicates significant differences between Scrambled vs siRNA transfected cells ($p \leq 0.05$ in unpaired T-student test); number of experiments between brackets.

COPβ1 is a component of COPI trafficking machinery, involved for both anterograde and retrograde transport between Golgi and ER (Gaynor and Emr, 1997; Wang *et al.*, 2010). In 3HA-ANO1-eGFP traffic screen, KD of COPβ1 increased ANO1 traffic to the PM, a result that was replicated with endogenous ANO1. Recently, Lee *et al.* (2016) reported that COPβ1 overexpression or KD resulted in lower or higher ANO1 PM expression/Cl^- currents, respectively. In addition, a direct interaction between COPβ1 and ANO1 proteins was described. Therefore, ANO1 PM expression increment caused by KD of COPβ1 is caused by blockage of protein-protein interaction, blocking ANO1 retrograde transportation.

ESYT family members have a role in tethering the ER to the PM in a PIP_2- and Ca^{2+}- dependent way (Giordano *et al.*, 2013). The ER forms an intricate network throughout the cell with a diversity of functions, including protein synthesis, lipid metabolism and Ca^{2+} storage for intracellular signalling. The ER membrane contact points with other membranes are hypothesised to be involved in exchanges of molecules such as lipids and, interestingly, in control of Ca^{2+} homeostasis (Giordano *et al.*, 2013). As previously proposed, ANO1 family members have a role in generating compartmentalised Ca^{2+} signals through their interaction with IP_3R, which tethers PM and ER membrane (Jin *et al.*, 2013; Kunzelmann *et al.*, 2016). Moreover,

yeast analogue of ANO1 (Ist2) is also present at these ER-PM junctions and acts as a tethering protein (Manford *et al.*, 2012). The three ESYTs proteins participate in the tethering function via C_2 domain-dependent interactions with the PM, which require PIP_2 for ESYT2 and ESYT3 and also the elevation of cytosolic Ca^{2+} for ESYT1 (Giordano *et al.*, 2013).

Although ESYTs are not necessary for the targeting of IP_3R in primary rat hepatocytes associated to ER Ca^{2+} release (Amaya *et al.*, 2014), these data show a link between ESYTs and ANO1 expression and receptor-mediated activation. Recently, two reports described that simultaneous loss of all three ESYTs did not affect development and survival of mice. Nevertheless, KD of ESYTs leads to the upregulation of other tethering proteins (ORP5/8, ORAI1, STIM1 and ANO110), compensating for ESYTs loss (Tremblay and Moss, 2016; Sclip *et al.*, 2016). Interestingly, two of the described upregulated proteins, ORAI1 and STIM1, are related to Ca^{2+} homeostasis (Stathopulos *et al.*, 2013; Benedetto *et al.*, 2017).

The positive regulation of ESYTs in ANO1 GPCR-mediated activation is due to the presence of higher number of ER-PM connections, provided by tethering proteins as ESYTs. The reduced distance between ER and PM increases local Ca^{2+} concentration next to ANO1, therefore, facilitating ANO1 activation (Fig. 17). Additionally, our findings also indicate that ESYTs promote ANO1 traffic to the PM, which probably occurs by enabling an alternative ANO1 traffic route bypassing the Golgi complex. This hypothesis is supported by the fact that currents from ANO1 are measurable after treatment of cells with brefeldin A (BFA), a compound that blocks protein transport from ER to the Golgi (data in chapter 2). Finally, tethering ER to the PM may increase the number of connections between ANO1 and IP_3R (present at ER membrane), ultimately stabilising ANO1.

ESYT1 KD was revealed to be a negative modulator of WT-CFTR current, decreasing it by approximately one third compared to scrambled transfected cells. This surprising result is also caused by a reduction of local Ca^{2+} availability in the cell. Indeed, several ADCYs involved in the control of cellular cAMP levels are activated by Ca^{2+} (ADCY1, 3, 8 and 10) (UniProt database; available at http://www.uniprot.org/; access on January 2018). Therefore, decreasing Ca^{2+}-sensitive ADCYs activation will reduce cellular cAMP concentration, ultimately decreasing I/F CFTR activation.

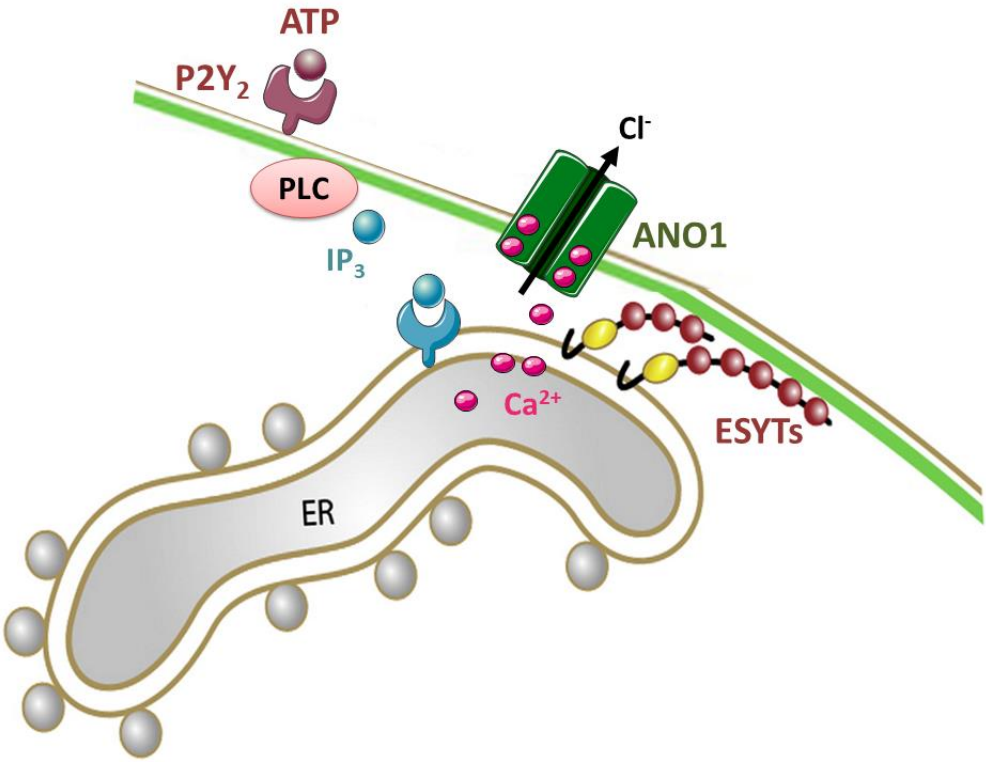

Fig. 17 Putative relationship between ESYTs and ANO1. ESYTs tether ER membrane to PM, allowing a larger IP_3R activation, increasing local Ca^{2+} release and, therefore, activating ANO1. [Adapted from Giordano *et al.* (2013)].

2.5. Validation of additional top hits

Additional interesting hits were chosen to be further validated by whole-cell patch-clamp. In this case, two siRNAs per gene were used in CFBE cells expressing F508del-CFTR. It is essential to bear in mind that all these hits are related to F508del-CFTR and/or WT-CFTR proteins' traffic, so it is interesting to assess the behaviour of both endogenous ANO1 and F508del-CFTR function. Two siRNA hits showed significant differences in their ATP-induced currents compared to control (scrambled transfected cells): CK2A2 as negative and PGLYRP3 as positive hits

(Fig. 18, Fig. 19). The other hits had no differences compared to control for ANO1 activation (Fig. 19, c). For I/F-induced currents, there were no significant differences to control, though there was a trend for higher currents with KD of IGS20 (F508del-CFTR traffic enhancer in a previous screen by Amaral's group) (Fig. 19, a, b, d). Concerning F508del-CFTR, its open probability is remarkably reduced compared to WT-CFTR (one-third of open probability), and its stabilisation at the PM is also decreased (Denning *et al.*, 1992; Lukacs *et al.*, 1994). Consequently, the increment in CFTR function may not be proportional to the increment in PM fraction, as is visible for ISG20 gene data. Indeed, KD of this gene resulted in a slight increment of F508del-CFTR function, regardless of a previous screen which shows a significant increase in F508del-CFTR.

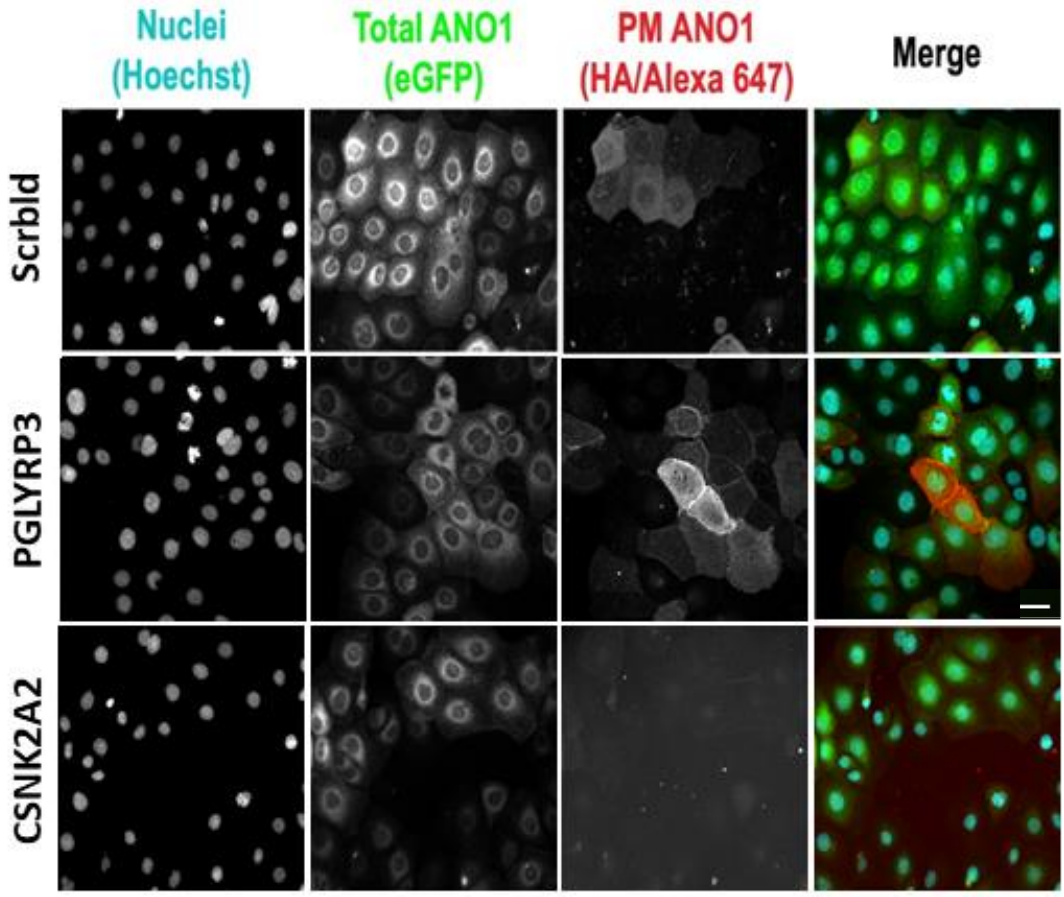

Fig. 18 Impact of screen hits siRNAs PGLYRP3 and CSNK2A2 on 3HA-ANO1-eGFP expression. CFBE-3HA-ANO1-eGFP cells were treated with distinct siRNAs and stained with anti-HA antibody. Images were acquired with Olympus Scan R microscope (objective 20x); scale bar = 50µM. [Images acquired by Madalena Pinto and included with permission].

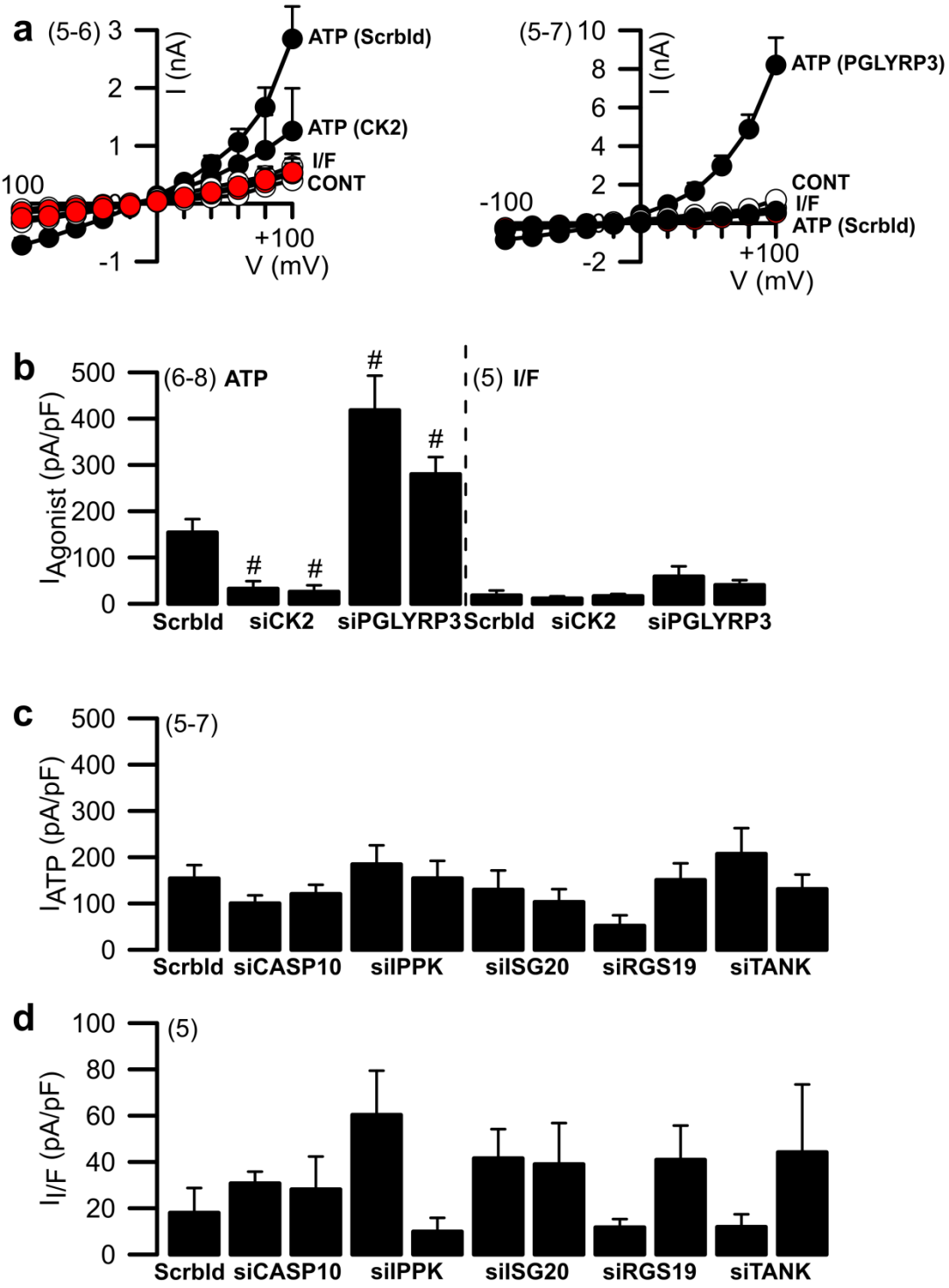

Fig. 19 Impact of screen hits on endogenous ANO1 and F508del-CFTR function. **(a)** Whole-cell patch-clamp data, shown as I/V curves -100mV to +100mV, obtained in CFBE-mCherry-flag-F508del-CFTR, transfected with siRNAs screen hits CSNK2 (siCSNK2) (left) or PGLYRP3 (siPGLYRP3) (right) as a control in Ringer (CONT) or after stimulation by ATP (100 µM) or IBMX/forskolin (I/F, 100 µM/2 µM); **(b)** Correspondent delta of the average of ATP- or I/F-induced current densities; **(c,d)** Delta of the average of ATP (100 µM) (c) or IBMX/Forskolin (I/F, 100 µM/2 µM) (d) current densities after treatment with distinct siRNAs. '#' indicates significant differences between Scrambled (Scrbld) vs siRNA transfected cells ($p \leq 0.05$ in unpaired T-student test); number of experiments between brackets.

CK2 is considered to have a wide array of physiological targets (>300 substrates) and to participate in different cellular functions (Litchfield, 2003; Meggio and Pinna, 2003). This gene has already been extensively linked to CFTR, with differences between WT- and F508del-CFTR. Indeed, Treharne *et al.* (2009) stated that only WT-CFTR is sensitive to CK2 inhibition and co-precipitates with CK2; contrarily, F508del-CFTR Cl^- currents are CK2 insensitive, and both do not co-precipitate. These data suggest that CK2 is a novel regulator of CFTR function and CK2-dependent regulation of F508del-CFTR is dysfunctional. Hence, disruption of CK2-CFTR interaction by F508del mutation might disrupt several CK2-dependent pathways. Other studies reported that F508del region of CFTR regulates CK2 activity (Pagano *et al.*, 2008; Venerando *et al.*, 2011). This kinase has also been linked to several other channels such as ENaC (Bachhuber *et al.*, 2008) or SLC4A2 (Ibrahim *et al.*, 2017), with reduction of their activity caused by CK2 inhibition. Additionally, ANO1 has binding sites that are recognised by CK2 (Adomaviciene *et al.*, 2013).

To further understand the effect of CK2 in ANO1 function, a CK2 inhibitor (TBB) was used in CFBE parental cells, endogenously expressing ANO1. The data herein obtained showed a significant reduction for ATP-induced currents in the presence of DMSO vs TBB in CFBE parental cells (Fig. 20). Contrarily, Tian *et al.* (2011) reported no inhibition of ANO1 currents using CK2 inhibitor TBB. Nevertheless, that study used HEK cells, which have different traffic regulation, and ANO1 was stimulated with ionomycin, in contrast to our assay with ATP. Additionally, Tian *et al.* (2011) used cells overexpressing ANO1, which is probably the leading cause of such differences. Indeed, ANO1 overexpression, in addition to increasing Cl^- currents after stimulation and also partially activating currents without stimulus (Schreiber *et al.*, 2010; Tian *et al.*, 2011), may alter ANO1 sensitivity to inhibitors and stimulators. ANO1 overexpression may, for instance, modify its placement in the lipid membrane and alter the accessible protein domains.

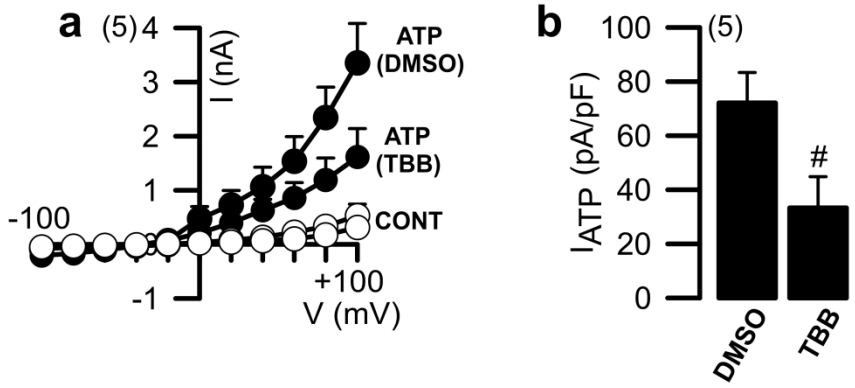

Fig. 20 Effect of CK2 inhibitor TBB in endogenous ANO1 function. (a) Whole-cell patch-clamp data, shown as I/V curves -100mV to +100mV, obtained for CFBE parental cells treated with DMSO or TBB (10 μM), a CSNK2 inhibitor; **(b)** Delta of the average of ATP-induced current densities. '#' indicates significant differences between TBB treated cells vs DMSO ($p \leq 0.05$ in unpaired T-student test); number of experiments between brackets.

Inhibition of ANO1 currents with KD of CK2 may be due to several reasons, namely (1) CK2 is vital for ANO1 traffic to PM; (2) CK2 has a role in ANO1 stabilisation and turnover and (3) CK2, though other proteins, interferes in ANO1 traffic/function. The first two hypotheses are supported by several reports the impaired traffic of proteins by CK2 inhibition or KD (Alconada *et al.*, 1996; Sarker *et al.*, 2008; Chan *et al.*, 2016), which includes WT-CFTR (Luz *et al.*, 2011). Indeed, Luz *et al.* (2011) reported that WT-CFTR traffic reduced with CK2 inhibition, caused by an increase of immature CFTR turnover and reduction of CFTR maturation efficiency. Possibly, CK2 KD affects ANO1 turnover and/or its passage through Golgi complex. Additionally, several studies have described complex interactions between CK2 and cytoskeleton proteins such as ankyrin (Wei and Tao, 1993), spectrin (Canton and Litchfield, 2006), adducin (Wei and Tao, 1993), dystrophin (Luise *et al.*, 1993), calmodulin (Canton and Litchfield, 2006), troponin (Risnik and Gusev, 1984), myosin (Singh *et al.*, 1983) and caldesmon (Vorotnikov *et al.*, 1993). Indeed, CK2 is suggested to be involved in the maintenance of intercellular junctions (Serres *et al.*, 2000) and its activation is related to increased actin filament assembly (Mullins *et al.*, 1998; Cory *et al.*, 2003). Finally, ANO1 interactome described by Perez-Cornejo *et al.* (2012) included the complex ezrin/radixin/moesin (ERM), which was previously related to CFTR stabilisation at the PM (Lobo *et al.*, 2016) and is essential for crosslink between actin and PM. Therefore, ERM may be affected by CK2 KD and, indirectly, affect ANO1 stabilisation at the PM.

Regarding the second suggestion, CK2 may indirectly interfere with the ANO1 function by phosphorylating other proteins. This would be in line with our data

showing ANO1 reduced currents in the presence of CK2 inhibitor TBB (Fig. 20). Both hypotheses are valid and are not mutually exclusive. Nevertheless, more data is needed to fully understand this complex interaction, such as assays of pulse-chase to assess a possible effect of CK2 KD on ANO1 turnover and immunostainings of cytoskeleton proteins with CK2 KD.

The other validated hit, PGLYRP3, belongs to secreted peptidoglycan recognition proteins family (PGRPs) with four members in mammals, critical for innate immunity patent recognition molecules (Kang *et al.*, 1998; Liu *et al.*, 2001). Interestingly, PGLYRP1-3 were identified as bactericidal and expressed in tissues that come in contact with the external environment, such as skin, eyes, salivary glands, throat, tongue, oesophagus, stomach and intestine (Lu *et al.*, 2006). The bactericidal action occurs through PGLYRPs interaction with gram-positive bacterial cell wall peptidoglycan, although a bacteriostatic action was also reported for some gram-negative bacteria (Lu *et al.*, 2006). Additionally, PGLYRP3 also has an anti-inflammatory effect on intestinal epithelial cells, by reducing bacterial peptidoglycan induced inflammatory cytokines production (IL-12p35, IL8 and TNF-α) and by having a negative regulation of the NF-κB pathway (Zenhom *et al.*, 2011, 2012).

Considering the link between ANO1 and inflammation/infection (Caputo *et al.*, 2008; Huang *et al.*, 2012; Scudieri *et al.*, 2012a), it is not surprising that such a protein would influence ANO1 expression and function. Our data shows that PGLYRP3 controls ANO1 by affecting its PM expression and function. Indeed, unrestrained upregulation of ANO1 has several problems, such as excessive mucus cell metaplasia and airway hyperreactivity, typical of asthma patients (Huang *et al.*, 2012; Scudieri *et al.*, 2012a). Since PGLYRPs are involved in immunity and ANO1 linked to inflammation, there may be a PGLYRP3 direct negative feedback when this protein is expressed, inhibiting ANO1 PM traffic, and therefore controlling the inflammation level. Moreover, PGLYRP3 anti-inflammatory effect, though only described for intestinal cells, may also indirectly reduce ANO1 expression by reducing cytokines production level in airway epithelial cells. Finally, Lin *et al.* (2015) reported that ANO1 channel acts upstream of NF-κB, so PGLYRP3 may also modulate ANO1 expression/activity through the same mechanism that it uses to modulate NF-kB pathway.

3. Conclusions

All data considered, this exogenous ANO1 expressing cell line system can be used to extrapolate its results to a more physiological system using endogenous ANO1, confirmed at least for four genes (COPβ1, ESYT1, PGLYRP3 and CK2). Indeed, the primary goal of this project was always to obtain data that could be used for development of drugs for CF patients. With this double-tagged ANO1 cell line system there are multiple possibilities of use, namely (1) identification of regulators of ANO1 (as potential drug targets); (2) development of compounds that modulate ANO1 traffic; (3) direct discovery of compounds that affect ANO1 traffic; (4) understanding the mechanisms of ANO1 secretory traffic. Although only CFBE-3HA-ANO1-eGFP cell line was used, two other cell lines also expressing either WT- or F508del-CFTR were produced, that will provide mechanistic insight into whether and how traffic of ANO1 and CFTR are co-regulated.

ANO1, in addition to its relevance in CF, also has a significant importance in other pathologic syndromes such as asthma, mucin secretion in airways (Scudieri *et al.*, 2012a; Huang *et al.*, 2012) or tumorigenesis (Wanitchakool *et al.*, 2014). In this last case, it would be noteworthy to discover new ANO1 negative regulators, which can also benefit from our described cell lines. Indeed, two negative ANO1 regulators were reported using this system (their KD increased ANO1 PM expression), PGLYRP3 and COPβ1, which were further functionally validated by whole-cell patch-clamp. The duality of this platform allows it to have broader purposes and, also, the 3HA-ANO1-eGFP construct can be used in other cellular models which could be more relevant to other pathologies besides CF. Finally, the cellular model and traffic assay reported here can help to improve ANO1-based drug development, with particular emphasis for CF.

CHAPTER 2

GPCRs importance in CFTR and ANO1 crosstalk

Data comprised in this chapter is included in:

Lérias J*, Pinto M*, Benedetto R, Schreiber R, Amaral MD, Aureli M, Kunzelmann K (2018). Compartmentalized crosstalk of CFTR and TMEM16A (ANO1) through EPAC and ADCY1. *Cell Signal* **44**:10-19 [*Shared first authorship].

1. Compartmentalized crosstalk of CFTR and ANO1 through EPAC1 and ADCY1

1.1. Relationship between GPCRs and ANO1

The data from double-tagged ANO1 traffic screen displayed an intriguing fact that a large number GPCRs were identified as positive ANO1 regulators, *i.e.*, KD of those receptors' genes would decrease ANO1 PM expression. Interestingly, Yang *et al.* (2008) related ANO1 activation with different GPCRs expression. The authors reported that currents of HEK cells expressing either GPCR or ANO1 had smaller currents compared to cells expressing both. Thus, we further studied this intricate relationship between GPCRs, ANO1 and also with WT-/F508del-CFTR.

For these assays, CFBE cells endogenously expressing ANO1 and also expressing WT-/F508del-CFTR were used to assess differences for ANO1 interaction with WT- or F508del-CFTR. Firstly, ANO1 whole-cell currents were measured after stimulation of purinergic receptors with ATP, which were higher for WT-CFTR expressing cells, as predictable (Ruffin *et al.*, 2013; Benedetto *et al.*, 2017) (Fig. 21, a-d). Expectedly, siRNA-knockdown of $P2RY_2$ (si$P2RY_2$) (KD efficiencies assessed by RT-PCR, Suppl. Fig. 5) reduced ATP-induced currents for both cell lines (Fig. 21, a-d).

Nevertheless, as ATP directly stimulates $P2RY_2$, an ionophore (ionomycin) was used to activate ANO1 by directly increasing intracellular Ca^{2+} without $P2RY_2$ stimulation. Surprisingly, $P2RY_2$ overexpression or KD either increased or decreased ionomycin-induced currents, respectively, for both cells lines expressing WT-/F508del-CFTR (Fig. 21, e-h).

The effect of $P2RY_2$ expression on ionomycin-induced currents implies that $P2RY_2$ is either increasing ANO1 PM expression or augmenting its activation by other means. Possibly, $P2RY_2$ cellular expression regulates Ca^{2+} increment upon ATP or ionomycin stimulus. Nonetheless, total intracellular Ca^{2+} measured by Fura-2 Ca^{2+} probe in WT- or F508del-CFTR expressing CFBE did not change with $P2RY_2$ overexpression after ATP or ionomycin stimulation (Fig. 22). Total cellular Ca^{2+} was also measured in cells transfected with si$P2RY_2$, with a significant reduction in intracellular Ca^{2+} after ATP stimulation, though not after ionomycin (Fig. 22).

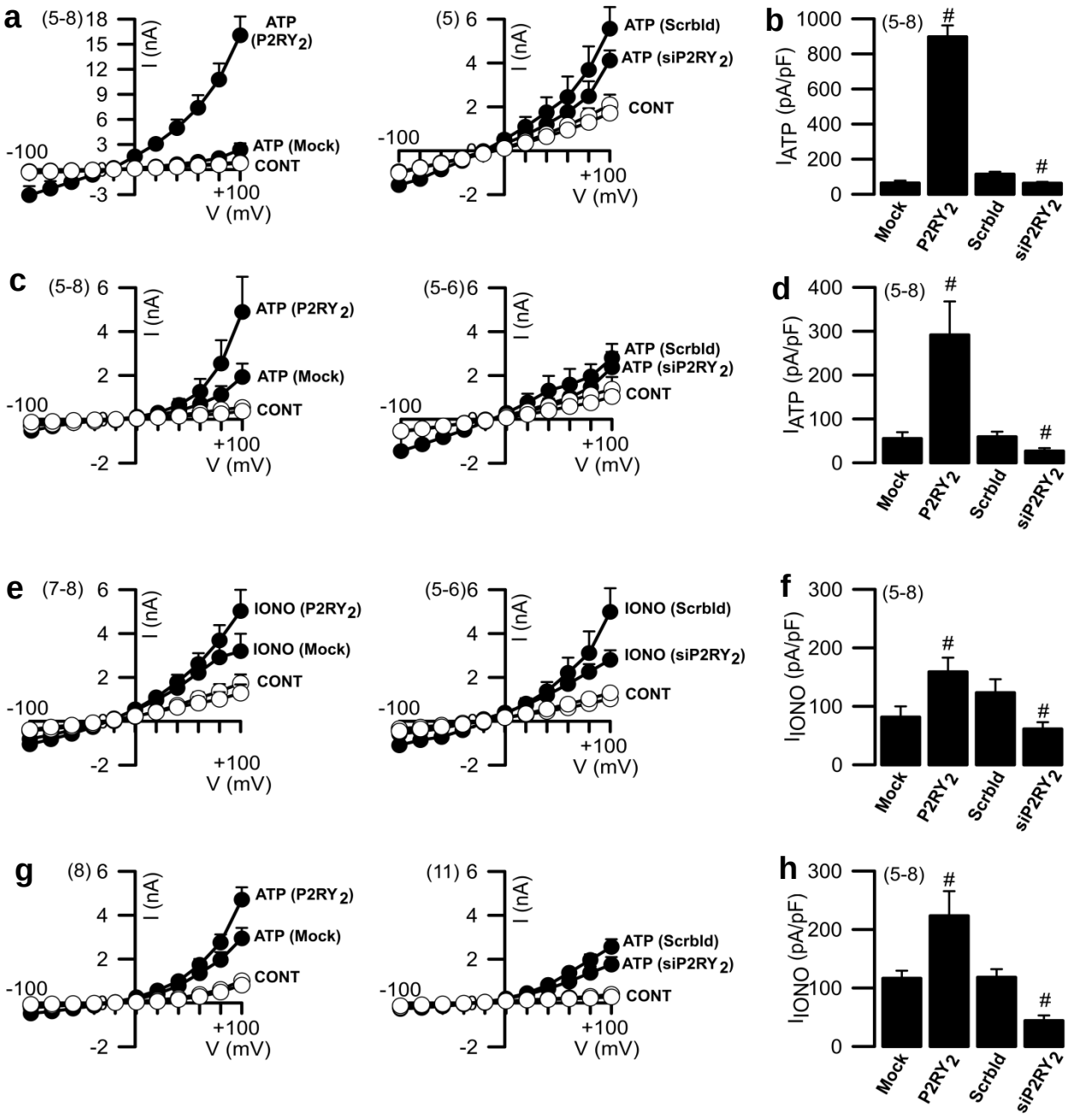

Fig. 21 Effect of $P2RY_2$ expression levels in ANO1 function in CFBE cells. (a,c) Whole-cell patch-clamp data, shown as I/V curves -100mV to +100mV, obtained for WT-CFTR/CFBE (a) or F508del-CFTR/CFBE (c) transfected with mock or $P2RY_2$ (left), scrambled (Scrbld) or siRNA against $P2RY_2$ ($siP2RY_2$) (right) as a control in Ringer (CONT) or after stimulation with ATP (100 μM); **(b,d)** Correspondent delta of the average of ATP-induced current densities for (a) and (c); **(e,g)** Whole-cell patch-clamp data, shown as I/V curves -100mV to +100mV, obtained for WT-CFTR/CFBE (e) or F508del-CFTR/CFBE (g) transfected with mock or $P2RY_2$ (left), scrambled (Scrbld) or siRNA against $P2RY_2$ ($siP2RY_2$) (right) as a control in Ringer (CONT) or after stimulation with ionomycin (IONO, 0.1 μM); **(f,h)** Correspondent delta of the average of IONO-induced current densities for (e) and (g). '#' indicates significant differences between cells transfected with mock vs $P2RY_2$ or Scrambled vs $siP2RY_2$ ($p \leq 0.05$ in unpaired T-student test); number of experiments between brackets.

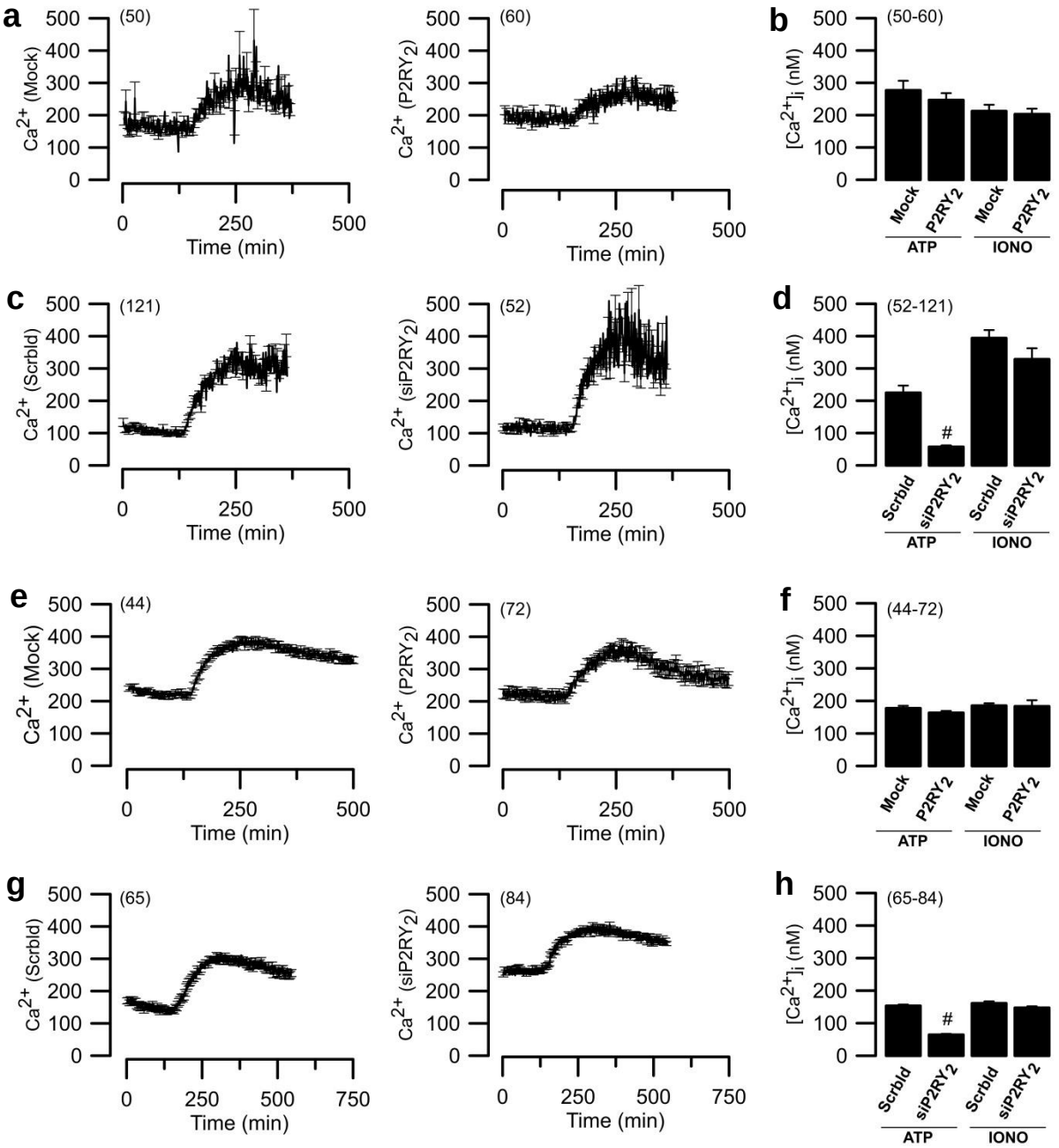

Fig. 22 Ca^{2+} measurements with different $P2RY_2$ expression levels in CFBE cells. (a,c) Ca^{2+} store release (nM) detected by Fura-2 fluorescence in WT-CFTR/CFBE stimulated by ionomycin (IONO, 0.1 μM) in cells transfected with Scrambled (Scrbld) (a) or $siP2RY_2$ (c); **(b,d)** Correspondent summary of Ca^{2+} store release for (a) and (c); **(e,g)** Ca^{2+} store release (nM) detected by Fura-2 fluorescence in F508del-CFTR/CFBE stimulated by ionomycin (IONO, 0.1 μM) in cells transfected with Scrambled (Scrbld) (e) or $siP2RY_2$ (g); **(f,h)** Correspondent summary of Ca^{2+} store release for (e) and (g). '#' indicates significant differences between cells transfected with Scrambled vs $siP2RY_2$ ($p \leq 0.05$ in unpaired T-student test); number of cells between brackets.

The Fura-2 measurements determined that the global Ca^{2+} increment is not the cause for such a difference in ANO1 function according to $P2RY_2$ expression levels. To assess if this effect could be mimicked using other receptors, we performed similar experiments using muscarinic M3 receptors (M3R). M3R expression allowed activation of not only carbachol-induced whole-cell currents, absent in mock-transfected cells, but also enhanced ATP-induced currents (Fig. 23). To further understand this relationship, we used another type of GPCR, histamine H1 receptors, which provided substantial histamine-induced currents in cells overexpressing $P2RY_2$ compared to mock-transfected cells (Fig. 24). These data suggest that (1) the expression of GPCRs translocates additional signalling proteins to PM that activate Cl^- currents through ANO1 and/or other channels and (2) Ca^{2+}-dependent whole-cell current is strongly CFTR-dependent, where differences were often present between WT- or F508del-CFTR expressing cells. Another hypothesis, not excluded from that which is the stated above, is that GPCRs could increase ANO1 PM expression, which would also contribute to such results.

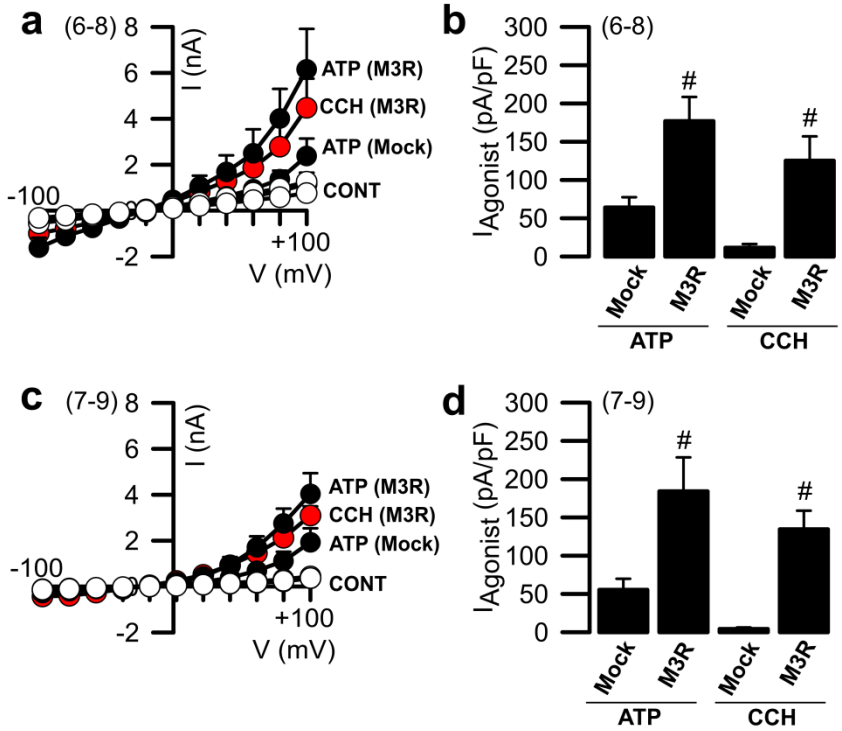

Fig. 23 Effect of M3R overexpression in ANO1 function in CFBE cells. (a,c) Whole-cell patch-clamp data shown as I/V curves -100mV to +100mV, obtained for WT-CFTR/CFBE (a) or F508del-CFTR/CFBE (c), transfected with mock or M3R as a control in Ringer (CONT) or after stimulation by ATP (100 µM) or carbachol (CCH, 100 µM); **(b,d)** Correspondent delta of average of ATP- or CCH-induced current densitites for (a) and (c). '#' indicates significant differences between cells transfected with mock vs $P2RY_2$/M3R ($p \leq 0.05$ in unpaired T-student test); number of experiments between brackets.

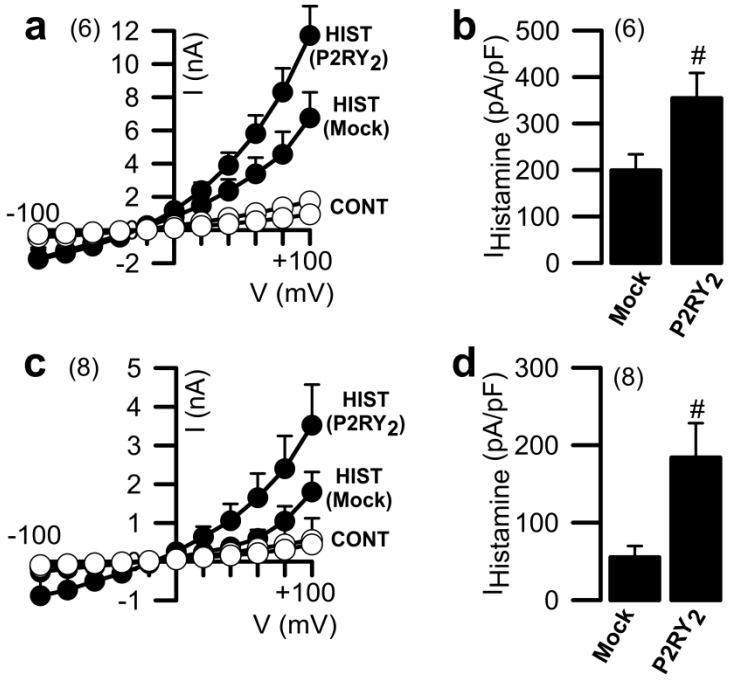

Fig. 24 Effect of $P2RY_2$ overexpression in histamine-induced currents in CFBE cells. (a,c) Whole-cell patch-clamp data shown as I/V curves -100mV to +100mV, obtained for WT-CFTR/CFBE (a) or F508del-CFTR/CFBE (c), transfected with mock or $P2RY_2$ as a control in Ringer (CONT) or after stimulation by histamine (HIST, 50 μM); **(b,d)** Correspondent delta of average of HIST-induced current densities for (a) and (c). '#' indicates significant differences between cells transfected with mock vs $P2RY_2$ ($p \leq 0.05$ in unpaired T-student test); number of experiments between brackets.

To test GPCRs effect on ANO1 expression, ANO1 total protein levels were evaluated by Western-Blot and the ANO1 PM fraction by immunofluorescence and chemiluminescence. Western-blot data, for both cell types expressing WT-/F508del-CFTR, revealed no ANO1 expression differences according to different $P2RY_2$ levels (Fig. 25).

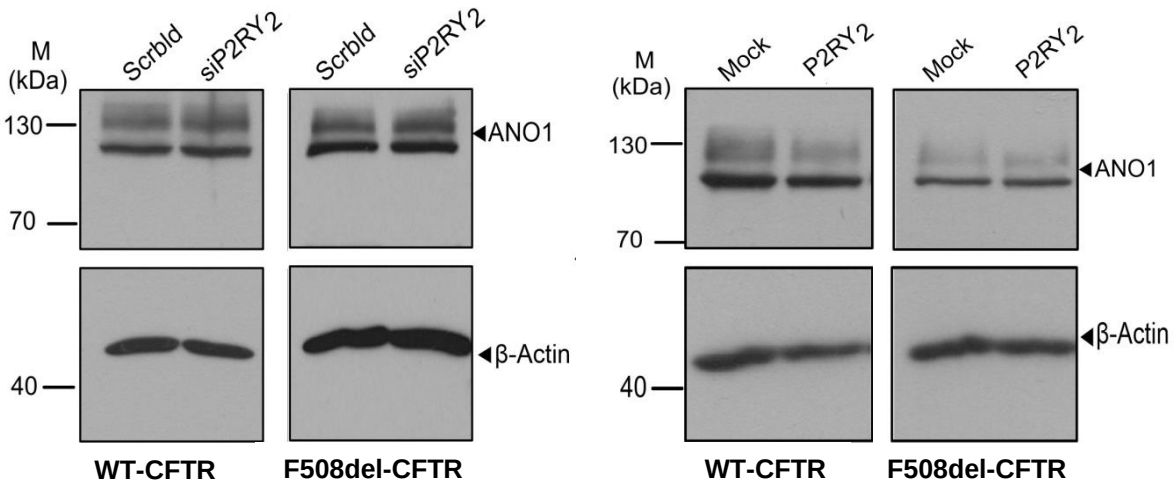

Fig. 25 Western-Blot for ANO1 in CFBE cells with different $P2RY_2$ expression levels. ANO1 expression in WT/CFBE (WT-CFTR) or F508del-CFTR/CFBE (F508del-CFTR), after transfection with scrambled (Scrbld) or siRNA against $P2RY_2$ ($siP2Y_2R$) (left) or after transfection with mock or $P2RY_2$ (right). There are no differences in ANO1 protein expression (~110kDa) despite different $P2RY_2$ protein expressions. β-actin was used as a loading control and molecular mass markers are shown on the left.

Regarding PM ANO1 expression, similar levels were determined regardless of $P2RY_2$ overexpression or KD in WT-/F508del-CFTR expressing CFBE cells (Fig. 26, a-f), or in HEK293T overexpressing ANO1 (Fig. 27, a, c). Also, a chemiluminescence assay in CFBE parental cells expressing 3HA-ANO1 construct had no differences in ANO1 PM levels with $P2RY_2$ overexpression (Fig. 26, g). Moreover, these data also exhibited higher ANO1 expression in WT- vs F508del-CFTR CFBE cells, as expected. Finally, similar data was obtained with another GPCR in WT-/F508del-CFTR CFBE cells, as M3R overexpression caused no differences in ANO1 PM expression assessed by immunostaining (Fig. 27, b, d)

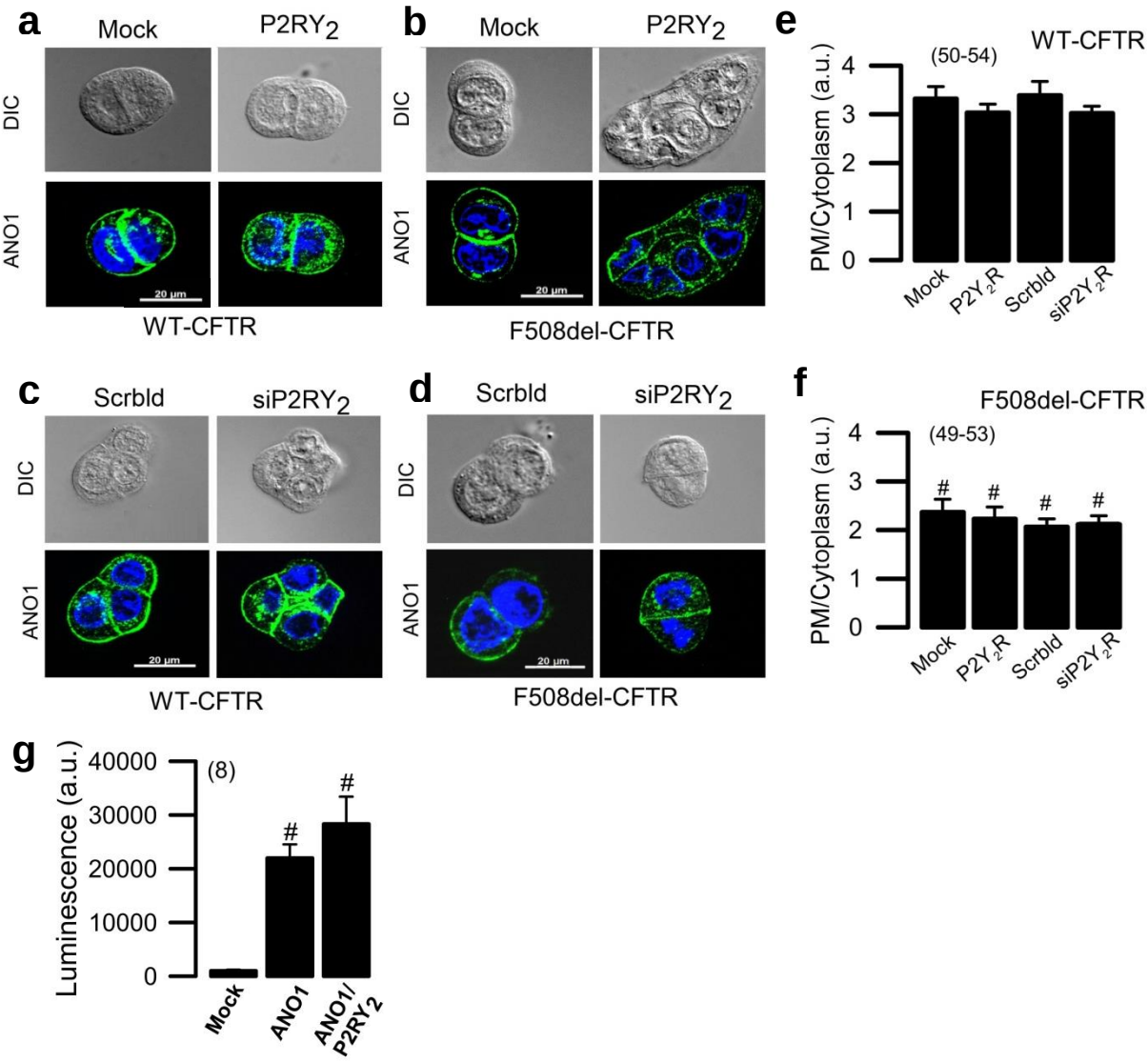

Fig. 26 ANO1 PM expression relationship to $P2RY_2$ levels in CFBE cells. (a-d) Immunofluorescence of ANO1 in WT-CFTR/CFBE (a,c) or F508del-CFTR/CFBE (b,d) transfected with mock or $P2RY_2$ (a,b) or transfected with scrambled (Scrbld) or siRNA against $P2RY_2$ ($siP2RY_2$) (c,d); images were acquired in Axiovert 200 microscope equipped with an ApoTome (objective 63x, oil); scale bar = 20 µM; **(e,f)** Analysis of cellular distribution of ANO1 in WT-CFTR/CFBE (e) and F508del-CFTR/CFBE (f) by quantitative assessment of fluorescence in plasma membrane/cytoplasm; **(g)** Membrane expression of ANO1 measured by chemiluminescence in CFBE parental cells transfected with mock, tagged ANO1 (ANO1) or tagged ANO1 and $P2RY_2$ (ANO1/$P2RY_2$). '#' indicates significant differences when compared to WT-CFTR (for 'f') or to mock (for 'g') ($p \leq 0.05$ in unpaired T-student test); number of experiments between brackets.

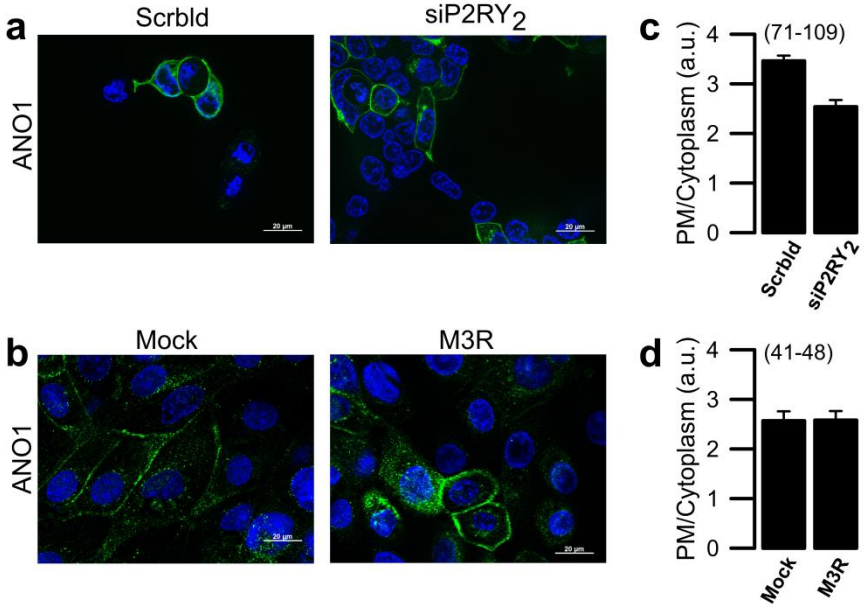

Fig. 27 ANO1 PM expression relationship to different GPCRs. (a,b) Immunofluorescence of ANO1 in HEK293T cells transfected with ANO1 and either scrambled (scrbld) or siRNA against $P2RY_2$ ($siP2RY_2$) or in WT-CFTR/CFBE cells transfected with mock or M3R; images were acquired in Axiovert 200 microscope equipped with an ApoTome (objective 63x, oil); scale bar = 20 µM; **(c,d)** Analysis of cellular distribution of ANO1 in HEK293T (c) or WT-CFTR/CFBE (f) by quantitative assessment of fluorescence in plasma membrane/cytoplasm. '#' indicates significant differences between scrambled vs $siP2RY_2$ or mock vs M3R ($p \leq 0.05$ in unpaired T-student test); number of experiments between brackets.

1.2. Relationship between GPCRs and WT-/F508del-CFTR

ANO1 and CFTR have a close relationship with several reports exhibiting differences in ANO1 expression/function according to WT-CFTR vs F508del-CFTR expression (Martins *et al.*, 2011b; Ruffin *et al.*, 2013). Therefore, GPCRs effect on ANO1 could be caused indirectly through CFTR, also affecting its expression and function. Similar assays were performed to evaluate GPCRs impact in CFTR and demonstrating that $P2RY_2$ enhances I/F-activated Cl^- currents in WT-CFTR. Rather surprisingly, comparable results were found in F508del-CFTR expressing CFBE cells (Fig. 28, a-d). Moreover, I/F-induced currents were suppressed by CFTR inhibitor 172, suggesting that CFTR stimulation was the cause of such currents. Additionally, M3R overexpression increased I/F-induced currents in F508del-CFTR expressing CFBE cells, which were inhibited by CFTR inhibitor 172. Regarding CFBE cells expressing WT-CFTR, M3R overexpressing did not increase I/F-induced currents, since mock transfected cells had particularly high current levels (Fig. 28, e-h).

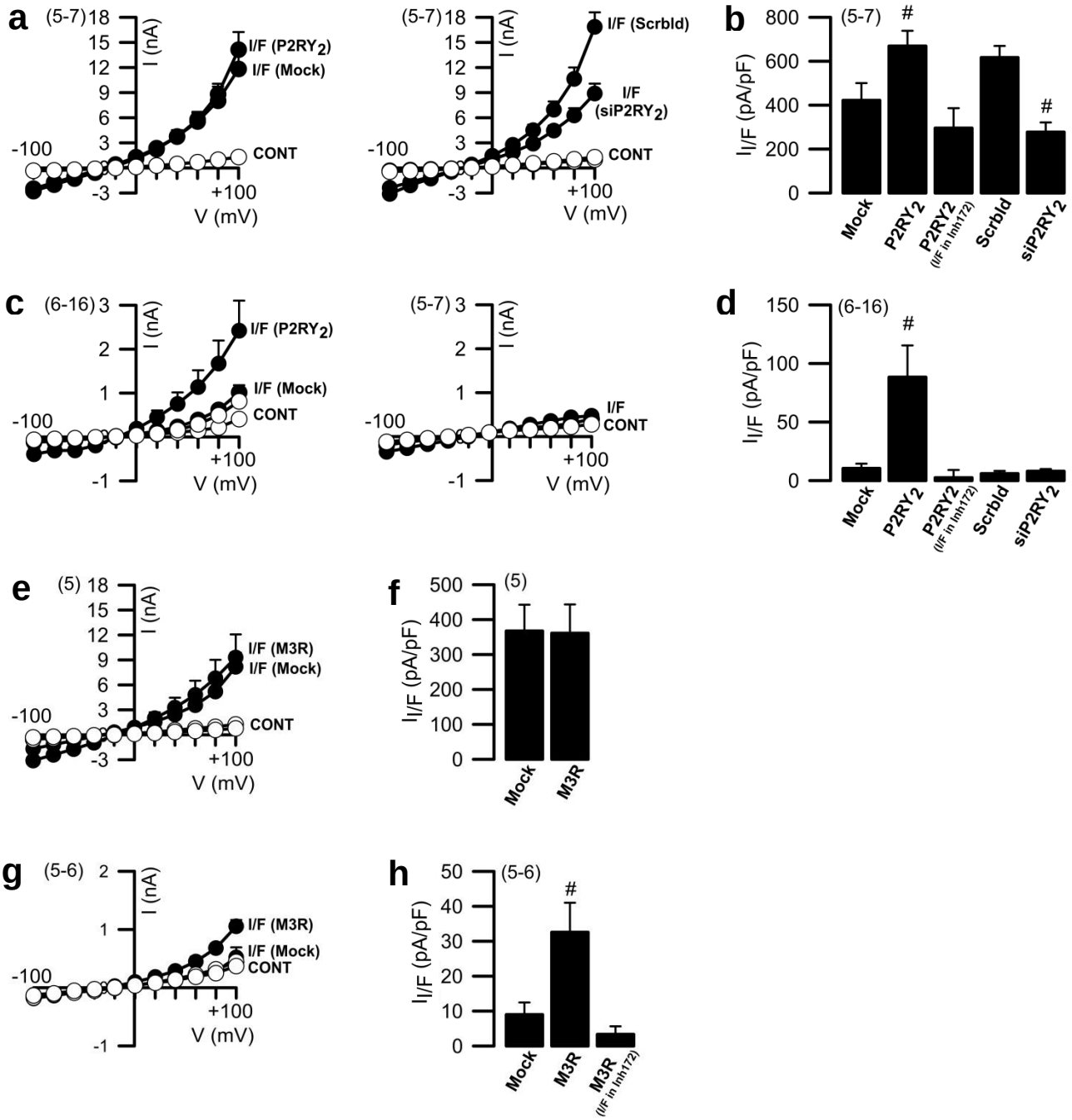

Fig. 28 Effect of different GPCRs expression levels in CFTR function in CFBE cells. (a,c) Whole-cell patch-clamp data shown as I/V curves -100mV to +100mV, obtained for WT-CFTR/CFBE (a) or F508del-CFTR/CFBE (c), transfected with mock or $P2RY_2$ as a control in Ringer (CONT) or after stimulation by IBMX/Forskolin (I/F, 100 μM/2 μM); **(b,d)** Correspondent delta of average of I/F-induced current densities for (a) and (c). **(e,g)** Whole-cell patch-clamp data shown as I/V curves -100mV to +100mV, obtained for WT-CFTR/CFBE (e) or F508del-CFTR/CFBE (g), transfected with mock or M3R as a control in Ringer (CONT) or after stimulation by IBMX/Forskolin (I/F, 100 μM/2 μM); **(f,h)** Correspondent delta of average of I/F-induced current densities for (e) and (g). '#' indicates significant differences between M3R/$P2RY_2$ vs mock ($p \leq 0.05$ in unpaired T-student test); number of experiments between brackets.

WT- and F508del-CFTR cellular expressions were assessed with different $P2RY_2$ levels by immunofluorescence and chemiluminescence. While WT-CFTR was well expressed in the PM, basically no F508del-CFTR reached the PM (Fig. 29, a-f), though I/F-induced currents were detected for both. Regarding $P2RY_2$ expression levels, they did not affect either WT- or F508del-CFTR PM expression, this being later confirmed by chemiluminescence (Fig. 29, g,h).

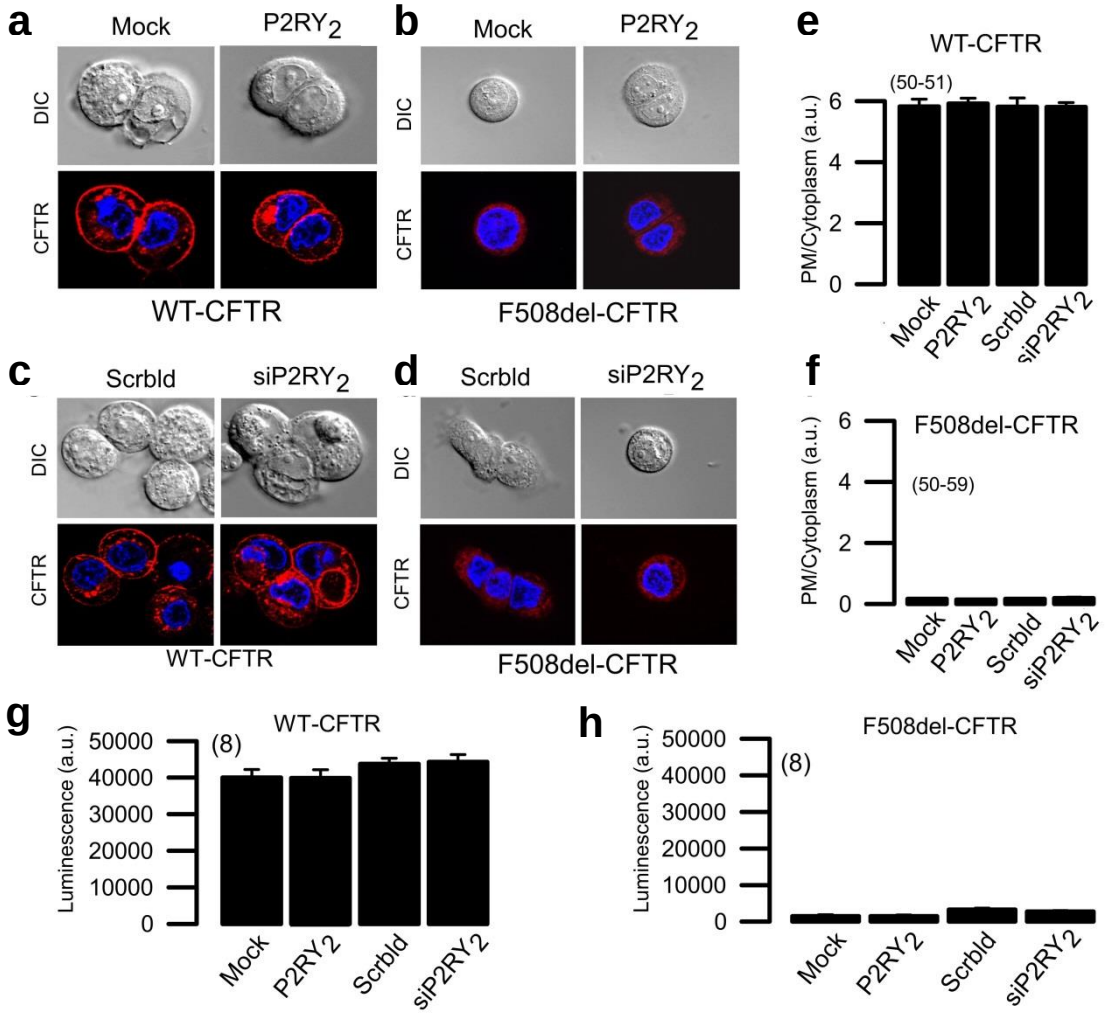

Fig. 29 CFTR PM expression relationship to $P2RY_2$ levels in CFBE cells. (a-d) Immunofluorescence of CFTR in WT-CFTR/CFBE (a,c) or F508del-CFTR/CFBE (b,d) transfected with mock or $P2RY_2$ (a,b) or transfected with scrambled (Scrbld) or siRNA against $P2RY_2$ ($siP2RY_2$) (c,d); images were acquired in Axiovert 200 microscope equipped with an ApoTome (objective 63x, oil); scale bar = 20 µM; **(e,f)** Analysis of cellular distribution of CFTR in WT-CFTR/CFBE (e) and F508del-CFTR/CFBE (f) by quantitative assessment of fluorescence in plasma membrane/cytoplasm; **(g,h)** Membrane expression of CFTR measured by chemiluminescence in WT-CFTR/CFBE (g) or F508del-CFTR/CFBE (h). a.u. arbitrary units; number of experiments between brackets.

1.3. Role of EPAC1 and ADCY1 in ANO1 and CFTR activation and their relation to GPCRs

The data described in the previous section determined that ANO1 as well as CFTR activated currents are dependent on $P2RY_2$ levels, without changing either ANO1 or CFTR PM expressions. Thus, these data suggest that $P2RY_2$ is exchanging molecules that link cAMP to Ca^{2+} signals, such as Ca^{2+}-sensitive ADCYs and EPAC. ADCYs catalyse the conversion of ATP to cAMP, directly activating CFTR through PKA activation (Hwang and Kirk, 2013). On the other hand, EPAC1 is cAMP-sensitive and activates ANO1 by an increase of intracellular Ca^{2+} through PLC pathway (Schmidt *et al.*, 2001; Hoque *et al.*, 2010). In addition, Lobo *et al.* (2016) described a stabilisation of CFTR at the PM promoted by EPAC activation.

To study the effect of such proteins, 8-substituted cAMP derivative (8-Br-cAMP) induced currents were measured with different GPCRs levels. Interestingly, such currents were independent of $P2RY_2$ or M3R levels in both WT-/F508del-CFTR CFBE cells (Fig. 30). These results suggest a role of ADCYs and EPAC1 for positive modulation of GPCRs on Cl^- activation by I/F or ionomycin. Indeed, since 8-substituted cAMP derivatives (*e.g.* 8-pCPT-2-O-Me-cAMP (007-AM) or 8-Br-cAMP) are also potent activators of EPAC1, ANO1 currents are also stimulated through 8-Br-cAMP. Therefore, the whole-cell patch-clamp currents obtained from 8-Br-cAMP stimulation are the activation of both channels through the mechanism described above.

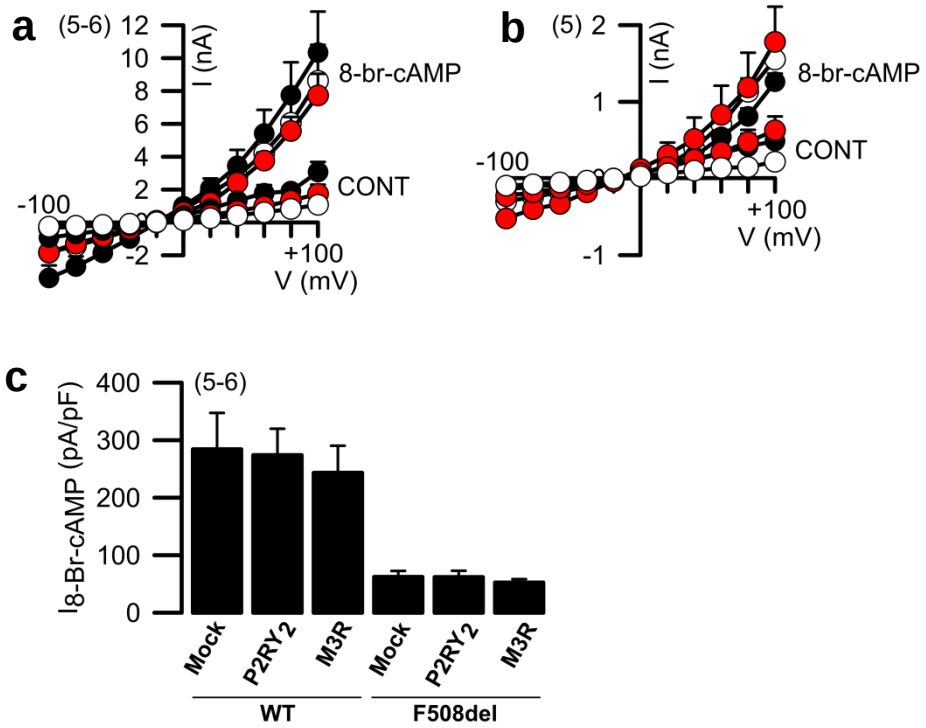

Fig. 30 Effect of different GPCRs overexpression in currents induced by 8-bromo-cAMP in CFBE cells. (a,b) Whole-cell patch-clamp data, shown as I/V curves -100mV to +100mV, obtained for WT-CFTR/CFBE (a) or F508del-CFTR/CFBE (b) transfected with mock (white), $P2RY_2$ (red) or M3R (black), as a control in Ringer (CONT) or after stimulation with 8-Bromo-cAMP (8-Br-cAMP, 25 μM); **(c)** Correspondent delta of the average 8-Bromo-cAMP-induced current densitites for WT-CFTR/CFBE (WT) or F508del-CFTR/CFBE (F508del). Number of experiments between brackets.

To further study the role of EPAC in the regulation of Cl^- currents, firstly its expression level was assessed. Both WT-/F508del-CFTR CFBE cells expressed EPAC1, with no differences between them (Suppl. Fig. 4). Then, Cl^- currents stimulated by an EPAC1 specific activator (007-AM) were measured in WT-CFTR expressing CFBE cells, revealing a linear current/voltage relationship. These currents were strongly inhibited by removal of extracellular Cl^- ($5Cl^-$), confirming the ionic nature of such currents (Fig. 31, f). Remarkably, both ANO1 inhibitor AO1 and CFTR inhibitor 172 partially suppressed 007-AM activated Cl^- currents, suggesting that both CFTR and ANO1 Cl^- secretory pathways are activated (Fig. 31, f). Furthermore, a Ca^{2+} chelator (BAPTA-AM) showed the same reduction as the inhibitors, demonstrating the involvement of Ca^{2+} storage depletion in EPAC1-induced Cl^- currents.

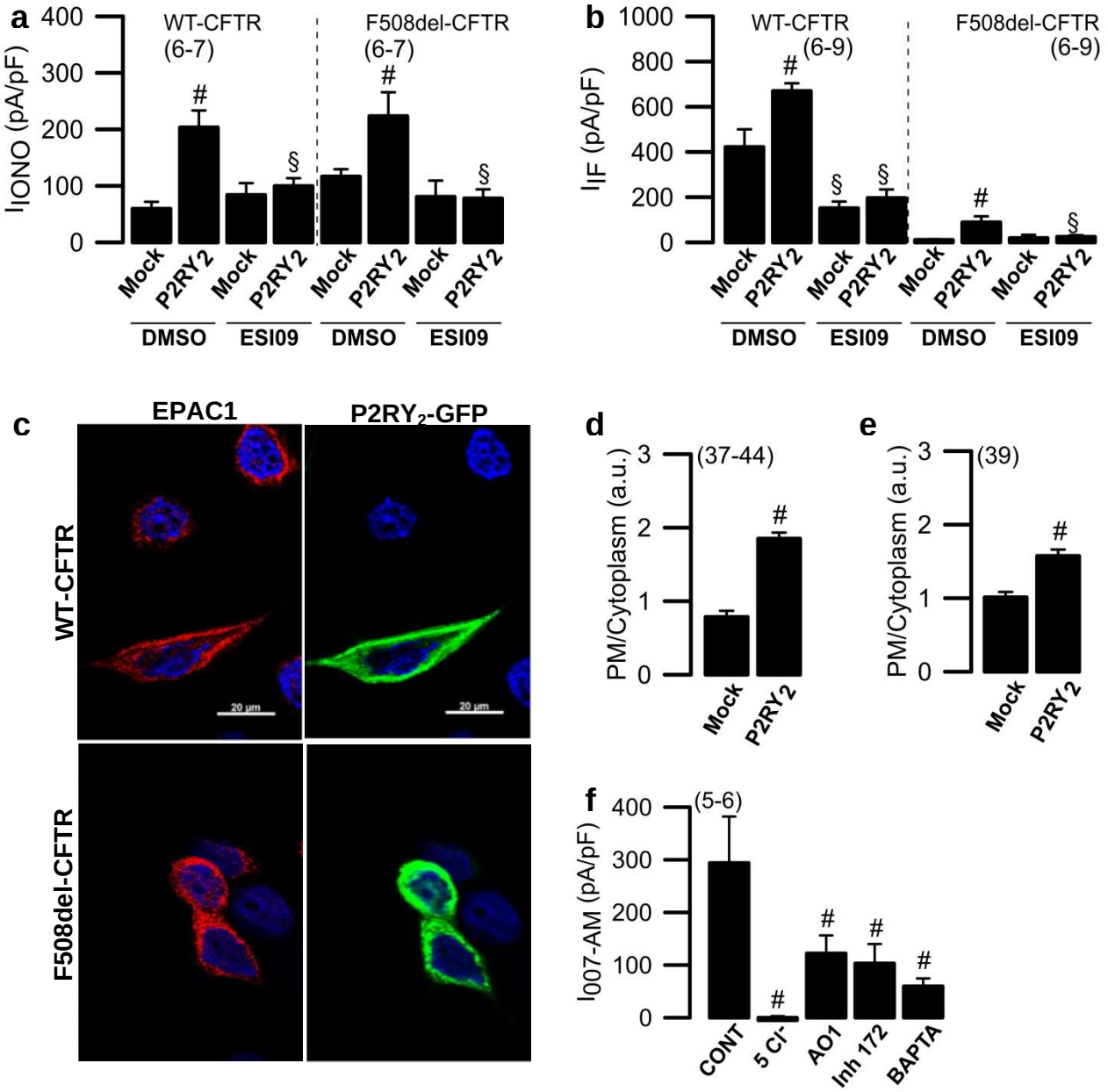

Fig. 31 EPAC1 impact in ANO1 and CFTR function in CFBE cells. (a,b) Inhibition of current densities by EPAC1 inhibitor ESI09 (10 µM) in WT-CFTR/CFBE (WT-CFTR) and F508del-CFTR/CFBE (F508del-CFTR) after stimulation with ionomycin (IONO, 0.1 µM) (a) or IBMX/Forskolin (I/F, 100 µM/2 µM) (b); **(c)** Immunostainings of EPAC1 and $P2RY_2$-GFP in WT-CFTR/CFBE (top panels) or F508del-CFTR/CFBE (bottom panels); images were acquired in Axiovert 200 microscope equipped with an ApoTome (objective 63x, oil); scale bar = 20 µM; **(d,e)** Analysis of cellular distribution of EPAC1 by quantitative assessment of fluorescence in plasma membrane/cytoplasm in WT-CFTR/CFBE (d) or F508del-CFTR/CFBE (e); **(f)** Summary of current densities measured in WT-CFTR/CFBE cells stimulated with EPAC1 activator 007-AM (CONT, 30 µM). Replacement of extracellular Cl^- by impermeable gluconate ($5Cl^-$), or application of CaCCinhAO1 (AO1, 20 µM), CFTRinh172 (Inh172, 20 µM) or Ca^{2+} chelator BAPTA-AM (BAPTA, 50 µM) inhibited current densities. a.u. arbitrary units; '#' indicates significant differences when compared to mock or CONT ($p \leq 0.05$, unpaired T-student test); '§' indicates significant differences between DMSO vs ESI09 (either both mock or both $P2RY_2$) ($p \leq 0.05$, unpaired T-student test); number of experiments between brackets.

To further understand the role EPAC1 in ANO1 and CFTR activation, an EPAC1 specific inhibitor (ESI09) was used. This inhibitor had no effect on ionomycin Cl^- currents measured in mock-transfected cells for both WT-/F508del-CFTR expressing CFBE. Nevertheless, the increment of Cl^- currents correlated to $P2RY_2$ overexpression was abolished in both cell types (Fig. 32, a, b). Furthermore, in mock-transfected WT-CFTR expressing CFBE cells, I/F-induced currents were inhibited by approximately 50% by ESI09. In addition, this inhibitor suppressed the increase of I/F-activated currents which are linked to a higher $P2RY_2$ expression for both cell lines (Fig. 32, a, b).

Finally, EPAC1 immunostaining in cells transfected with $P2RY_2$-GFP suggested its localization to be close to PM, compared to non-transfected cells for both WT-/F508del-CFTR expressing CFBE (Fig. 31, c-e). Altogether, these data indicate that a significant part of I/F-activated Cl^- currents is EPAC1-dependent.

ADCYs are responsible for cellular cAMP levels and divided into Ca^{2+}- dependent (ADCY1, 3, 8 and 10) or independent (ADCY2, 4, 5, 6, 7 and 9) (UniProt database; available at http://www.uniprot.org/; access on January 2018). Notably, ADCY1 and ADCY3 (but not ADCY8 or ADCY10) are expressed in both cell lines, and ADCY1 levels are independent of $P2RY_2$ expression in WT-CFTR CFBE (Suppl. Fig. 7). Nonetheless, regardless of their expression, ADCYs activity may differ according to GPCRs levels. To further understand this, intracellular cAMP was measured after stimulation with ATP or I/F in mock or $P2RY_2$ transfected cells. The stimulation of purinergic receptors increased intracellular cAMP, further enhanced by a higher $P2RY_2$ expression for both WT-/F508del-CFTR CFBE cells (Fig. 32, c). Interestingly, ATP-induced rise of intracellular cAMP upon $P2RY_2$ overexpression was comparable to intracellular cAMP induced by I/F (Fig. 32, c). These data confirm the link between ATP-induced Ca^{2+} release and increment in cAMP levels caused by Ca^{2+}-sensitive ADCYs higher activity.

Namkung *et al.* (2010) reported a vital role of ADCY1 in CFTR-dependent Cl^- secretion in airway epithelial cells and suggested to be part of Ca^{2+}/cAMP crosstalk for CFTR activation. Therefore, an ADCY1 specific inhibitor (ST034) was used to further assess the ADCY1 role for Ca^{2+}-activated Cl^- secretion modulated by GPCRs expression. This inhibitor did not affect ionomycin-induced currents in mock-transfected cells for both cell lines. However, ST034 suppressed the increment in currents caused by $P2RY_2$ overexpression for both WT-/F508del-CFTR expressing

CFBE cells (Fig. 32, a). Moreover, ST034 remarkably reduced I/F-induced currents in WT-CFTR CFBE for both mock and $P2RY_2$ transfected cells. For both cell lines, ADCY1 inhibitor abolished the increment in I/F currents related to $P2RY_2$ overexpression (Fig. 32, b). These data indicate the dominant role of ADCY1 in the generation of cAMP and suggests a robust relationship between GPCRs expression and ADCY1 activity.

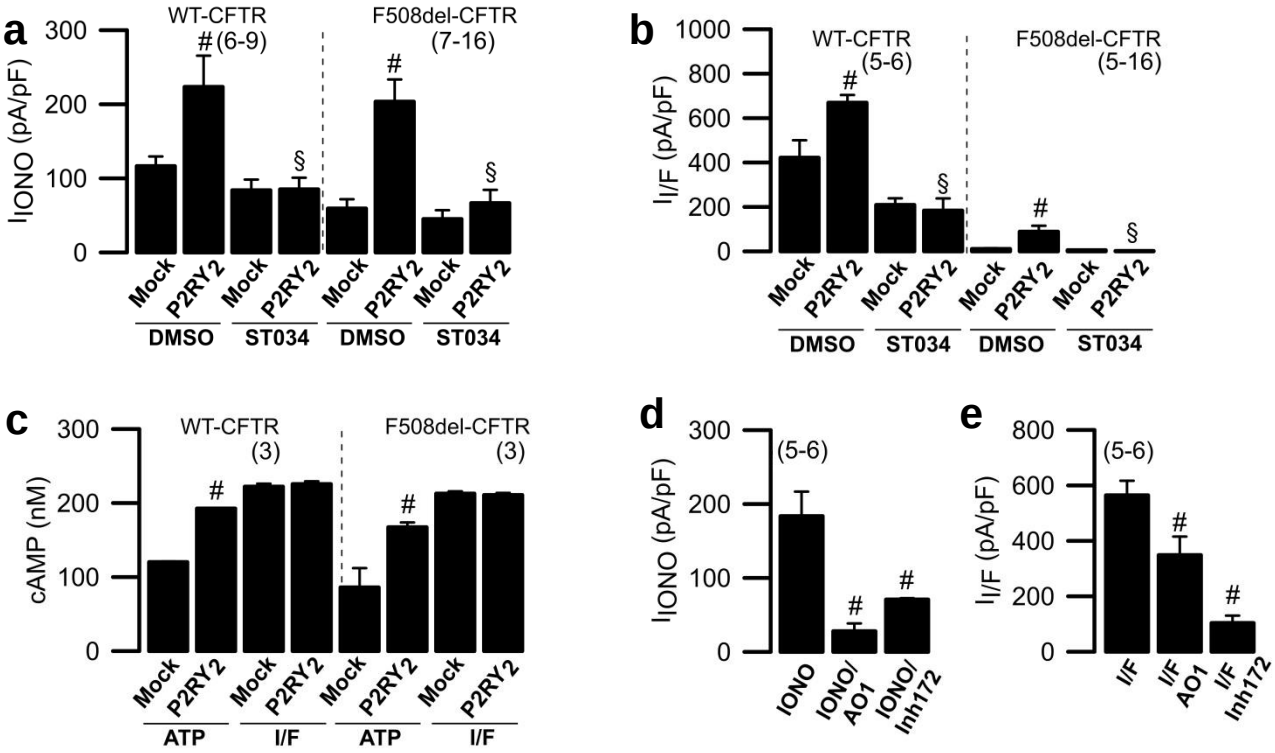

Fig. 32 ADCY1 in ANO1 and CFTR functions. (a,b) Inhibition of current densities by ADCY1 inhibitor ST034307 (ST034, 30 μM) in WT-CFTR/CFBE and F508del-CFTR/CFBE after stimulation with ionomycin (IONO, 0.1 μM) (a) or IBMX/forskolin (I/F, 100 μM/2 μM) (b); **(c)** Increase in intracellular cAMP levels (nM) after stimulation with ATP (100 μM) or IMBX/forskolin (I/F, 100 μM/2 μM) in WT-CFTR/CFBE or F508del-CFTR/CFBE; **(d)** Delta of current densities of Cl^- currents in CFBE parental after stimulation with ionomycin (IONO, 0.1 μM) or in the presence of the inhibitors $CaCC_{inh}AO1$ (AO1, 20 μM) or CFTR inhibitor $CFTR_{inh}172$ (Inh172, 20 μM); **(e)** Delta of current densities of Cl^- currents in HEK293T transfected with WT-CFTR after stimulation with IBMX/Forskolin (I/F, 100 μM/ 2 μM) or in the presence of the inhibitors $CaCC_{inh}AO1$ (AO1, 20 μM) or CFTR inhibitor $CFTR_{inh}172$ (Inh172, 20 μM). '#' indicates significant differences when compared to mock or control ($p \leq 0.05$, unpaired T-student test); '§' indicates significant differences between DMSO vs ST034 (either both mock or both $P2RY_2$) ($p \leq 0.05$, unpaired T-student test); number of experiments between brackets.

Bearing in mind all these results, an intensive crosstalk between cAMP- and Ca^{2+}-dependent signalling is present in CFBE cells with EPAC1 and ADCY1 both playing an essential role. In addition, this crosstalk prevents a clear discrimination

between Cl^- secretion by adrenergic/CFTR or purinergic/ANO1 activation. Indeed, inhibitors considered to be specific for CFTR, such as CFTR inhibitor 172, or for ANO1, such as CaCC inhibitor AO1, block both Ca^{2+} (ATP) and cAMP (I/F) activated currents (Fig. 32, d, e). Benedetto *et al.* (2017) also described an absence of specificity of these inhibitors in CFBE cells, suggesting that their use may be limited to separate CFTR and ANO1 induced Cl^- currents.

Previously in this chapter, it was established that different $P2RY_2$ expression leads to no changes in global intracellular Ca^{2+} levels. Nevertheless, Ca^{2+} variation in the presence of GPCRs may occur at a more compartmentalised level, such as at the PM. Using the Ca^{2+} sensor G-CAMP6 fused to CFTR C-terminus, several components were tested to determine variations of local compartmentalised Ca^{2+}.

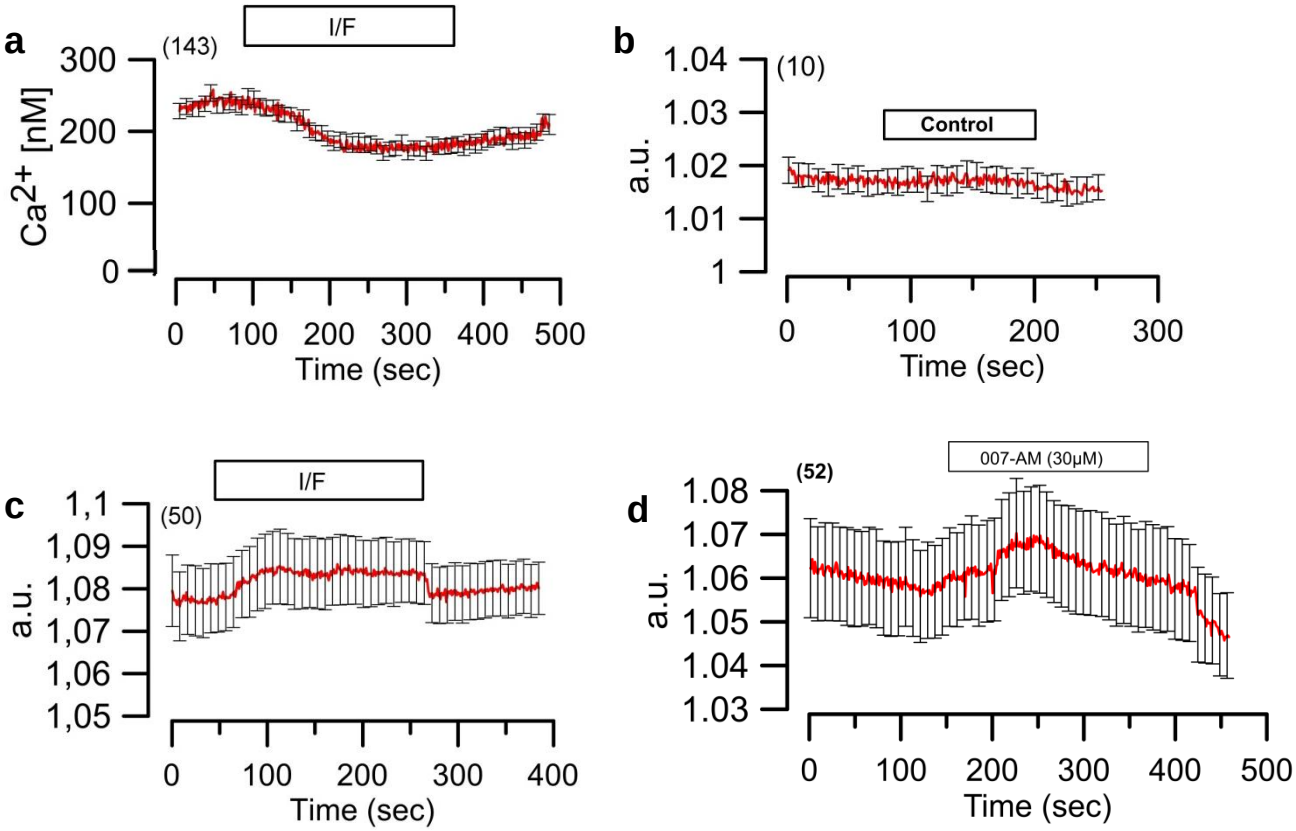

Fig. 33 Intracellular Ca^{2+} measurements in WT-CFTR/CFBE. (a) Intracellular Ca^{2+} measured by Fura-2 in WT-CFTR/CFBE cells with IBMX/Forskolin (I/F, 100 µM/2 µM) stimulation; **(b-d)** Intracellular Ca^{2+} levels detected by the Ca^{2+}-sensor G-CAMP6 fused to CFTR C-terminal with ringer (control) (b), IBMX/Forskolin (I/F, 100 µM/2 µM) (c) or 007-AM stimulation (30 µM) (d). a.u. arbitary units; number of cells between brackets.

Indeed, I/F stimulation triggered a peak of Ca^{2+} concentration in CFTR proximity, compared to control experiments with ringer (Fig. 33, b, c). This Ca^{2+} increment indicates that higher cellular cAMP concentration through I/F stimulation results in

more abundant local Ca^{2+}, probably by EPAC1 activation. Comparable data was obtained with EPAC1 activation by 007-AM, resulting in a local Ca^{2+} increment (Fig. 33, d).

1.4 ANO1 and CFTR Golgi bypass

The traffic of proteins to PM classically reaches the ER and then follows to the Golgi complex, where post-translational modifications occurs, such as protein glycosylation (Stanley, 2011). Nevertheless, an unconventional route bypassing the Golgi complex occurs in specific cellular conditions for several proteins such as Kv4 K^+ or CFTR channels (Grieve and Rabouille, 2011). Indeed, CFTR trafficking from the ER (core-glycosylated, band B) to the Golgi complex (complex-glycosylated, band C) is regulated by COPII, but can also follow an unconventional route bypassing Golgi complex for both WT- and F508del-CFTR (Yoo *et al.*, 2002; Gee *et al.*, 2011).

To test this hypothesis, BFA was used to block the canonical protein traffic pathway. This compound is a potent inhibitor of membrane recruitment for ARF1, involved in the first step of the formation of COPI-coated vesicles and its use collapses the Golgi complex. Accordingly, it blocks the exit of glycosylated protein from the Golgi to the PM (Nickel and Rabouille, 2009). Both CFTR and ANO1 proteins are glycosylated in cells, indicating they undergo the classic trafficking route (Yang *et al.*, 2008; Farinha *et al.*, 2013). Indeed, blocking Golgi-PM protein transport with BFA removed glycosylated forms of CFTR and ANO1 (Fig. 34, a). It also changed WT-CFTR cellular localization, since it was mostly cytoplasmic, though ANO1 PM expression remained mostly unchanged (Fig. 34, b-e). Remarkably, although WT-CFTR was utterly absent from the cell membrane in BFA-treated cells, I/F-induced currents were still present (approximately 50% compared to non-treated cells currents) (Fig. 35, b). Surprisingly, in BFA-treated cells, $P2RY_2$ higher expression would still increase I/F-induced currents to the same level as non-treated cells overexpressing $P2RY_2$ (Fig. 35, b). For F508del-CFTR, similar data was obtained, with higher I/F-induced currents positively correlated to $P2RY_2$ levels, regardless of BFA treatment (Fig. 35, b).

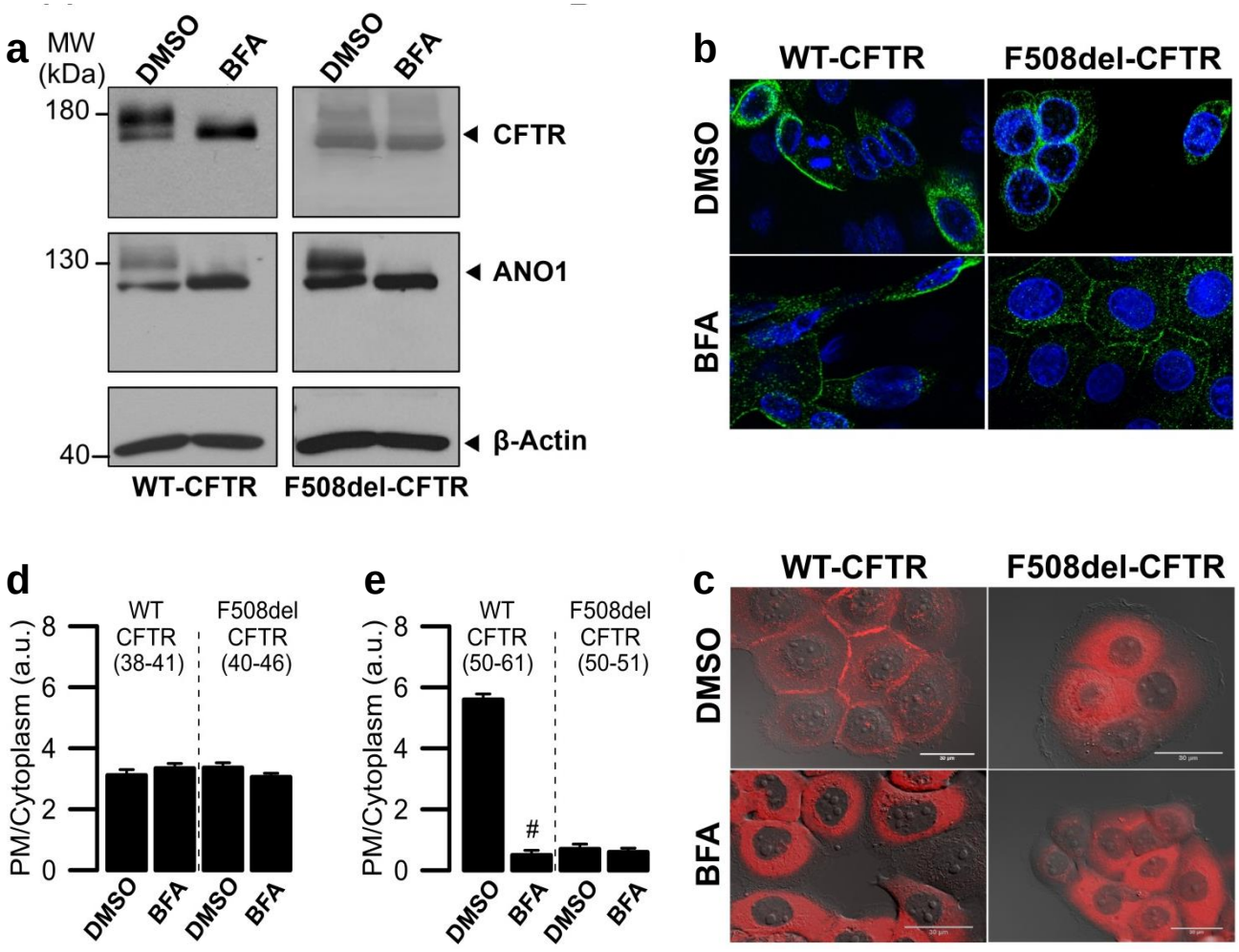

Fig. 34 ANO1 and CFTR expression after BFA treatment in CFBE cells. (a) Western-blot of CFTR and ANO1 in WT-CFTR/CFBE (WT-CFTR) and F508del-CFTR/CFBE (F508del-CFTR) incubated with DMSO or BFA (10 μM), showing that BFA eliminates glycosylated form of CFTR (band c) and ANO1 (upper band at 130kDa); **(b)** Expression of ANO1 in WT-CFTR/CFBE (left panels) or F508del-CFTR/CFBE (right panels) incubated with DMSO or BFA (10 μM); **(c)** Expression of CFTR (mCherry fluorescence in living cells) in WT-CFTR/CFBE (left panels) or F508del-CFTR/CFBE (right panels) incubated with DMSO or BFA (10 μM); images were acquired in Axiovert 200 microscope equipped with an ApoTome (objective 63x, oil); scale bar = 30μM; **(d,e)** Analysis of cellular distribution of ANO1 (d) or CFTR (e) by quantitative assessment of fluorescence in plasma membrane/cytoplasm. a.u. arbitrary units; '#' indicates significant differences between DMSO vs BFA ($p \leq 0.05$, unpaired T-student test);

As expected, since BFA does not affect ANO1 PM trafficking, ionomycin-induced currents also remained equal between BFA-treated and non-treated cells, with higher currents for cells transfected with $P2RY_2$ (Fig. 35, a).

These surprising outcomes suggest several implications, namely (1) ANO1 and $P2RY_2$ have an alternative PM traffic route that bypasses Golgi complex; (2) cAMP-activated Cl^- currents can move partially through ANO1, probably by EPAC1

activation and (3) $P2RY_2$ different expression levels affect ANO1 that is already placed at the PM.

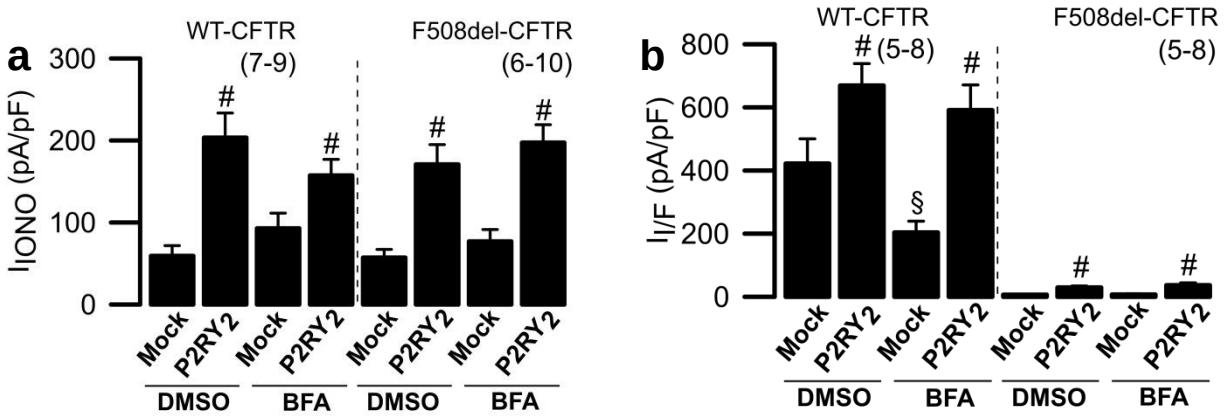

Fig. 35 ANO1 and CFTR functions after BFA treatment in CFBE cells. (a,b) Delta of current densities of ionomycin-induced (IONO, 0.1 µM) (a) or IBMX/Forskolin-induced (100 µM/2 µM) (b) currents in WT-CFTR/CFBE (WT-CFTR) or F508del-CFTR/CFBE (F508del-CFTR) incubated with DMSO or BFA (10 µM) and transfected with mock or $P2RY_2$. a.u. arbitrary units; '#' indicates significant differences between mock vs $P2RY_2$ ($p \leq 0.05$, unpaired T-student test); '§' indicates significant differences between DMSO vs BFA (either both mock or both $P2RY_2$) ($p \leq 0.05$, unpaired T-student test); number of experiments between brackets.

2. Conclusions

ANO1 and CFTR have an intricate relationship, which was further explored in this chapter. Indeed, a strong co-regulation between CFTR or ANO1-activated currents was evident, which limits a total separation between them. A recent study by Benedetto *et al.* (2017) reported that tissue-specific knockout of ANO1 gene in mouse intestine and airways eliminated not only Ca^{2+}-activated Cl^- currents, but also CFTR-mediated Cl^- secretion, abolishing cAMP-activated whole-cell currents. Another previous report by Faria *et al.* (2009) described a two-phase activation by ATP in oocytes coexpressing $P2RY_2$ and CFTR, an instantaneous current followed by a non-transient one. The first current (appearing very fast) likely corresponds to ANO1 and the second one (slower to appear) to CFTR, possibly corresponding to CFTR activation by $P2RY_2$ stimulation, and probably through Ca^{2+}-sensitive ADCYs. These interesting data are in line with our results shown here, demonstrating new roles of ANO1 in CFTR function.

Several elements are vital to this complex relationship, namely EPAC1 and ADCY1, both necessary for cAMP and Ca^{2+} cross-activation. This overlap is located

in a shielded membrane compartment (microdomain), suggested by the fact that total Ca^{2+} measurements with Fura-2 underwent no alterations with GPCRs different expressions (Fig. 22), though CFTR with a G-CAMP6 Ca^{2+} sensor could detect such alterations (Fig. 33). Lipid rafts are PM microdomains with enrichment in cholesterol and sphingolipids involved in compartmentalization of molecules at the cell surface. It has been proposed that lipid rafts have a higher level of several signalling molecules, namely GPCRs (Barnett-Norris *et al.*, 2005), which transform these specific parts of the membrane particularly prone to compartmentalized signalling talk.

Membrane bound ADCYs were described to co-localize with PLC-coupled GPCRs possibly in lipid raft-like membrane compartments (Ostrom and Insel, 2004). Interestingly, CFTR and ANO1 are also found in lipid rafts and EPAC1 was reported to co-localize with CFTR (Kowalski and Pier, 2004; Jin *et al.*, 2013; Lobo *et al.*, 2016). Relative to EPAC1, this molecule has a known role in cAMP/Ca^{2+} crosstalk. In previous reports, both forskolin and EPAC1 activator (007-AM) could produce Cl^- currents in intestinal cells, which were sensitive to Ca^{2+} chelation and PKA inhibition, though 007-AM was only sensitive to Ca^{2+} chelation (Hoque *et al.*, 2010). Similar results were obtained from Domingue *et al.* (2016), reporting two components of Cl^- currents in T84 cells, PKA dependent and independent, probably correspondent either to CFTR or ANO1 activation, respectively. These results are in line with the data of this research, suggesting an intricate relationship between cAMP and Ca^{2+}-induced Cl^- currents.

EPAC1 activator induced a Cl^- current suppressed by Ca^{2+} chelator BAPTA-AM, implying that this current is related to intracellular Ca^{2+} (Fig. 31, f). Moreover, I/F-induced currents in WT-CFTR expressing CFBE cells were partially inhibited by an ADCY1 inhibitor (Fig. 32, b), as expected, but also by an EPAC1 inhibitor (Fig. 31, b), indicating a central role of EPAC1 in Cl^- secretion regulation. Regarding BFA experiments, even though this compound inhibited CFTR membrane localisation, there was still a partial Cl^- current activated by I/F and it was unaffected by $P2RY_2$ expression (Fig. 35, b). These surprising results indicated that part of cAMP-activated Cl^- current may move through ANO1.

It is interesting to consider that the KD of ESYT1 affected ATP and I/F-induced currents, correspondent mainly to Ca^{2+}- or cAMP-activated currents, respectively. Indeed, this further indicates the intimate relationship between ANO1 and CFTR and co-localization of the signalling machinery that allows Ca^{2+}/cAMP crosstalk.

In conclusion, receptors, such as GPCRs, translocate Ca^{2+}-sensitive ADCY1 and EPAC1 to PM compartments containing GPCRs, CFTR and ANO1, therefore facilitating crosstalk between Ca^{2+}- and cAMP-dependent signalling and cross-activation between both channels (Fig. 36). These findings are significant for the CF field since ANO1 is already responsible for part of Cl^- current classically attributed solely to CFTR and so there is a chance for it to entirely replace CFTR function as a Cl^- channel in CF.

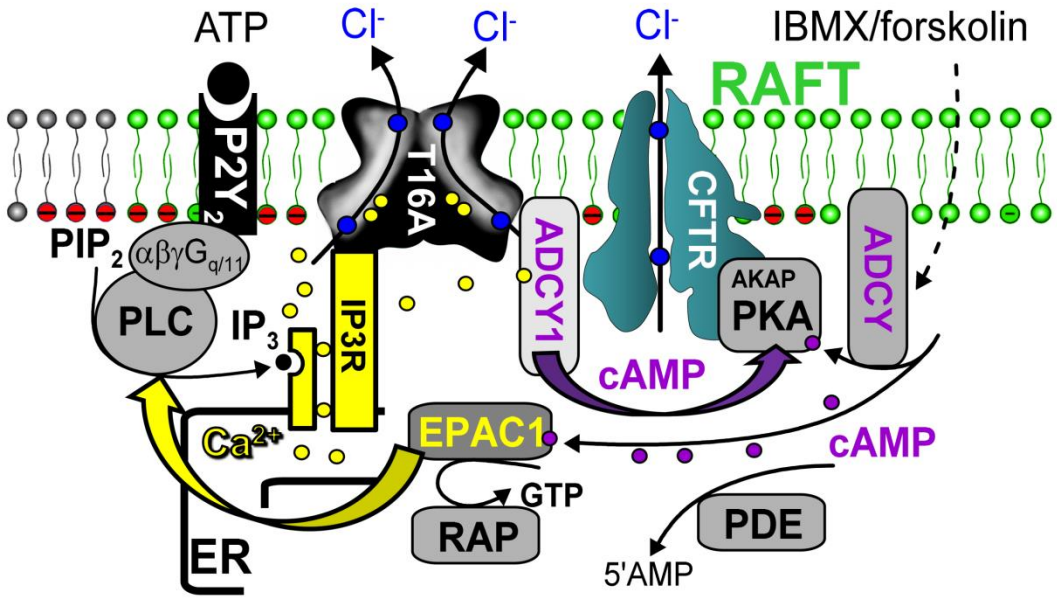

Fig. 36 cAMP/Ca^{2+}-crosstalk activates CFTR and ANO1. Stimulation of purinergic receptors ($P2Y_2$) leads to ER Ca^{2+} store release through IP_3R. Ca^{2+} not only activates ANO1 (T16A), but also stimulates ADCY1 to produce cAMP and to activate CFTR via protein kinase A (PKA). Vice versa, activation of ADCYs by IBMX/forskolin (or through ß-adrenergic stimulation) generates cAMP and activates not only CFTR, but also ANO1 via EPAC1, small GTP-binding protein RAP, PLC and local increase in intracellular Ca^{2+}. Receptors, ANO1, CFTR and signaling molecules are probably co-localized in raft-like plasma membrane microdomains. [Figure by Prof. Dr. Karl Kunzelmann, included with permission].

CHAPTER 3

ANO1 and mucins

1. ANO1 and IL4-induced mucus production

ANO1 is upregulated by several cytokines involved in inflammation and also has a role in goblet cell metaplasia (Caputo *et al.*, 2008; Scudieri *et al.*, 2012a). Indeed, Scudieri *et al.* (2012) reported the ANO1 association with mucin expression in cells related with IL4 treatment, suggesting that ANO1 upregulation by IL4 is an early event for goblet cell differentiation. Furthermore, excessive mucus production is a hallmark of CF and a relevant target to improve the quality of life of CF patients (Amaral, 2015).

Double-tagged ANO1 was used to study the interaction between ANO1 and MUC5AC, one of the most represented mucins in airways (Thornton *et al.*, 2008). For this assay, immunostainings were performed, and four conditions considered: (1) induction of 3HA-ANO1-eGFP expression with dox, (2) induction with dox and treatment with IL4, (3) non-induced cells and (4) cells only treated with IL-4. The results showed that IL4 increases MUC5AC expression in non-induced cells, *i.e.*, cells expressing only endogenous ANO1, as expected. Rather unexpectedly, a higher ANO1 expression by endogenous and double-tagged ANO1 (dox-induced cells) did not increase MUC5AC production. In addition, the higher ANO1 expression removed effect of increasing MUC5AC expression due to IL4 (Fig. 37). The differences in the variation of MUC5AC levels due to IL4 between only endogenous (non-induced) or also double-tagged ANO1 (induced cells) may be caused by negative feedback from an abnormally high level of ANO1. Indeed, Veit *et al.* (2012) reported that CFBE cells overexpressing ANO1 had a significantly attenuated secretion of pro-inflammatory cytokines, compared to cells expressing only endogenous ANO1. The authors suggest that endogenous ANO1 activity is insufficient to modulate the secretion of cytokines, but overexpressed ANO1 can have that effect. Therefore, in our experiment, possibly cells overexpressing ANO1 had lower cytokines concentration than cells only expressing endogenous ANO1, before treatment with IL4. Considering that MUC5AC is partially regulated by higher levels of cytokines such as IL4 and IL8 (Dabbagh *et al.*, 1999; Bautista *et al.*, 2009), in our experiments, ANO1 overexpression possibly modulated MUC5AC expression after IL4 treatment by having an initial lower production of cytokines. Nevertheless, Lin *et al.* (2015) reported that ANO1 overexpression in HBE16 cells promoted mucus production, whereas loss of ANO1 had the opposite effect. However, these variations

are explained by different cell types used and by different levels of overexpression, since in our experiments and those conducted by Veit *et al.* (2012), cells used were CFBE stably expressing ANO1.

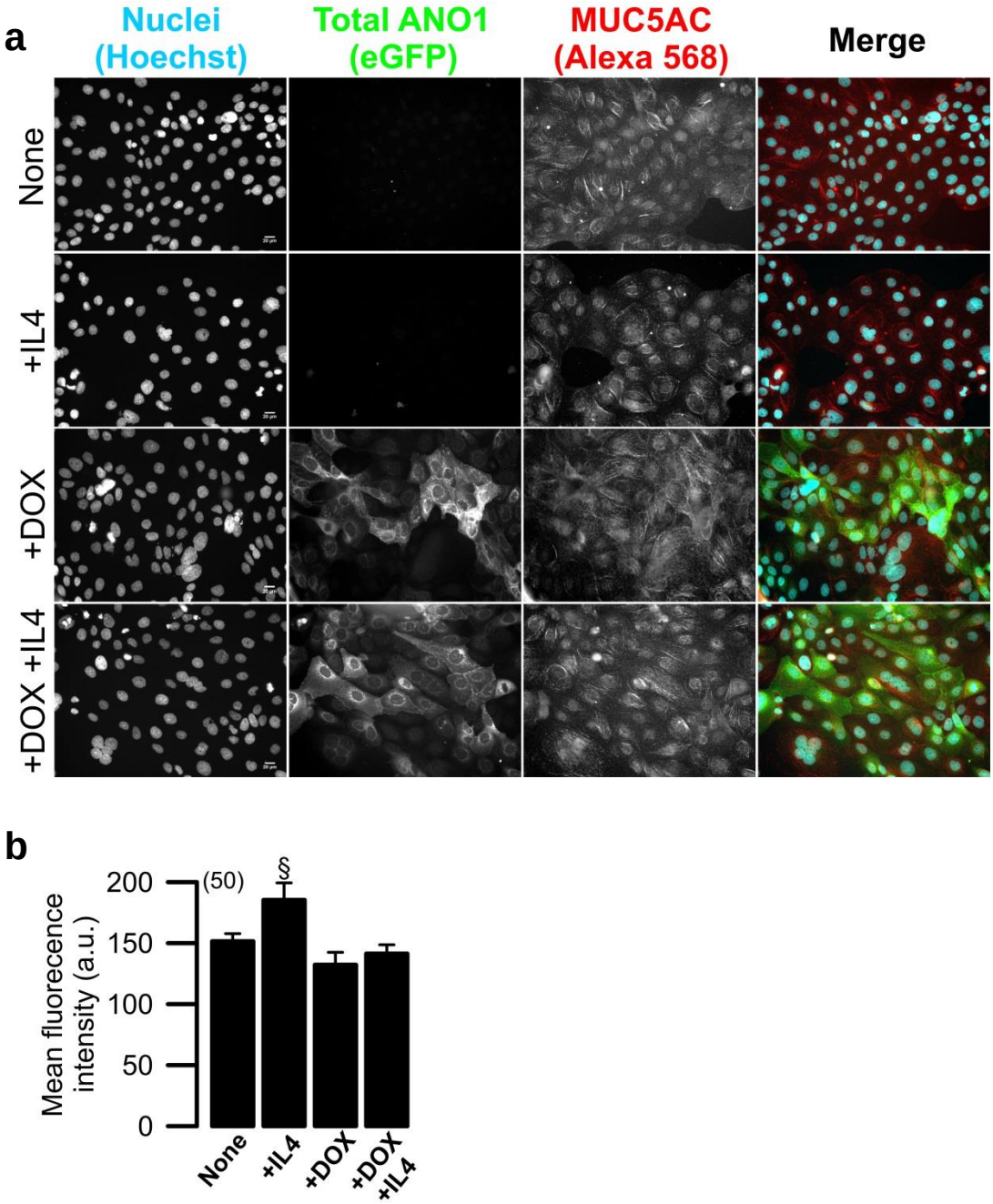

Fig. 37 MUC5AC expression in CFBE-3HA-ANO1-eGFP. (a) CFBE-3HA-ANO1-eGFP cells were treated with DMSO (none), IL4 (+IL4, 10 ng/mL for 48h), induced with dox (+DOX, 1 µg/mL for 48h) or induced with dox and treated with IL4 (+DOX+IL4). Cells were stained with MUC5AC antibody. Images were acquired with Leica DMI 6000B (objective 63x, water); scale bar = 20µM; **(b)** Quantitative assessment of mean fluorescence intensity of MUC5AC fluorescence. a.u. arbitrary units; '§' indicates significant differences compared to all groups ($p \leq 0.05$ in unpaired T-student test); number of analysed cells between brackets.

2. ANO1 and CLCA1 regulation

CLCA1 is a secreted self-cleaving metalloprotease, able to activate Ca^{2+}-dependent Cl^- currents and is linked to chronic inflammatory airway diseases, with particular emphasis on mucus production and release (Alevy *et al.*, 2012; Brett, 2015). Alevy *et al.* (2012) reported that a signalling pathway initiated by environmental stimuli (*e.g.* allergen or virus), stimulates IL13 production, which induces CLCA1 gene expression. Secreted CLCA1 then activates MAPK13 and ultimately increases MUC5AC gene expression and mucus production in airway cells. In another study, Sala-Rabanal *et al.* (2015) described ANO1 modulation by secreted CLCA1. Indeed, CLCA1 mediated an increase of PM ANO1 expression resulting in higher Ca^{2+}-dependent Cl^- currents.

Since CLCA1 is related to both MUC5AC expression and ANO1 expression/activation, it is interesting to further understand this relationship. Therefore, HT-29 cell line was chosen due to its high endogenous ANO1 expression (Namkung *et al.*, 2011; Tian *et al.*, 2012). ATP-induced currents were assessed for HT-29 cells for three conditions: transfection with mock plasmid, transfection with CLCA1 plasmid or neighbouring cells, *i.e.*, non-transfected cells sitting next to CLCA1 expressing cells. By determining the currents of neighbouring cells as well, the secreted CLCA1 paracrine effect in ANO1 was evaluated as previously described by Sala-Rabanal *et al.* (2015).

The results showed higher ATP-induced currents for CLCA1 expressing cells, followed by neighbouring cells and then by mock-transfected cells (Fig. 38). These data suggests that induced ATP-activated currents are modulated by CLCA1 in an autocrine (cells expressing CLCA1) and paracrine (neighboring cells) fashion. Sala-Rabanal *et al.* (2015) suggest that CLCA1 acts in ANO1 PM stabilisation by increasing ANO1 dimerization or reducing its recycling, ultimately also increasing ANO1 currents.

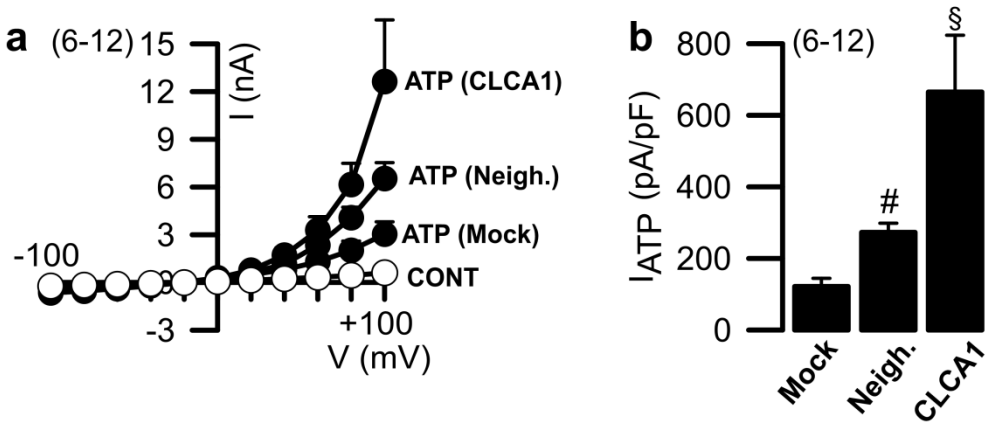

Fig. 38 Effect of CLCA1 in HT29 cells endogenous ANO1 function. (a) Whole-cell patch-clamp data, shown as I/V curves -100mV to +100mV, obtained for HT-29 cells transfected with mock, CLCA1 or neighboring cells (neigh.), *i.e.*, cells sitting next to CLCA1 transfected cells, as a control in Ringer (CONT) or after stimulation by ATP (100 µM); **(b)** Correspondent delta of the average of ATP-induced current densities. '#' indicates significant differences between mock vs CLCA1/Neigh. ($p \leq 0.05$, unpaired T-student test); '§' indicates significant differences compared to all groups ($p \leq 0.05$, unpaired T-student test); number of experiments between brackets.

The CLCA1 effect was also tested in a different cell line, as HT-29 cells are derived from human colon adenocarcinoma (Hekmati *et al.*, 1990) and the primary interest of this project is to study ANO1 in airway cells. Therefore, CFBE cells expressing 3HA-ANO1-eGFP and WT-CFTR were used in similar experiments. Hypothetically, since the double-tagged ANO1 is mostly cytoplasmic (Fig. 9, Fig. 10), higher levels of CLCA1 could switch ANO1 localisation to PM. Moreover, these cells have a minor CLCA-1 expression for both induced and non-induced (Suppl. Fig. 6).

Cells were either transfected with a CLCA1 plasmid or incubated with CLCA1 enriched media to test the possible paracrine effect of this protein (Suppl. Fig. 8). Neither CLCA1 expressing cells nor cells incubated with enriched CLCA1 media showed any difference regarding ANO1 or WT-CFTR PM expression (Fig. 39) or ATP-induced currents (Fig. 40). The differences between CFBE data compared to Sala-Rabanal *et al.* (2015) data and HT-29 cell line results are related either to the use of different cell lines or exogenous vs endogenous ANO1 features. Although endogenous ANO1 in CFBE cells may be affected by CLCA1, the exogenous fraction, which accounts for the majority of total ANO1 expressed in this cell line (Fig. 8), seemingly is not. Hence neither total ANO1 expression nor its function is being significantly affected by CLCA1.

According to these data, 3HA-ANO1-eGFP is not regulated by CLCA1, though we cannot reject the hypothesis that CLCA1 regulates endogenous ANO1 in CFBE cells.

Similar experiments using CFBE cells expressing endogenous ANO1 would have to be performed to assess CLCA1 modulation adequately.

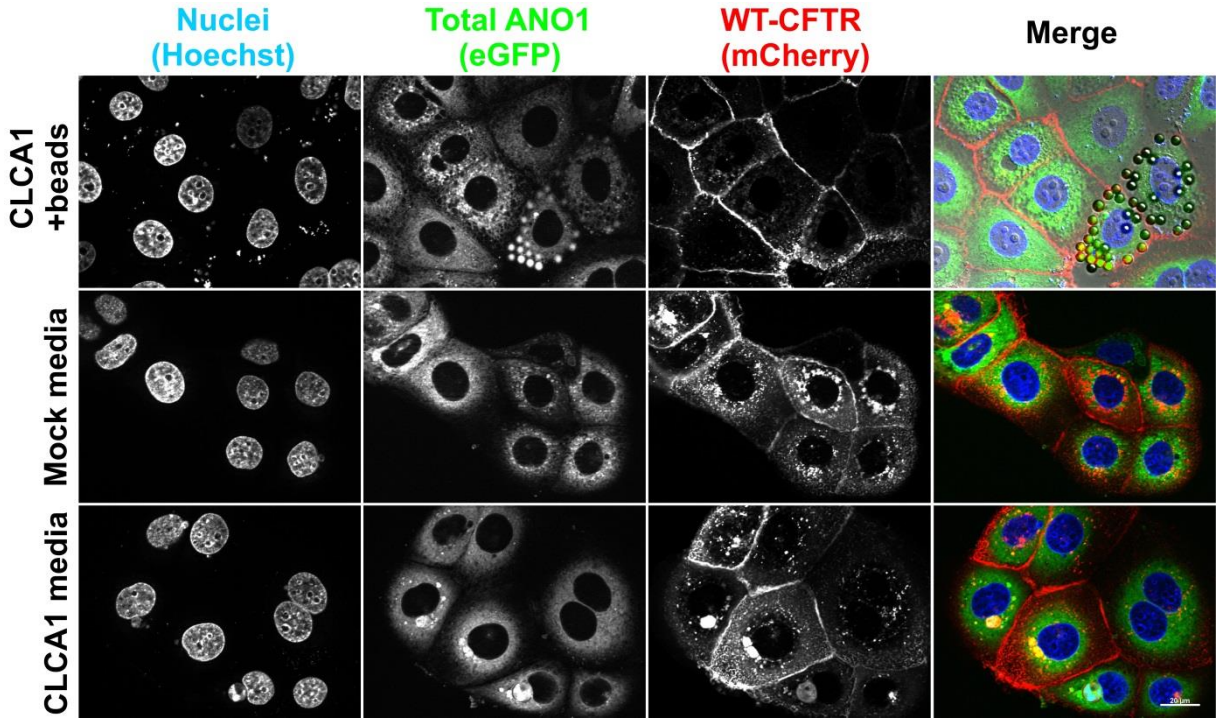

Fig. 39 Effect of CLCA1 in CFBE overexpressing 3HA-ANO1-eGFP and mCherry-flag-WT-CFTR. Live cell imaging of 3HA-ANO1-eGFP (eGFP) and mCherry-WT-CFTR (mCherry). Cells were transfected with CLCA1 and CD8 expressing plasmids (CLCA1+beads), which allows the use of beads coupled to CD8 antibody to detect transfected cells; incubated with mock enriched media or CLCA1 enriched media; images were acquired in Axiovert 200 microscope equipped with an ApoTome (objective 63x, oil); scale bar = 20 µM.

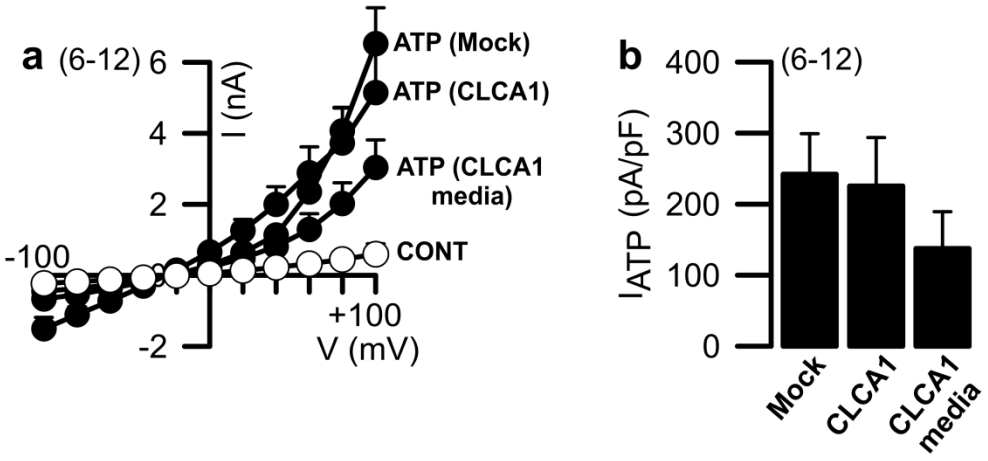

Fig. 40 Effect of CLCA1 in function of CFBE overexpressing 3HA-ANO1-eGFP and mCherry-flag-WT-CFTR. (a) Whole-cell patch-clamp data, shown as I/V curves -100mV to +100mV, obtained for cells transfected with mock or CLCA1 or incubated with CLCA1 enriched media, as a control in Ringer (CONT) or after stimulation by ATP (100 μM); **(b)** Correspondent delta of the average of ATP-induced current densities. Number of experiments between brackets.

3. Conclusions

ANO1 is involved in inflammation and mucus production and release, though there is still some controversy in this field (Caputo *et al.*, 2008). Indeed, ANO1, along with CFTR, are permeable to HCO_3^- (Kunzelmann *et al.*, 1991; Jung *et al.*, 2013), an ion essential for expansion and release of anchored mucus, by removing Ca^{2+} and H^+ cations from condensed mucins (Quinton, 2007, 2008). The lack of functional CFTR in CF reduces HCO_3^- secretion, affecting viscoelastic properties of mucus, namely in airways and pancreas, which culminates with persistent airway infections and pancreas failure (De Boeck and Amaral, 2016). Therefore, it is essential to consider all these factors before accepting ANO1 as an alternative Cl^- channel for CF therapy.

The data herein obtained for CFBE overexpressing 3HA-ANO1-eGFP and also the results reported by Veit *et al.* (2012), indicate that higher ANO1 levels negatively modulate MUC5AC by reducing cytokines production. This feature values the increase in ANO1 cellular expression in CF patients since hypothetically it can reduce inflammation and augment mucin release. Regarding CLCA1 interaction with ANO1, exogenous ANO1 expressed in CFBE cells was not regulated by secreted CLCA1, though we could not reject the possibility that endogenous ANO1 in these cells was also not modulated by such a mechanism.

Finally, double-tagged ANO1, though not entirely mimicking the features of endogenous ANO1 in CFBE cells, is a powerful tool to study ANO1 pathways involved in its traffic, with an impact for mucus therapies.

CHAPTER 4

ANO1, ANO6 and CFTR interaction

1. Effect of ANO1 and ANO6 on CFTR function and expression

ANO6 has a dual function; as a Ca^{2+}-regulated phospholipid scramblase, but also as a component of outwardly rectifying Cl^- channel. Moreover, CFTR positively modulates ANO6 produced Cl^- currents and its expression at the PM (Martins *et al.*, 2011a; Simões *et al.*, 2017). ANO1 and ANO6 are both affected by CFTR and are considered alternative channels with possible application for CF therapy (Bell *et al.*, 2015), so it is fundamental to understand such a relationship adequately.

Several whole-cell patch-clamp assays and immunostainings were performed in Calu-3 cells, which express these three proteins endogenously (Martins *et al.*, 2011a; Jia *et al.*, 2015). The data showed that ANO6 KD alone or together with ANO1 KD, significantly reduced CFTR PM expression, thereby demonstrating CFTR expression dependence on ANO6. However, PM CFTR expression with KD of ANO1 alone revealed no differences compared to scrambled transfected cells (Fig. 41) (KD levels in Suppl. Fig. 9).

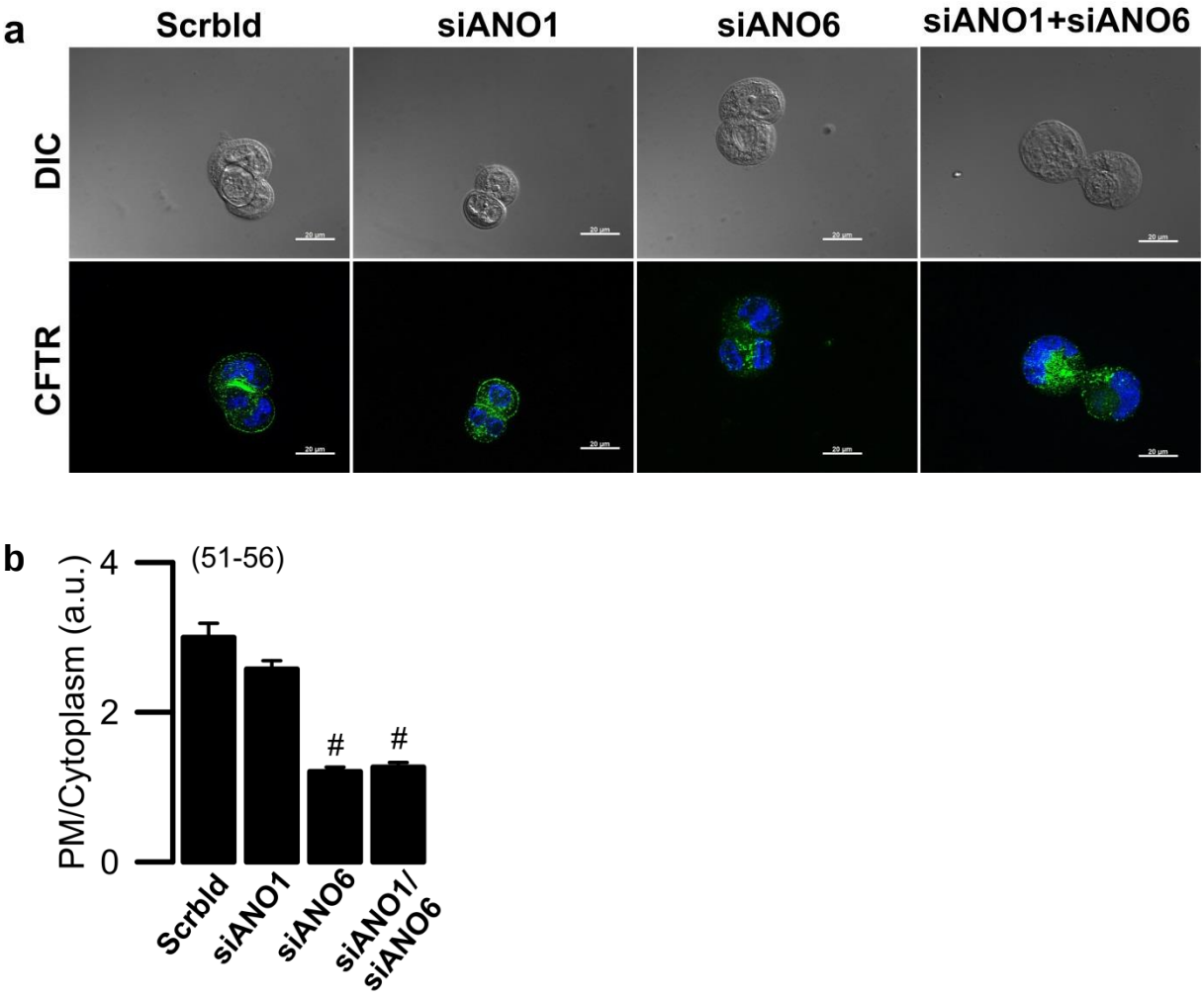

Fig. 41 Effect of siANO1 and siANO6 in CFTR expression in Calu-3 cells. (a) Immunofluorescence of CFTR in Calu-3 cells transfected with scrambled (scrbld), siANO1, siANO6 or both siANO1 and siANO6 (siANO1/siANO6); images were acquired in Axiovert 200 microscope equipped with an ApoTome (objective 63x, oil); scale bar = 20 µM; **(b)** Analysis of cellular distribution of CFTR in Calu-3 cells by quantitative assessment of fluorescence in plasma membrane/cytoplasm. a.u., arbitary units; '#' indicates significant differences compared to scrambled ($p \leq 0.05$, unpaired T-student test); number of cells between brackets.

To further understand this relationship, I/F-induced currents were measured in Calu-3 cells under the same conditions used in the immunostainings. Similarly to expression data, ANO1 KD did not affect Cl^- currents, in contrast to KD of ANO6 alone or in combination with ANO1, which significantly reduced CFTR currents (Fig. 42, a, b). This decreased activity correlates with diminished CFTR PM fraction, but possibly also with Ca^{2+} reduction near CFTR.

As mentioned above, CFTR Cl^- activity is affected by lower Ca^{2+} availability caused by reduced activation of Ca^{2+}-sensitive ADCYs. Indeed, it is suggested that ANO6 proteins couple Ca^{2+} signals to membrane-localised channels (Kunzelmann, 2015; Cabrita *et al.*, 2017). To test this hypothesis, currents were measured with I/F and an ionophore (to increase global Ca^{2+}) in scrambled or siANO6 transfected cells. Added ionomycin raised Cl^- currents compared to I/F alone, though not significantly (Fig. 42, c, d).

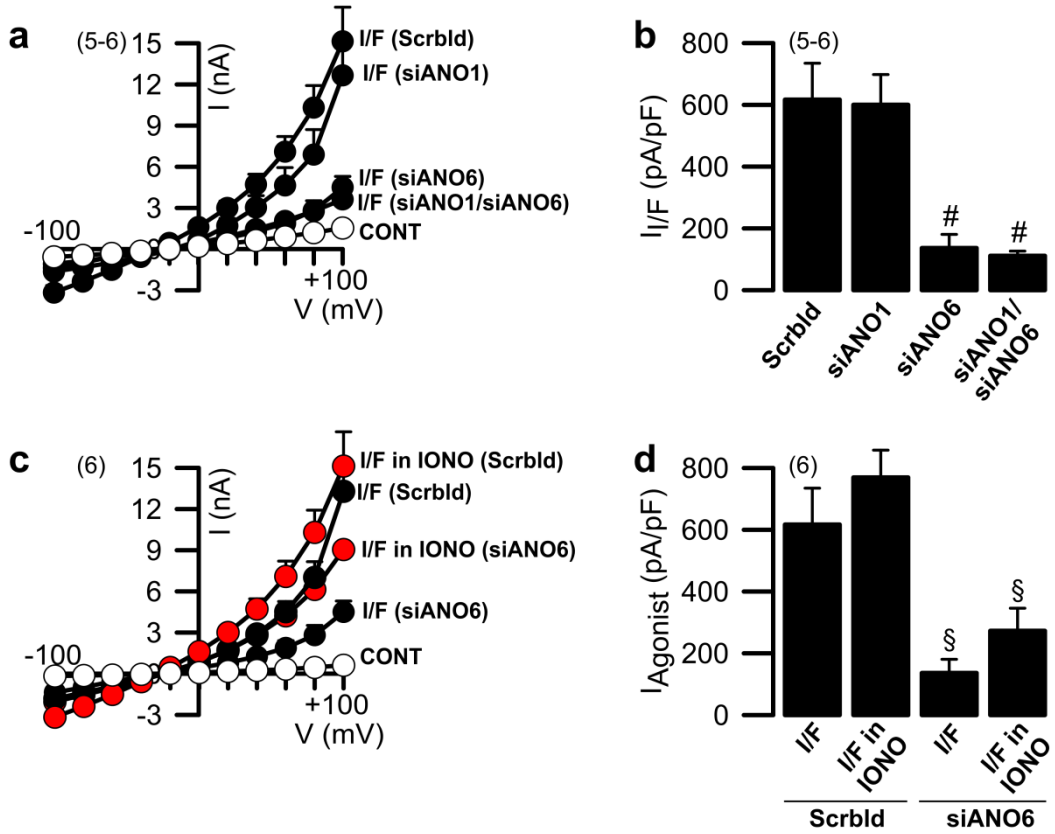

Fig. 42 Effect of siANO1 and siANO6 in CFTR function in Calu-3 cells. (a) Whole-cell patch-clamp data, shown as I/V curves -100mV to +100mV, obtained for Calu-3 cells transfected with Scrambled (Scrbld), siANO1, siANO6 or both siANO1 and siANO6 (siANO1/siANO6), as a control in Ringer (CONT) or after stimulation with IBMX/Forskolin (I/F, 2 µM/100 µM); **(b)** Correspondent delta of the average I/F-induced current densities; **(c)** Whole-cell patch-clamp data, shown as I/V curves -100mV to +100mV, obtained for cells transfected with Scrambled (Scrbld) or siANO6 as a control in Ringer (CONT) or after stimulation with IBMX/Forskolin (I/F, 2 µM/100 µM) or IBMX/Forskolin in ionomycin (I/F (2 µM/100 µM) in IONO (1 µM)); **(d)** Delta of the average of I/F- or I/F in IONO-induced current densities. '#' indicates significant differences compared to scrambled ($p \leq 0.05$ in unpaired T-student test); '§' indicates significant differences in cells transfected with scrambled vs siANO6 with the same stimulus (either both I/F of I/F in IONO) ($p \leq 0.05$ in unpaired T-student test); number of experiments between brackets.

In Calu-3 cells, ANO6, but not ANO1, is essential for CFTR PM expression/activation either by increasing its traffic and stabilisation at PM (*e.g.* by

reducing CFTR recycling), or by local Ca^{2+} changes at the PM. These results suggest that CFTR requires that at least one member of anoctamin family traffics to the PM in order to maintain its PM localisation and also for its function as a Cl^- channel. CFTR cytoplasmic expression observed only with ANO6 KD is probably related to ANO1 and ANO6 different cellular localisation. Indeed, Calu-3 cells ANO1 expression is mainly cytoplasmic, while ANO6 is mostly located at PM (Suppl. Fig. 9).

The reduction in CFTR activation associated with ANO6 KD is caused (at least partially) by a decrease of CFTR levels at the PM, but other factors may also be involved. Indeed, recently Cabrita *et al.* (2017) reported that ANO1, ANO5, ANO6 and ANO10 affect release of Ca^{2+} from ER stores. Seemingly, by modulating cellular Ca^{2+} signalling, anoctamins activate CFTR by SOcAMPs and Ca^{2+}-sensitive ADCYs. Indeed, the SOcAMPs pathway empties ER Ca^{2+} store thereby increasing cAMP levels, regardless of cytosolic Ca^{2+} levels, therefore connecting cellular Ca^{2+} stores directly to cAMP signalling (Lefkimmiatis *et al.*, 2009; Benedetto *et al.*, 2017).

Regarding the functional data from cells stimulated with I/F and ionomycin, there was a trend for higher currents compared to I/F alone, though not significant. Ionomycin directly increases Ca^{2+} cellular availability, which increases cAMP levels by activating Ca^{2+}-sensitive ADCYs, ultimately inducing CFTR. However, Lefkimmiatis *et al.* (2009) described in NCM460 cells that stimulation with forskolin and ionomycin caused an initial reduction in cAMP levels followed by its gradual augmentation. Therefore, in our experiments, the stimulation may not have been long enough to increase cAMP levels to the same level as scrambled transfected cells. Furthermore, since ANO6 KD dramatically reduced CFTR fraction at PM, ionomycin effect is diluted.

In accordance with the previous data, HEK293T cells overexpressing WT-CFTR and transfected with siANO1 and siANO6 registered a reduction in I/F-induced currents comparable to that obtained by CFTR inhibitor 172 (Fig. 43, a, b). This further suggests the requirement of anoctamin members for proper CFTR activation.

Finally, to study a possible role of ANO6 in ANO1 activation, HEK293T cells were transfected with ANO1, ANO6 or both, and stimulated with ATP. Expression of ANO6 alone, as expected, showed no ATP-induced activation, as ANO6 Cl^- channel activity is strongly activated by ionomycin, but only weakly activated by GPCRs stimulation (Tian *et al.*, 2012). Surprisingly, ATP-induced currents were considerably higher in the presence of both ANO1 and ANO6, in comparison to ANO1 alone (Fig. 43, c, d).

Indeed, ANO6 synergistically acts in ANO1 activation, probably by increasing Ca^{2+} availability, followed by higher ANO1 derived currents.

Bearing in mind previous data in Calu-3 cells, ANO6 has a central role in CFTR and ANO1 function as Cl^- channels, probably by modulating Ca^{2+} availability at the cell. Therefore, ANO6 is also a viable candidate for future CF therapy, as it may increase overall Cl^- activity through CFTR and ANO1.

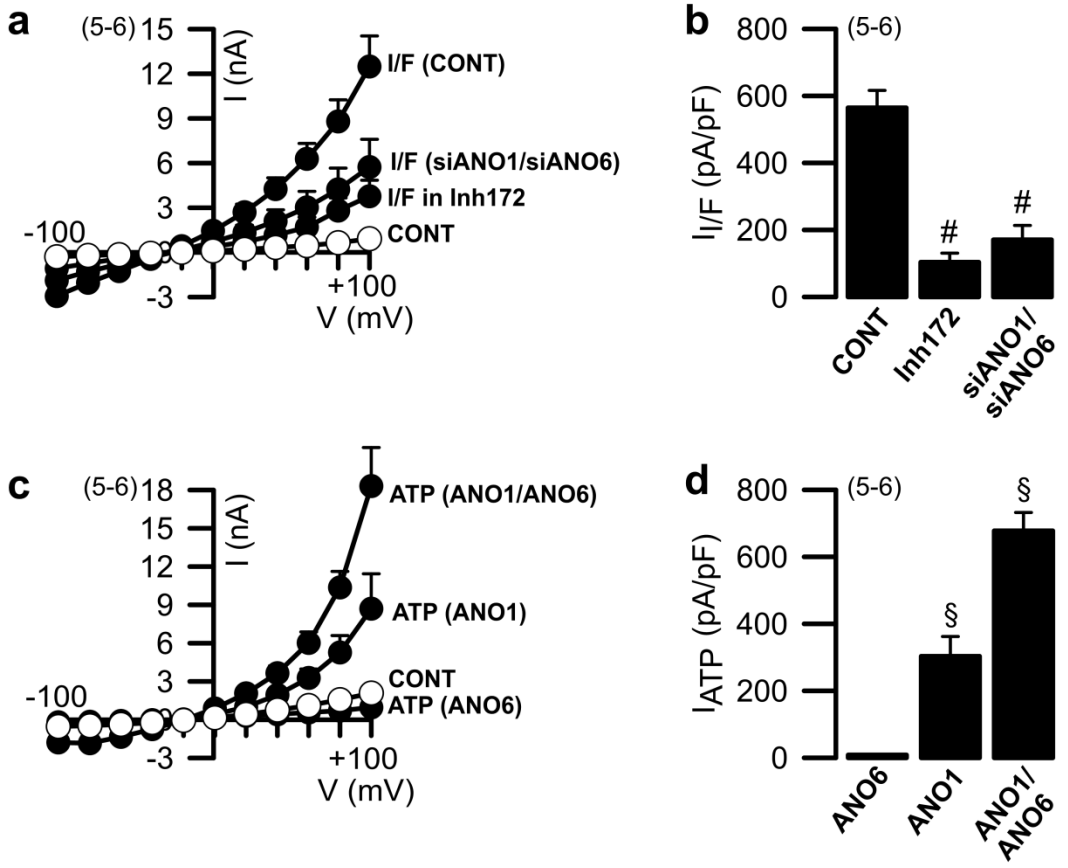

Fig. 43 Effect of ANO1 and ANO6 expression levels on CFTR function in HEK293T cells. (a) Delta of the average IMBX/Forskolin-induced currents (I/F, 2 µM/100 µM) currents in cells transfected with CFTR (CONT) and inhibited by CFTR inhibitor 172 (Inh 172, 20 µM) or by transfection with siANO1 and siANO6 (siANO1/siANO6); **(b)** Correspondent delta of the average I/F-induced current densities; **(c)** Whole-cell patch-clamp data, shown as I/V curves -100mV to +100mV, obtained in cells transfected with ANO1, ANO6 or both (ANO1/ANO6), as a control in Ringer (CONT) or after stimulation with ATP (100 µM); **(d)** Correspondent delta of the average ATP-induced current densities. '#' indicates significant differences compared to control (CONT); '§' indicates significant differences compared to all groups ($p \leq 0.05$ in unpaired T-student test); number of experiments between brackets.

2. Conclusions

Anoctamins have long been associated with CFTR and considered as alternative channels for CF therapy. Indeed, this concept allows the bypassing of CFTR channel, so that theoretically can be used for all CF patients, regardless of CFTR mutation class (Bell *et al.*, 2015). Both ANO1 and ANO6 are possible candidates for such therapy, and that is why understanding their relationship and co-regulation with CFTR, and possible shared pathways is valuable in the CF field. The data described in this chapter suggests that CFTR requires at least one member of anoctamin family for its proper PM expression and function. In addition, ANO6 potentiates ANO1 channel Cl^- activity, likely by increasing Ca^{2+} cellular availability.

As a proposed approach for CF therapy, it would be beneficial to pharmacologically increase expression of both ANO1 and ANO6. Indeed, this would allow (1) the improvement of CFTR PM expression and function in cases where CFTR is still functional; (2) the increase of Cl^- secretion directly due to higher PM expression of ANO1 and (3) the increase of Cl^- secretion by a synergistic action of ANO6 in ANO1. The results described here provide new knowledge on the relationship and co-regulation of anoctamins and CFTR and could have a significant impact on the discovery of new drugs for CF.

V. General Discussion and Future Perspectives

Although significant efforts have been made to discover novel therapeutic approaches for CF, most treatments are still symptom-guided, and existing drugs are not applicable to all patients. The symptomatic treatments involve mucolytics, antibiotics for existing infections or as a preventive measure, anti-inflammatory drugs to reduce chronic lung infection, and, ultimately, lung transplant (De Boeck and Amaral, 2016).

Nowadays, only three FDA approved drugs exist, ivacaftor (potentiator, VX-770), lumacaftor (corrector, VX-809) and tezacaftor (corrector, VX-661), which only benefit patients with specific mutations. Indeed, ivacaftor benefits patients with gating mutations (approximately 5% of all patients) and some with residual function mutations, and lumacaftor in combination with ivacaftor benefiting patients who are homozygous for F508del (approximately 40-45% of all patients) (De Boeck *et al.*, 2014; Moss *et al.*, 2015). Nevertheless, treatment with such drugs is costly, which is a significant issue for a large number of patients (Bush and Simmonds, 2012; Whiting *et al.*, 2014).

Nowadays, 'mutation agnostic' pharmacological treatments are not available, which ideally could be applicable for all patients. These treatments could include gene therapy, cell-based therapies, activation of alternative ion channels that bypass CFTR (*e.g.* anoctamins) or inhibition of ENaC channel. ANO1 channel is expressed in a multiplicity of tissues affected by CF, such as lungs and pancreas and it can transport both Cl^- and HCO_3^- (Kunzelmann *et al.*, 2011). Furthermore, ANO1 is present in both CF and WT epithelial tissues, though in different levels (Ruffin *et al.*, 2013). Therefore, to search for drug candidates that act more efficiently and can be used in a broader range of patients, it is essential to discover new anoctamin traffic modulators and also to understand better the relationship between anoctamins and CFTR.

A novel cell-based traffic assay to identify potential ANO1 traffic regulators

The first goal of this doctoral thesis was to create a cellular platform to identify ANO1 traffic regulators by applying a similar technique already used by our group in CFTR (Botelho *et al.*, 2015). A double-tagged ANO1 was used, with an eGFP tag at C-terminus to determine total ANO1 expression, and a 3HA tag at the first extracellular loop, accounting for the PM ANO1 fraction. Hence, traffic enhancement or inhibition is determined by 3HA/eGFP ratio (PM ANO1/total ANO1). Importantly,

the 3HA-ANO1-eGFP was cloned to a lentiviral vector with inducible features (pLVX-TRE3G), *i.e.*, the ANO1 expression only begins after cells' incubation with dox. This feature is of critical importance to properly evaluate the effect of siRNAs or drugs before starting ANO1 traffic.

Three original cell lines expressing 3HA-ANO1-eGFP were produced and characterised for ANO1 expression, function and inducibility. The results obtained determined that double-tagged ANO1 resemble endogenous ANO1 characteristics and thus is physiologically relevant. Undeniably, our goal is to use a non-physiological system (exogenous ANO1) to discover enriched gene pathways important for drug development for CF patients. Indeed, from the nine genes that altered 3HA-ANO1-eGFP traffic and were further validated by whole-cell patch-clamp, four of them also changed endogenous ANO1 function. Therefore, these double-tagged ANO1 cellular systems have several usages, such as (1) identification of ANO1 regulators by using siRNA molecules, data which may be applied either to (2) drug development or (3) to identify compounds modulators of ANO1 traffic.

It is noteworthy that two CFBE cell lines expressing 3HA-ANO1-eGFP and CFTR were created and characterised. In future, these cell lines may be used to further understand the relationship between ANO1 and WT-/F508del-CFTR. Finally, the 3HA-ANO1-eGFP construct can be used in other cellular systems more relevant in clinical fields besides CF, opening new doors for the possibilities of such a system. ANO1 has a role in other respiratory diseases such as asthma or specific respiratory pathological symptoms as excessive mucus secretion (Scudieri *et al.*, 2012a; Huang *et al.*, 2012), and also in tumorigenesis (Wanitchakool *et al.*, 2014). In these cases, it may be necessary to use the double-tagged ANO1 in other cell types or to search for ANO1 negative traffic modulators, which it was also achieved here with this 3HA-ANO1-eGFP.

Compartmentalized crosstalk of CFTR and ANO1

An unexpected result from the primary ANO1 traffic screen was the recognition of a singular link between GPCRs and ANO1, further revealed during this doctoral thesis. Indeed, a positive association between $P2RY_2$ expression levels and ANO1 and WT-/F508del-CFTR currents was identified. Similar assays were performed overexpressing different GPCRs with related results, confirming that this relationship was not $P2RY_2$ specific, but related to global GPCRs expression.

The resulting data inferred that cAMP- and Ca^{2+}-dependent Cl^- currents in airway epithelial cells overlap due to intracellular crosstalk involving EPAC1 and Ca^{2+}-sensitive ADCYs. These results further clarified previous reports regarding the 2-phases/components of Cl^- currents observed in oocytes overexpressing WT-CFTR (Faria *et al.*, 2009) or in intestinal T84 cells (Domingue *et al.*, 2016). Additionally, this overlap occurs in a shielded membrane compartment, with localised Ca^{2+} rise not interfering in its global concentration.

Our data demonstrates new roles of ANO1 in CFTR function, determining that CFTR Cl^- currents can partially pass through ANO1 channels. Therefore, drugs that activate ANO1 will also increase CFTR function, further enhancing Cl^- secretion in CF patients. Moreover, as this overlap requires EPAC1 and Ca^{2+}-sensitive ADCYs, targeting these molecules could also be interesting for future drug development. By affecting pathways interfering with GPCRs expression, cell membrane may be enriched with lipid rafts compartments and both ANO1 and CFTR function may be indirectly increased without changing their expression. The next step to validate the application of these results would be to compare with similar experiments in primary lung cells or nasal cells of patients.

ANO1 and mucins

The wide range of applications of the 3HA-ANO1-eGFP cellular system allowed us to explore other topics, such as the relationship of this protein with mucus, namely mucin production. As extensively reported, mucins and ANO1 are intimately related, but controversial concepts are present within this field. Indeed, ANO1 inhibitors reduce mucin secretion (Huang *et al.*, 2012), but, as this channel also conducts HCO_3^- ions, ANO1 may also be important for mucin expansion and release (Scudieri *et al.*, 2012a; Jung *et al.*, 2013). Another factor adding to this controversy is the difference between exogenous and endogenous ANO1 modulation of cytokines production, as previously reported by Veit *et al.* (2012) and confirmed by the data of this research. These differences are probably caused by a remarkably higher level of ANO1 in overexpressing cells, which is not enough if solely endogenous ANO1 is considered. Therefore, by increasing ANO1 activation, cytokines level may reduce with diminished mucin production, ultimately improving patients' health. In addition, ANO1 higher function may also increase mucin expansion and release due to its permeability to HCO_3^-, thereby reducing mucus thickness.

Finally, the data herein obtained demonstrate that double-tagged ANO1 can also be used to assess molecules or pathways as potential modulators of mucin production and secretion.

Anoctamin family members and CFTR

Recent data has highlighted the importance of anoctamin family in CFTR expression and function (Benedetto *et al.*, 2017; Simões *et al.*, 2017). As both ANO1 and ANO6 are possible alternative Cl^- channels in CF therapy, it was interesting to further assess the relationship between these proteins. Interestingly, the results suggested that CFTR requires at least one anoctamin member for its expression at the PM. Moreover, according to these data and previous reports, it is suggested that ANO1 or ANO6 (1) travel together with CFTR; (2) stabilise CFTR at the PM and/or (3) provide a Ca^{2+} source and further activate CFTR by Ca^{2+}-sensitive ADCYs. These data prove that stimulating common pathways for both ANO1 and ANO6, instead of ANO1 only, may be valuable in increasing Cl^- currents to a more considerable value.

Future perspectives

Despite the extensive scientific data published in the CF field, the life expectancy of CF patients is still low (~37.5 years), being often a lung transplant required to increase survival (MacKenzie *et al.*, 2014). In addition, treatments are mostly symptom-guided, and available drugs are costly and do not serve all CF patients. There is thus an urgent unmet need for a drug that can be used regardless of CFTR mutation class, i.e., ‘mutation-agnostic’. Activation of alternative channels already expressed in CF-affected organs is a possibility which has been widely explored. Nevertheless, a drug targeting $P2RY_2$ activating ANO1 (INS37217, denufosol) failed to show any benefit on phase III of clinical trials with CF patients (Moss, 2013), emphasizing the need to develop new compounds.

A future task would be to test the validated hits in the other two new cell lines that express both double tagged ANO1 and CFTR. On the other hand, the relationship of GPCRs with CFTR and ANO1 also provides a hint to a new pathway of novel drug targets for CF treatment. Indeed, by affecting the expression of such proteins and not by directly stimulating them, overall Cl^- currents can be increased by increasing localized Ca^{2+} signalling, activating ANO1 as well as CFTR.

The data obtained from this doctoral thesis are a step forward to the cure of this life-shortening disease as they provided further knowledge on alternative channels and possible modulatory pathways for their expression and activation. Potential follow-up to this work is:

1. Determining the mechanism of action from the functional validated hits in ANO1 protein;
2. Defining the effect of such hits on CFBE overexpressing both 3HA-ANO1-eGFP and WT-/F508del-CFTR to further understand their role in ANO1 and CFTR;
3. Validating the impact of the expression of GPCRs in a more physiological system, *i.e.*, CF patients' primary cells;
4. Testing small compounds/drugs in these new cell lines to obtain novel traffic modulators of ANO1 and CFTR channels.

VI. Appendix – Supplementary Figures

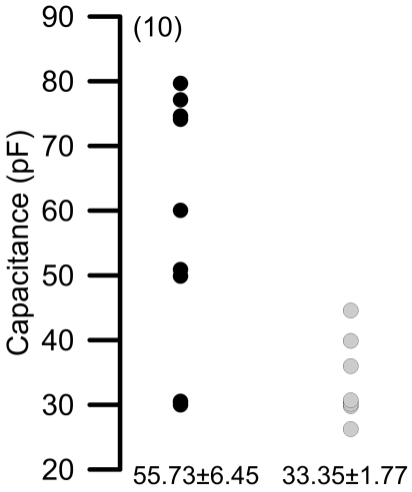

Suppl. Fig. 1 Capacitance measurements for CFBE-3HA-ANO1-eGFP cells. Values of capacitance (pF) measured in CFBE-3HA-ANO1-eGFP cells non-induced (black circles) or induced for 48h with dox (grey circles). Capacitance values, which can be used as a measurement of cell size, are higher in non-induced compared with induced cells. At the bottom, values of average ± SEM.

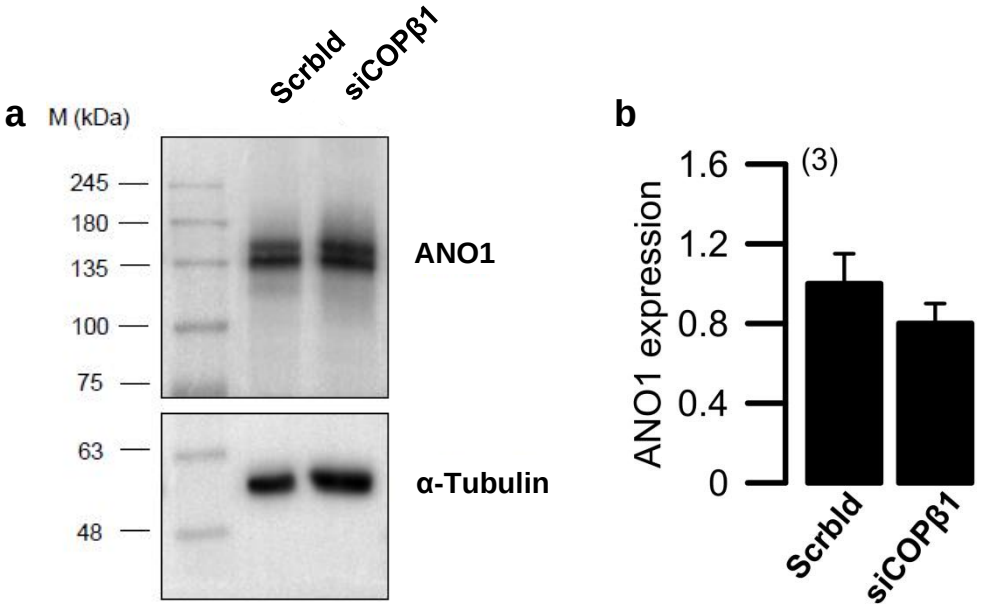

Suppl. Fig. 2 ANO1 expression after KD of COPβ1 in CFBE-3HA-ANO1-eGFP. **(a)** Western-Blot of CFBE-3HA-ANO1-eGFP cells transfected with siRNA against COPβ1 (siCOPβ1) or scrambled (Scrbld), where cells were induced with dox. α-Tubulin was used as a loading control and molecular mass markers are shown on the left; **(b)** KD of COPβ1 does not change the expression of double-tagged ANO1. 3HA-ANO1-eGFP expression was normalized for α-Tubulin levels. [Data obtained by Madalena Pinto and included with permission].

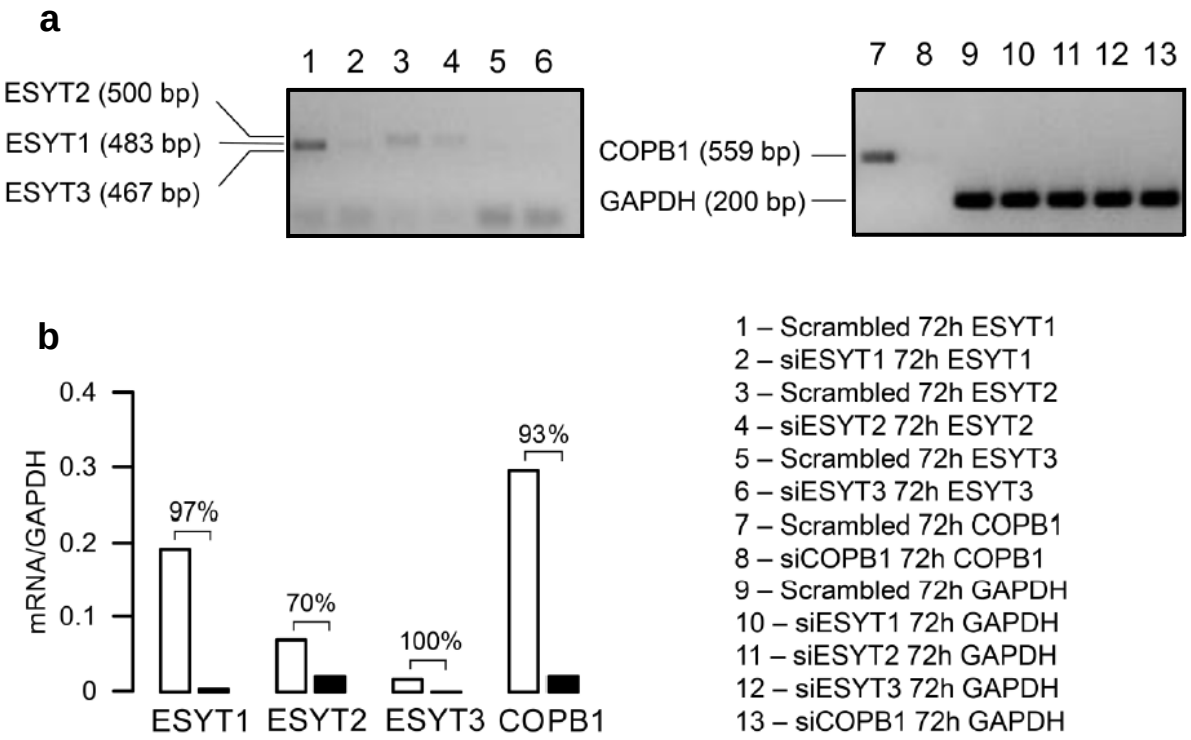

Suppl. Fig. 3 Endogenous levels of extended synaptotagmins (ESYT1, 2 and 3) and COPβ1 in CFBE-3HA-ANO1-eGFP cells and effect of siRNA KD. (a) Products of RT-PCR performed in CFBE-3HA-ANO1-eGFP cells induced for 48h with dox to assess endogenous levels of ESYT1, ESYT2, ESYT3 and COPβ1. Cells were transfected either with Scrambled or with siRNAs targetting those genes; **(b)** Summary of data in (a), where KD efficiencies (shown as numbers above bars) were determined by comparing the mRNA levels of ESYT1-3 or COPβ1 in the siRNA transfected cells with those in cells transfected with Scrambled.

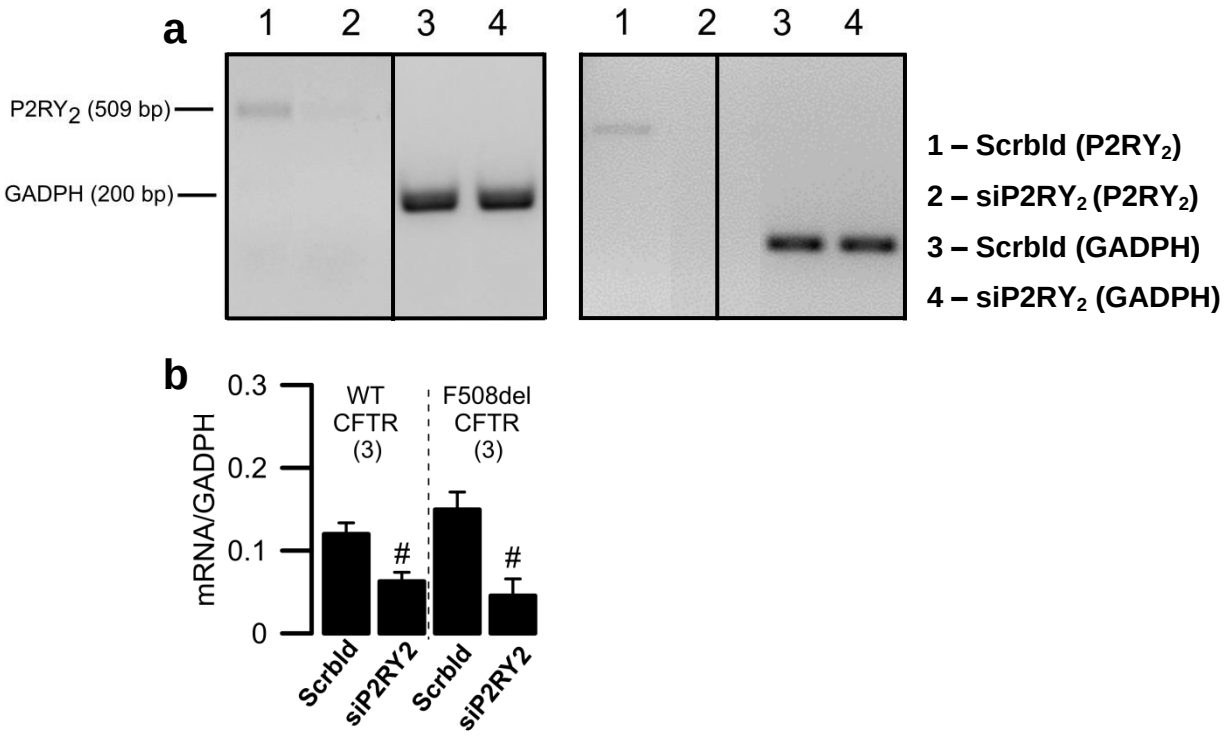

Suppl. Fig. 5 Endogenous levels of $P2RY_2$ in CFBE cells and effect of siRNA KD. (a) Products of RT-PCR in WT-CFTR/CFBE (left) or F508del-CFTR/CFBE (right) to assess endogenous levels of $P2RY_2$. Cells were transfected either with Scrambled (Scrbld) or with siRNA targeting $P2RY_2$ ($siP2RY_2$); **(b)** Summary of data in (a), showing KD of $P2RY_2$. '#' indicates significant differences between Scrambled vs $siP2RY_2$ ($p \leq 0.05$, unpaired T-student test).

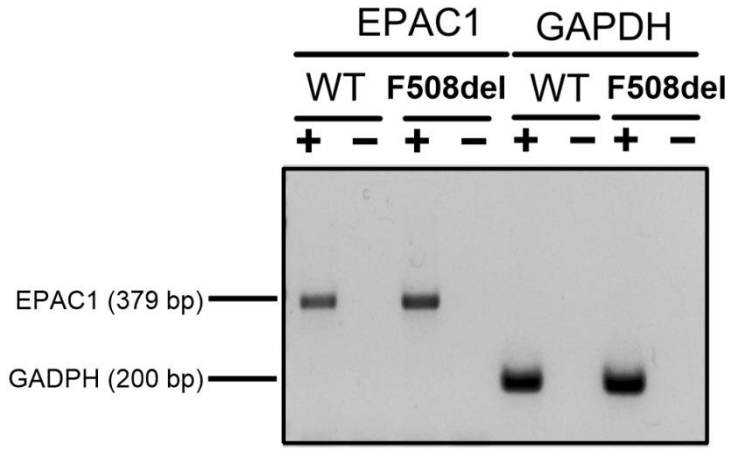

Suppl. Fig. 4 EPAC1 expression in CFBE cells. RT-PCR demonstrating expression of EPAC1 in WT-CFTR/CFBE cells (WT) and F508del-CFTR/CFBE cells (F508del).

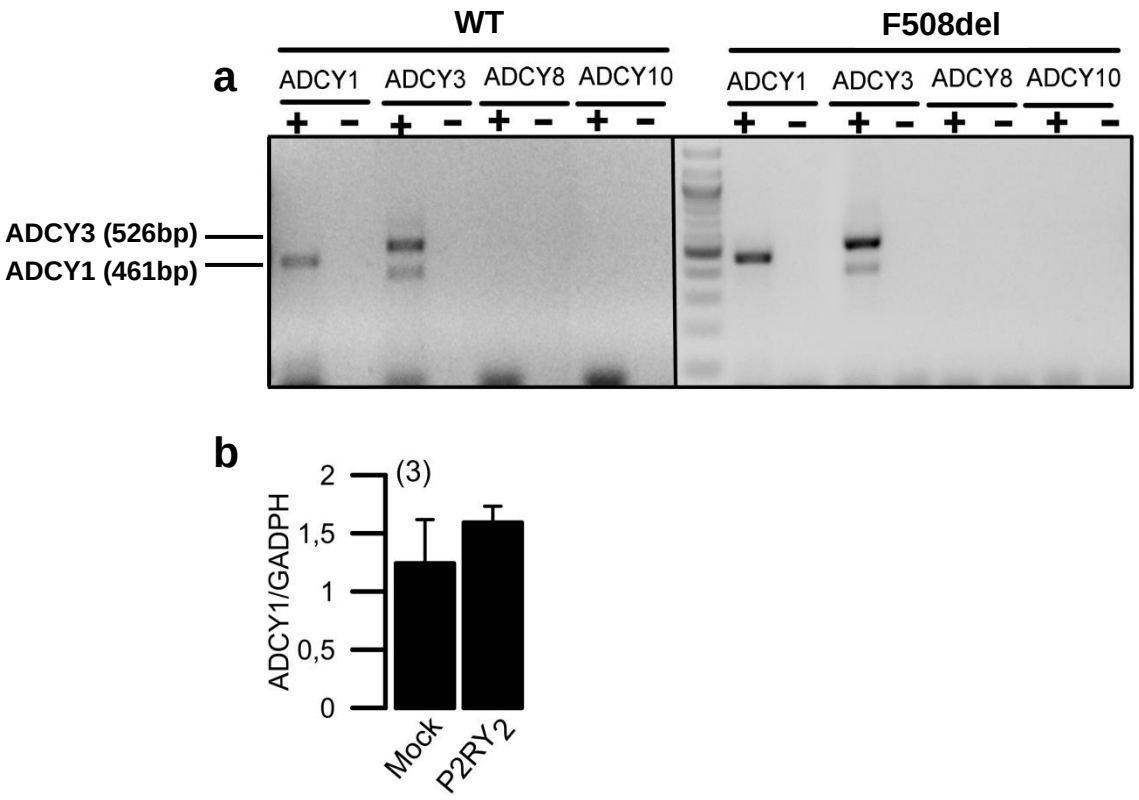

Suppl. Fig. 7 ADCYs expression in CFBE cells. (a) RT-PCR indicating expression of Ca^{2+}-sensitive ADCY1 and 3, but not 8 and 10 in WT-CRFTR/CFBE (WT) or F508del-CFTR/CFBE (F508); **(b)** Relative expression of ADCY1-mRNA in mock or $P2RY_2$ transfected WT-CFTR/CFBE cells.

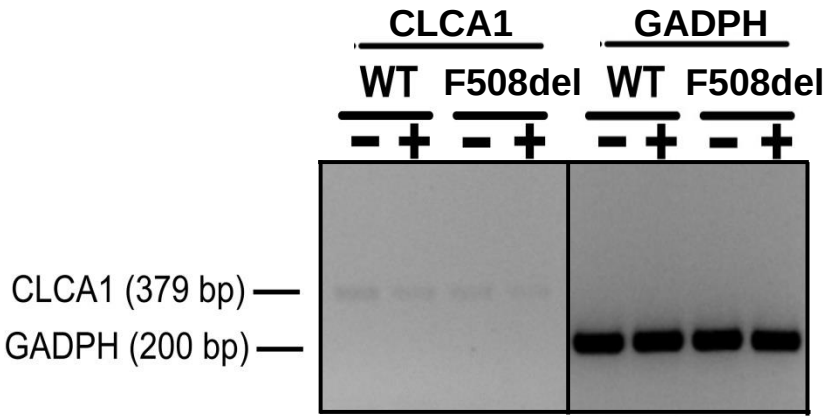

Suppl. Fig. 6 CLCA1 expression in CFBE cells. RT-PCR demonstrating the low expression of CLCA1 in WT-CFTR/CFBE cells (WT) and F508del-CFTR/CFBE cells (F508del) non-induced (-) or induced for 48h with dox (+).

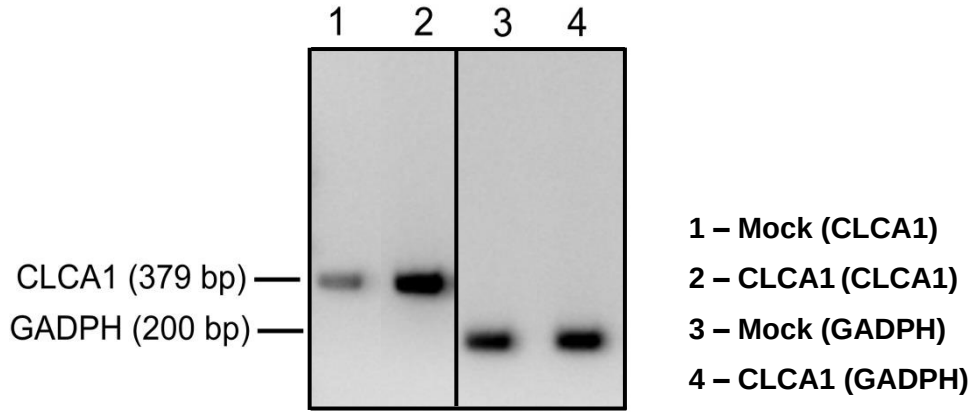

Suppl. Fig. 8 CLCA1 expression in HEK293T cells. RT-PCR demonstrating CLCA1 expression in HEK293T cells transfected with mock or CLCA1 expressing plasmids.

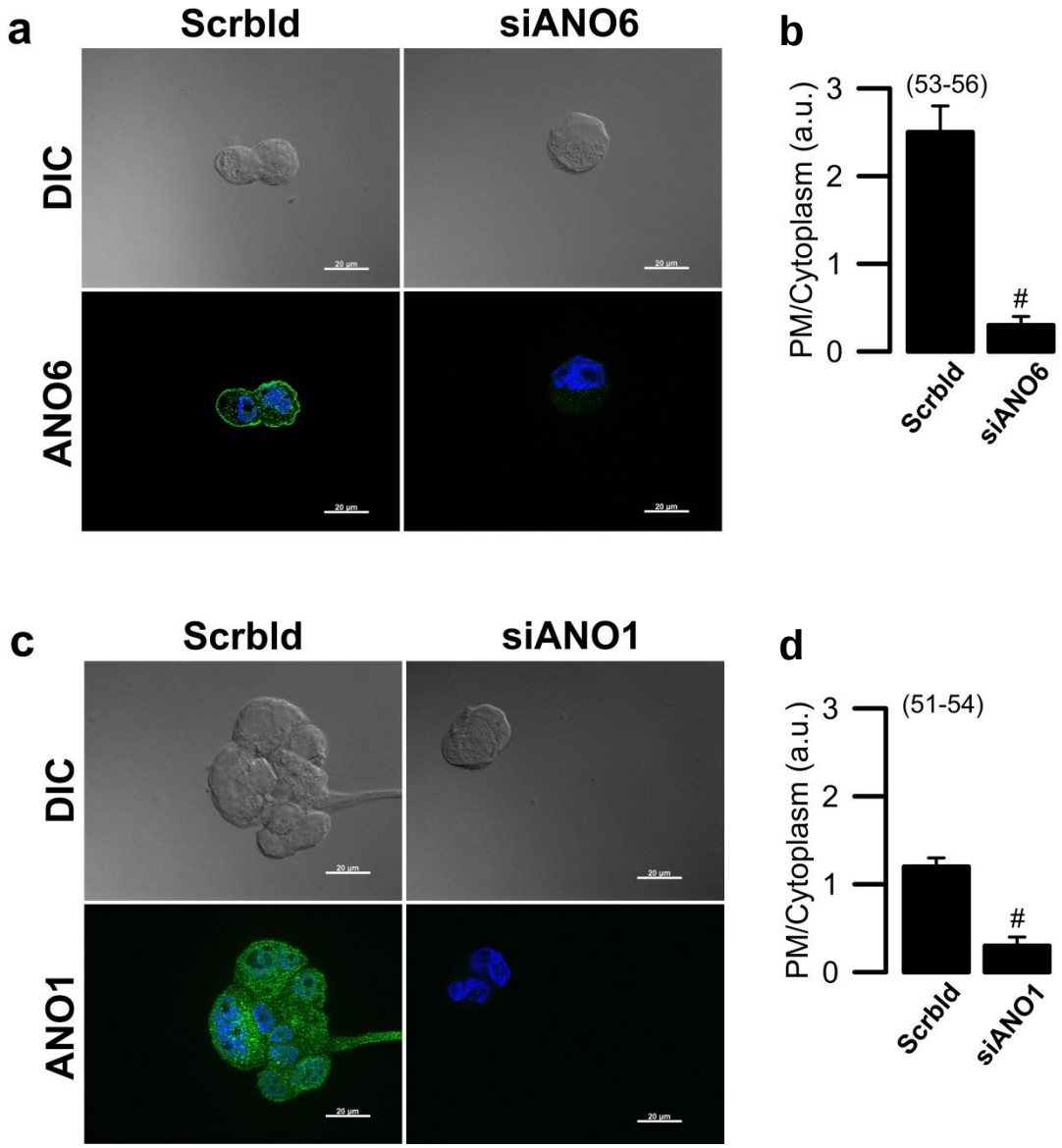

Suppl. Fig. 9 Assessment of ANO6 KD and ANO1 KD in Calu-3 cells. (a,b) Immunofluorescence of ANO6 in Calu-3 cells transfected with scrambled (Scrbld) or siANO6 (a) and respective analysis of cellular ANO6 distribution by quantitative assessment of fluorescence in plasma membrane/cytoplasm (b); images were acquired in Axiovert 200 microscope equipped with an ApoTome (objective 63x, oil); scale bar = 20 µM; **(c,d)** Immunofluorescence of ANO1 in Calu-3 cells transfected with scrambled (Scrbld) or siANO1 (c) and respective analysis of cellular ANO1 distribution by quantitative assessment of fluorescence in plasma membrane/cytoplasm (d); images were acquired in Axiovert 200 microscope equipped with an ApoTome (objective 63x, oil); scale bar = 20 µM. a.u. arbitrary units; '#' indicates significant differences between Scrambled vs siANO6/siANO1 ($p \leq 0.05$, unpaired T-student test); number of analyzed cells between brackets.

VII. References

References

Cystic Fibrosis Mutation Database. CFMDB Statistics (2018, January). Retrieved from http://www.genet.sickkids.on.ca/cftr/

Uniprot Database (2018, January). Retrieved from http://www.uniprot.org

Vertex Pharmaceuticals Incorporated. A Study Evaluating the Safety and Efficacy of VX-440 Combination Therapy in Subjects With Cystic Fibrosis (2018, January). Retrieved from http://clinicaltrials.gov/ct2/show/NCT02951182.

Adomaviciene, A., K.J. Smith, H. Garnett, and P. Tammaro. 2013. Putative pore-loops of TMEM16/anoctamin channels affect channel density in cell membranes. *J. Physiol.* 591:3487–3505.

Alconada, A., U. Bauer, and B. Hoflack. 1996. A tyrosine-based motif and a casein kinase II phosphorylation site regulate the intracellular trafficking of the varicella-zoster virus glycoprotein I, a protein localized in the trans-Golgi network. *EMBO J.* 15:6096–110.

Alevy, Y.G., A.C. Patel, A.G. Romero, D.A. Patel, J. Tucker, W.T. Roswit, C.A. Miller, R.F. Heier, D.E. Byers, T.J. Brett, and M.J. Holtzman. 2012. IL-13-induced airway mucus production is attenuated by MAPK13 inhibition. *J. Clin. Invest.* 122:4555–4568.

Altschuler, S.J., and L.F. Wu. 2010. Cellular Heterogeneity: Do Differences Make a Difference? *Cell*. 141:559–563.

Amaral, M.D. 2015. Novel personalized therapies for cystic fibrosis: Treating the basic defect in all patients. *J. Intern. Med.* 277:155–166.

Amaral, M.D., and K. Kunzelmann. 2007. Molecular targeting of CFTR as a therapeutic approach to cystic fibrosis. *Trends Pharmacol. Sci.* 28:334–341.

Amaya, M.J., A.G. Oliveira, L.K. Schroeder, E.S. Allgeyer, J. Bewersdorf, and M.H. Nathanson. 2014. Apical Localization of Inositol 1,4,5-Trisphosphate Receptors Is Independent of Extended Synaptotagmins in Hepatocytes. *PLoS One*. 9:e114043.

Andersen, D.H. 1938. Cystic Fibrosis of the Pancreas and its relation to celiac disease. *Am. J. dieases Child.* 344–399.

Bachhuber, T., J. Almaça, F. Aldehni, A. Mehta, M.D. Amaral, R. Schreiber, and K. Kunzelmann. 2008. Regulation of the epithelial Na+ channel by the protein kinase CK2. *J. Biol. Chem.* 283:13225–32.

Barnett-Norris, J., D. Lynch, and P.H. Reggio. 2005. Lipids, lipid rafts and caveolae: Their importance for GPCR signaling and their centrality to the endocannabinoid system. *Life Sci.* 77:1625–1639.

Bautista, M. V, Y. Chen, V.S. Ivanova, M.K. Rahimi, A.M. Watson, and M.C. Rose. 2009. IL-8 regulates mucin gene expression at the posttranscriptional level in lung epithelial cells. *J. Immunol.* 183:2159–2166.

Bell, S.C., K. De Boeck, and M.D. Amaral. 2015. New pharmacological approaches for cystic fibrosis: Promises, progress, pitfalls. *Pharmacol. Ther.* 145:19–34.

References

Benedetto, R., J. Ousingsawat, P. Wanitchakool, Y. Zhang, M.J. Holtzman, M. Amaral, J.R. Rock, R. Schreiber, and K. Kunzelmann. 2017. Epithelial Chloride Transport by CFTR Requires TMEM16A. *Sci. Rep.* 7:1–13.

Botelho, H.M., I. Uliyakina, N.T. Awatade, M.C. Proença, C. Tischer, L. Sirianant, K. Kunzelmann, R. Pepperkok, and M.D. Amaral. 2015. Protein Traffic Disorders: an Effective High-Throughput Fluorescence Microscopy Pipeline for Drug Discovery. *Sci. Rep.* 5:1–8.

Brett, T.J. 2015. CLCA1 and TMEM16A: The link towards a potential cure for airway diseases. *Expert Rev. Respir. Med.* 9:503–506.

Bruce, J.I.E., S. V. Straub, and D.I. Yule. 2003. Crosstalk between cAMP and CA2+ signaling in non-excitable cells. *Cell Calcium*. 34:431–444.

Brunner, J.D., N.K. Lim, S. Schenck, A. Duerst, and R. Dutzler. 2014. X-ray structure of a calcium-activated TMEM16 lipid scramblase. *Nature*. 516:207–212.

Bush, A., and N.J. Simmonds. 2012. Hot off the breath: “l”ve a cost for’ - the 64 million dollar question. *Thorax*. 67:380–382.

Cabrita, I., R. Benedetto, A. Fonseca, P. Wanitchakool, L. Sirianant, B. V. Skryabin, L.K. Schenk, H. Pavenstädt, R. Schreiber, and K. Kunzelmann. 2017. Differential effects of anoctamins on intracellular calcium signals. *FASEB J.* 31:2123–2134.

Canton, D.A., and D.W. Litchfield. 2006. The shape of things to come: An emerging role for protein kinase CK2 in the regulation of cell morphology and the cytoskeleton. *Cell. Signal.* 18:267–275.

Caputo, A., E. Caci, L. Ferrera, N. Pedemonte, C. Barsanti, E. Sondo, U. Pfeffer, R. Ravazzolo, O. Zegarra-Moran, and L.J. V. Galietta. 2008. TMEM16A, A Membrane Protein Associated with Calcium-Dependent Chloride Channel Activity. *Science (80-.).* 322:590–594.

Chan, T., F.S.G. Cheung, J. Zheng, X. Lu, L. Zhu, T. Grewal, M. Murray, and F. Zhou. 2016. Casein Kinase 2 Is a Novel Regulator of the Human Organic Anion Transporting Polypeptide 1A2 (OATP1A2) Trafficking. *Mol. Pharm.* 13:144–154.

Cory, G.O.C., R. Cramer, L. Blanchoin, and A.J. Ridley. 2003. Phosphorylation of the WASP-VCA domain increases its affinity for the Arp2/3 complex and enhances actin polymerization by WASP. *Mol. Cell*. 11:1229–1239.

Dabbagh, K., K. Takeyama, H.-M. Lee, I.F. Ueki, J.A. Lausier, and J.A. Nadel. 1999. IL-4 Induces Mucin Gene Expression and Goblet Cell Metaplasia In Vitro and In Vivo. *J. Immunol.* 162:6233–6237.

De Boeck, K., and M.D. Amaral. 2016. Progress in therapies for cystic fibrosis. *Lancet Respir. Med.* 4:662–674.

De Boeck, K., A. Munck, S. Walker, A. Faro, P. Hiatt, G. Gilmartin, and M. Higgins. 2014. Efficacy and safety of ivacaftor in patients with cystic fibrosis and a non-G551D gating mutation. *J. Cyst. Fibros.* 13:674–680.

References

Denning, G.M., M.P. Anderson, J.F. Amara, J. Marshall, A.E. Smith, and M.J. Welsh. 1992. Processing of mutant cystic fibrosis transmembrane conductance regulator is temperature-sensitive. *Nature*. 358:761–764.

Domingue, J.C., M. Ao, J. Sarathy, and M.C. Rao. 2016. Chenodeoxycholic acid requires activation of EGFR, EPAC, and Ca2+ to stimulate CFTR-dependent Cl- secretion in human colonic T84 cells. *Am J Physiol Cell Physiol*. 311:777–792.

Duran, C., and C. Hartzell. 2011a. Physiological Roles and Diseases of Tmem16/Anoctamin Proteins: Are They All Chloride Channels? *Acta Pharmacol. Sin.* 32:685–692.

Duran, C., and H.C. Hartzell. 2011b. Physiological roles and diseases of tmem16/anoctamin proteins: Are they all chloride channels? *Acta Pharmacol. Sin.* 32:685–692.

Edlund, A., J.L. Esguerra, A. Wendt, M. Flodström-Tullberg, and L. Eliasson. 2014. CFTR and Anoctamin 1 (ANO1) contribute to cAMP amplified exocytosis and insulin secretion in human and murine pancreatic beta-cells. *BMC Med.* 12:1–12.

Erfle, H., B. Neumann, U. Liebel, P. Rogers, M. Held, T. Walter, J. Ellenberg, and R. Pepperkok. 2007. Reverse transfection on cell arrays for high content screening microscopy. *Nat. Protoc.* 2:392–399.

Faria, D., J.R. Rock, A.M. Romao, F. Schweda, S. Bandulik, R. Witzgall, E. Schlatter, D. Heitzmann, H. Pavenstädt, E. Herrmann, K. Kunzelmann, and R. Schreiber. 2014. The calcium-activated chloride channel Anoctamin 1 contributes to the regulation of renal function. *Kidney Int.* 85:1369–1381.

Faria, D., R. Schreiber, and K. Kunzelmann. 2009. CFTR is activated through stimulation of purinergic P2Y2 receptors. *Pflugers Arch. Eur. J. Physiol.* 457:1373–1380.

Farinha, C.M., P. Matos, and M.D. Amaral. 2013. Control of cystic fibrosis transmembrane conductance regulator membrane trafficking: Not just from the endoplasmic reticulum to the Golgi. *FEBS J.* 280:4396–4406.

Gaynor, E.C., and S.D. Emr. 1997. COPI-independent anterograde transport: Cargo-selective ER to Golgi protein transport in yeast COPI mutants. *J. Cell Biol.* 136:789–802.

Gee, H.Y., S.H. Noh, B.L. Tang, K.H. Kim, and M.G. Lee. 2011. Rescue of Δf508-CFTR trafficking via a GRASP-dependent unconventional secretion pathway. *Cell*. 146:746–760.

Giordano, F., Y. Saheki, O. Idevall-Hagren, S.F. Colombo, M. Pirruccello, I. Milosevic, E.O. Gracheva, S.N. Bagriantsev, N. Borgese, and P. De Camilli. 2013. PI(4,5)P2-Dependent and Ca2+-Regulated ER-PM interactions mediated by the extended synaptotagmins. *Cell*. 153:1494–1509.

Grieve, A.G., and C. Rabouille. 2011. Golgi bypass: Skirting around the heart of classical secretion. *Cold Spring Harb. Perspect. Biol.* 3:1–15.

Hekmati, M., Y. Ben-Shaul, and S. Polak-Charcon. 1990. A morphological study of a human adenocarcinoma cell line (HT29) differentiating in culture. Similarities to intestinal embryonic development. *Cell Differ. Dev.* 31:207–218.

References

Herdman, C., and T. Moss. 2016. Extended-Synaptotagmins (E-Syts); The extended story. *Pharmacol. Res.* 107:48–56.

Hoque, K.M., O.M. Woodward, D.B. van Rossum, N.C. Zachos, L. Chen, G.P.H. Leung, W.B. Guggino, S.E. Guggino, and C.-M. Tse. 2010. Epac1 mediates protein kinase A-independent mechanism of forskolin-activated intestinal chloride secretion. *J. Gen. Physiol.* 135:43–58.

Huang, F., H. Zhang, M. Wu, H. Yang, M. Kudo, C.J. Peters, P.G. Woodruff, O.D. Solberg, M.L. Donne, X. Huang, D. Sheppard, J. V. Fahy, P.J. Wolters, B.L.M. Hogan, W.E. Finkbeiner, M. Li, Y.-N. Jan, L.Y. Jan, and J.R. Rock. 2012. Calcium-activated chloride channel TMEM16A modulates mucin secretion and airway smooth muscle contraction. *Proc. Natl. Acad. Sci.* 109:16354–16359.

Hwang, T., and K.L. Kirk. 2013. The CFTR Ion Channel : Gating, Regulation, and Anion Permeation. *Cold Spring Harb Perspect Med*. 3:1–16.

Ibrahim, S.H., M.J. Turner, V. Saint-Criq, J. Garnett, I.J. Haq, M. Brodlie, C. Ward, C. Borgo, M. Salvi, A. Venerando, and M.A. Gray. 2017. CK2 is a key regulator of SLC4A2-mediated Cl^-/HCO_3^- exchange in human airway epithelia. *Pflugers Arch. Eur. J. Physiol.* 1073–1091.

Igreja, S., L.A. Clarke, H.M. Botelho, L. Marques, and M.D. Amaral. 2016. Correction of a Cystic Fibrosis Splicing Mutation by Antisense Oligonucleotides. *Hum. Mutat.* 37:209–215.

Jia, L., W. Liu, L. Guan, M. Lu, and K.W. Wang. 2015. Inhibition of calcium-activated chloride channel ANO1/TMEM16A suppresses tumor growth and invasion in human lung cancer. *PLoS One*. 10:1–17.

Jin, X., S. Shah, Y. Liu, H. Zhang, M. Lees, Z. Fu, J.D. Lippiat, D.J. Beech, A. Sivaprasadarao, S.A. Baldwin, H. Zhang, and N. Gamper. 2013. Activation of the Cl- Channel ANO1 by Localized Calcium Signals in Nociceptive Sensory Neurons Requires Coupling with the IP3 Receptor. *Sci. Signal.* 6:1–28.

Jung, J., J.H. Nam, H.W. Park, U. Oh, J.-H. Yoon, and M.G. Lee. 2013. Dynamic modulation of ANO1/TMEM16A HCO3- permeability by Ca2+/calmodulin. *Proc. Natl. Acad. Sci.* 110:360–365.

Kang, D., G. Liu, A. Lundstrom, E. Gelius, and H. Steiner. 1998. A peptidoglycan recognition protein in innate immunity conserved from insects to humans. *Proc. Natl. Acad. Sci.* 95:10078–10082.

Kerem, B., J. Rommens, J. Buchanan, D. Markiewicz, T. Cox, A. Chakravarti, M. Buchwald, and L.-C. Tsui. 1989. Identification of the cystic fibrosis gene: genetic analysis. *Science (80-.).* 245:1073–1080.

Knowles, A.M.R., M.J. Stutts, A. Spock, N. Fischer, and J.T. Gatzy. 1983. Abnormal Ion Permeation through Cystic Fibrosis Respiratory Epithelium. *Science (80-.).* 221:1067–1070.

Kongsuphol, P., D. Cassidy, F. Romeiras, A. Mehta, and K. Kunzelmann. 2010. Cellular Physiology Biochemistry and Biochemistr y Metformin Treatment of Diabetes Mellitus Increases the Risk for Pancreatitis in Patients Bearing the CFTR-mutation S573C. *Cell. Physiol. Biochem.* 25:389–396.

Kowalski, M.P., and G.B. Pier. 2004. Localization of Cystic Fibrosis Transmembrane Conductance Regulator to Lipid Rafts of Epithelial Cells Is Required for Pseudomonas aeruginosa-Induced Cellular Activation. *J. Immunol.* 172:418–425.

Kunzelmann, K. 2015. TMEM16, LRRC8A, bestrophin: Chloride channels controlled by Ca2+ and cell volume. *Trends Biochem. Sci.* 40:535–543.

Kunzelmann, K., T. Bachhuber, R. Regeer, D. Markovich, J. Sun, and R. Schreiber. 2004. Purinergic inhibition of the epithelial Na+ transport via hydrolysis of PIP2. *FASEB J.* 19:142–143.

Kunzelmann, K., I. Cabrita, P. Wanitchakool, J. Ousingsawat, L. Sirianant, R. Benedetto, and R. Schreiber. 2016. Modulating Ca^{2+} signals: a common theme for TMEM16, Ist2, and TMC. *Pflügers Arch. Eur. J. Physiol.* 468:475–490.

Kunzelmann, K., L. Gerlach, U. Fröbe, and R. Greger. 1991. Bicarbonate permeability of epithelial chloride channels. *Pflügers Arch. Eur. J. Physiol.* 417:616–621.

Kunzelmann, K., and M. Mall. 2001. Pharmacological treatment of the ion transport defect in cystic fibrosis. *Expert Opin. Investig. Drugs*. 28:857–867.

Kunzelmann, K., and M. Mall. 2003. Pharmacotherapy of the ion transport defect in cystic fibrosis: role of purinergic receptor agonists and other potential therapeutics. *Am J Respir Med*. 2:299–309.

Kunzelmann, K., M. Mall, M. Briel, A. Hipper, R. Nitschke, S. Ricken, and R. Greger. 1997. The cystic fibrosis transmembrane conductance regulator attenuates the endogenous Ca2+ activated Cl- conductance of Xenopus oocytes. *Pflugers Arch. Eur. J. Physiol.* 435:178–181.

Kunzelmann, K., and R. Schreiber. 2014b. Chloride secretion, anoctamin 1 and Ca 2+ signaling. *Channels*. 8:387–388.

Kunzelmann, K., E.M. Schwiebert, P.L. Zeitlin, W.L. Kuo, B.A. Stanton, and D.C. Gruenert. 1993. An immortalized cystic fibrosis tracheal epithelial cell line homozygous for the delta F508 CFTR mutation. *Am. J. Respir. Cell Mol. Biol.* 8:522–529.

Kunzelmann, K., Y. Tian, J.R. Martins, D. Faria, P. Kongsuphol, J. Ousingsawat, F. Thevenod, E. Roussa, J. Rock, and R. Schreiber. 2011. Anoctamins. *Pflugers Arch.* 462:195–208.

Kunzelmann, K., Y. Tian, J.R. Martins, D. Faria, P. Kongsuphol, J. Ousingsawat, L. Wolf, and R. Schreiber. 2012. Airway epithelial cells - Functional links between CFTR and anoctamin dependent Cl- secretion. *Int. J. Biochem. Cell Biol.* 44:1897–1900.

Lee, Y.S., Y. Bae, N. Park, J.C. Yoo, C.H. Cho, K. Ryoo, E.M. Hwang, and J.Y. Park. 2016. Surface expression of the Anoctamin-1 (ANO1) channel is suppressed by protein-protein interactions with β-COP. *Biochem. Biophys. Res. Commun.* 475:216–222.

Lefkimmiatis, K., M. Srikanthan, I. Maiellaro, M.P. Moyer, S. Curci, and A.M. Hofer. 2009. Store-operated cyclic AMP signalling mediated by STIM1. *Nat. Cell Biol.* 11:433–442.

Lin, J., Y. Jiang, L. Li, Y. Liu, H. Tang, and D. Jiang. 2015. TMEM16A mediates the hypersecretion of mucus induced by Interleukin-13. *Exp. Cell Res.* 334:260–269.

Litchfield, D.W. 2003. Protein kinase CK2: structure, regulation and role in cellular decisions of life and death. *Biochem. J.* 369:1–15.

Liu, C., Z. Xu, D. Gupta, and R. Dziarski. 2001. Peptidoglycan recognition proteins: A novel family of four human innate immunity pattern recognition molecules. *J. Biol. Chem.* 276:34686–34694.

Lobo, M.J., M.D. Amaral, M. Zaccolo, and C.M. Farinha. 2016. EPAC1 activation by cAMP stabilizes CFTR at the membrane by promoting its interaction with NHERF1. *J. Cell Sci.* 129:2599–2612.

Long, K.J., and K.B. Walsh. 1997. Iodide efflux measurements with an iodide-selective electrode : A non-radioactive procedure for monitoring cellular chloride transport. 212:207–212.

Lu, X., M. Wang, J. Qi, H. Wang, X. Li, D. Gupta, and R. Dziarski. 2006. Peptidoglycan recognition proteins are a new class of human bactericidal proteins. *J. Biol. Chem.* 281:5895–5907.

Luise, M., C. Presotto, L. Senter, R. Betto, S. Ceoldo, S. Furlan, S. Salvatori, R.A. Sabbadini, and G. Salviati. 1993. Dystrophin is phosphorylated by endogenous protein kinases. *Biochem. J.* 293 (Pt 1:243–7.

Lukacs, G.L., A. Mohamed, N. Kartnerl, X.-B. Chang, J.R. Riordan, and S. Grinstein. 1994. Conformational maturation of CFTR but not its mutant counterpart (AF508) occurs in the endoplasmic reticulum and requires ATP. *EMBO J.* 13:6076–6086.

Luz, S., P. Kongsuphol, A.I. Mendes, F. Romeiras, M. Sousa, R. Schreiber, P. Matos, P. Jordan, A. Mehta, M.D. Amaral, K. Kunzelmann, and C.M. Farinha. 2011. Contribution of casein kinase 2 and spleen tyrosine kinase to CFTR trafficking and protein kinase A-induced activity. *Mol. Cell. Biol.* 31:4392–404.

MacKenzie, T., A.H. Gifford, K.A. Sabadosa, H.B. Quinton, E.A. Knapp, C.H. Goss, and B.C. Marshall. 2014. Longevity of patients with cystic fibrosis in 2000 to 2010 and beyond: Survival analysis of the Cystic Fibrosis Foundation Patient Registry. *Ann. Intern. Med.* 161:233–241.

Manford, A.G., C.J. Stefan, H.L. Yuan, J.A. MacGurn, and S.D. Emr. 2012. ER-to-Plasma Membrane Tethering Proteins Regulate Cell Signaling and ER Morphology. *Dev. Cell*. 23:1129–1140.

Martins, J.R., D. Faria, P. Kongsuphol, B. Reisch, R. Schreiber, and K. Kunzelmann. 2011a. Anoctamin 6 is an essential component of the outwardly rectifying chloride channel. *Proc. Natl. Acad. Sci.* 108:18168–18172.

Martins, J.R., P. Kongsuphol, E. Sammels, S. Dahimène, F. AlDehni, L.A. Clarke, R. Schreiber, H. De Smedt, M.D. Amaral, and K. Kunzelmann. 2011b. F508del-CFTR increases intracellular Ca 2+ signaling that causes enhanced calcium-dependent Cl - conductance in cystic fibrosis. *Biochim. Biophys. Acta - Mol. Basis Dis.* 1812:1385–1392.

Meggio, F., and L.A. Pinna. 2003. One-thousand-and-one substrates of protein kinase CK2? *FASEB J.* 17:349–368.

Moniz, S., M. Sousa, B.J. Moraes, A.I. Mendes, M. Palma, C. Barreto, J.I. Fragata, M.D. Amaral, and P. Matos. 2013. HGF stimulation of Rac1 signaling enhances pharmacological correction of the most prevalent cystic fibrosis mutant F508del-CFTR. *ACS Chem. Biol.* 8:432–442.

References

Moss, R.B. 2013. Pitfalls of drug development: Lessons learned from trials of denufosol in cystic fibrosis. *J. Pediatr.* 162:676–680.

Moss, R.B., P.A. Flume, J.S. Elborn, J. Cooke, M. Rowe, S.A. Mccolley, R.C. Rubenstein, and M. Higgins. 2015. Efficacy and safety of ivacaftor treatment: randomized trial in subjects with cystic fibrosis who have an R117H-CFTR mutation. *Lancet Respir. Med.* 3:524–533.

Mullins, R.D., J.A. Heuser, and T.D. Pollard. 1998. The interaction of Arp2/3 complex with actin: Nucleation, high affinity pointed end capping, and formation of branching networks of filaments. *Proc. Natl. Acad. Sci.* 95:6181–6186.

Namkung, W., W.E. Finkbeiner, and A.S. Verkman. 2010. CFTR-Adenylyl Cyclase I Association Responsible for UTP Activation of CFTR in Well-Differentiated Primary Human Bronchial Cell Culture. *Mol. Biol. Cell*. 21:2639–2648.

Namkung, W., P.W. Phuan, and A.S. Verkman. 2011. TMEM16A inhibitors reveal TMEM16A as a minor component of calcium-activated chloride channel conductance in airway and intestinal epithelial cells. *J. Biol. Chem.* 286:2365–2374.

Nickel, W., and C. Rabouille. 2009. Mechanisms of regulated unconventional protein secretion. *Nat. Rev. Mol. Cell Biol.* 10:148–155.

O'Sullivan, B.P., and S.D. Freedman. 2009. Cystic fibrosis. *Lancet*. 373:1891–1904.

Ostrom, R.S., and P.A. Insel. 2004. The evolving role of lipid rafts and caveolae in G protein-coupled receptor signaling: implications for molecular pharmacology. *Br. J. Pharmacol.* 143:235–245.

Pagano, M.A., G. Arrigoni, O. Marin, S. Sarno, F. Meggio, K.J. Treharne, A. Mehta, and L.A. Pinna. 2008. Modulation of protein kinase CK2 activity by fragments of CFTR encompassing F508 may reflect functional links with cystic fibrosis pathogenesis. *Biochemistry*. 47:7925–7936.

Paradiso, a M., C.M. Ribeiro, and R.C. Boucher. 2001. Polarized signaling via purinoceptors in normal and cystic fibrosis airway epithelia. *J. Gen. Physiol.* 117:53–67.

Paulino, C., V. Kalienkova, A.K.M. Lam, and Y. Neldner. 2017. Activation mechanism of the calcium-activated chloride channel TMEM16A revealed by cryo-EM. *Nature* 552:421-425.

Paulino, C., Y. Neldner, A.K.M. Lam, V. Kalienkova, J.D. Brunner, S. Schenck, and R. Dutzler. 2017b. Structural basis for anion conduction in the calcium-activated chloride channel TMEM16A. *Elife*. 6:1–23.

Pedemonte, N., G.L. Lukacs, K. Du, E. Caci, O. Zegarra-moran, L.J. V Galietta, and A.S. Verkman. 2005. Small-molecule correctors of defective ΔF508-CFTR cellular processing identified by high-throughput screening. *J. Clin. Invest.* 115:2564–2571.

Perez-Cornejo, P., A. Gokhale, C. Duran, Y. Cui, Q. Xiao, H.C. Hartzell, and V. Faundez. 2012. Anoctamin 1 (Tmem16A) Ca2+-activated chloride channel stoichiometrically interacts with an ezrin-radixin-moesin network. *Proc. Natl. Acad. Sci.* 109:10376–10381.

Plant, B.J., C.H. Goss, W.D. Plant, and S.C. Bell. 2013. Management of comorbidities in older patients with cystic fibrosis. *Lancet Respir. Med.* 1:164–174.

Quinton, P. 1983. Chloride Impermeability in Cystic Fibrosis. *Nature*. 301:421–422.

Quinton, P.M. 2007. Too much salt, too little soda: cystic fibrosis. *Acta Physiol. Sin.* 59:397–415.

Quinton, P.M. 2008. Cystic fibrosis: impaired bicarbonate secretion and mucoviscidosis. *Lancet*. 372:415–417.

Riordan, J.R., J.M. Rommens, B. Kerem, N. Alon, R. Rozmahel, Z. Grzelczak, J. Zielenski, S. Lok, N. Plavsic, J.-L. Chou, M.L. Drumm, M.C. Iannuzzi, F.S. Collins, and L. Tsui. 1989. Identification of the Cystic Fibrosis Gene: Cloning and Characterization of Complementary DNA. *Science (80-.).* 245:1066–1072.

Risnik, V. V, and N.B. Gusev. 1984. Some properties of the nucleotide-binding site of troponin T kinase-casein kinase type II from skeletal muscle. *Biochimic*. 790:108–116.

Rommens, J.M., M.C. Iannuzzi, B. Kerem, M.L. Drumm, G. Melmer, M. Dean, R. Rozmahel, J.L. Cole, D. Kennedy, N. Hidaka, M. Zsiga, M. Buchwald, J.R. Riordan, L. Tsui, and F.S. Collins. 1989. Identification of the Cystic Fibrosis Gene: Chromossome Walking and Jumping. *Science (80-.).* 122:1059–1065.

Roth, E.K., S. Hirtz, J. Duerr, D. Wenning, I. Eichler, H.H. Seydewitz, M.D. Amaral, and M.A. Mall. 2011. The K + channel opener 1-EBIO potentiates residual function of mutant CFTR in rectal biopsies from cystic fibrosis patients. *PLoS One*. 6.

Ruffin, M., M. Voland, S. Marie, M. Bonora, E. Blanchard, S. Blouquit-Laye, E. Naline, P. Puyo, P. Le Rouzic, L. Guillot, H. Corvol, A. Clement, and O. Tabary. 2013. Anoctamin 1 dysregulation alters bronchial epithelial repair in cystic fibrosis. *Biochim. Biophys. Acta - Mol. Basis Dis.* 1832:2340–2351.

Sala-Rabanal, M., Z. Yurtsever, C.G. Nichols, and T.J. Brett. 2015. Secreted CLCA1 modulates TMEM16A to activate Ca2+-dependent chloride currents in human cells. *Elife*. 2015:1–14.

Sarker, R., M. Gronborg, B. Cha, S. Mohan, Y. Chen, A. Pandey, D. Litchfield, D. M, and X. Li. 2008. Casein Kinase 2 binds to the C terminus of Na+/H+ exchanger 3 (NHE3) and Stimulated NHE3 Basal Activity by Phosphorylating a Separate Site in NHE3. *Mol. Biol. Cell*. 19:3859–3870.

Schmidt, M., S. Evellin, P. a Weernink, F. von Dorp, H. Rehmann, J.W. Lomasney, and K.H. Jakobs. 2001. A new phospholipase-C-calcium signalling pathway mediated by cyclic AMP and a Rap GTPase. *Nat. Cell Biol.* 3:1020–1024.

Schreiber, R., D. Faria, B. V. Skryabin, P. Wanitchakool, J.R. Rock, and K. Kunzelmann. 2014. Anoctamins support calcium-dependent chloride secretion by facilitating calcium signaling in adult mouse intestine. *Pflugers Arch. Eur. J. Physiol.* 467:1203–1213.

Schreiber, R., I. Uliyakina, P. Kongsuphol, R. Warth, M. Mirza, J.R. Martins, and K. Kunzelmann. 2010. Expression and function of epithelial anoctamins. *J. Biol. Chem.* 285:7838–7845.

Schroeder, B.C., T. Cheng, Y.N. Jan, and L.Y. Jan. 2008. Expression Cloning of TMEM16A as a Calcium-Activated Chloride Channel Subunit. *Cell*. 134:1019–1029.

Sclip, A., T. Bacaj, L.R. Giam, and T.C. Südhof. 2016. Extended Synaptotagmin (ESyt) Triple Knock-Out Mice Are Viable and Fertile without Obvious Endoplasmic Reticulum Dysfunction. *PLoS One*. 11:1–17.

Scudieri, P., E. Caci, S. Bruno, L. Ferrera, M. Schiavon, E. Sondo, V. Tomati, A. Gianotti, O. Zegarra-Moran, N. Pedemonte, F. Rea, R. Ravazzolo, and L.J. V. Galietta. 2012a. Association of TMEM16A chloride channel overexpression with airway goblet cell metaplasia. *J. Physiol.* 590:6141–6155.

Scudieri, P., E. Sondo, L. Ferrera, and L.J. V Galietta. 2012b. The anoctamin family: TMEM16A and TMEM16B as calcium-activated chloride channels. *Exp. Physiol.* 97:177–83.

Serres, M., O. Filhol, H. Lickert, C. Grangeasse, E.M. Chambaz, J. Stappert, C. Vincent, and D. Schmitt. 2000. The disruption of adherens junctions is associated with a decrease of E-cadherin phosphorylation by protein kinase CK2. *Exp. Cell Res.* 257:255–264.

Simões, F., J. Ousingsawat, P. Wanitchakool, A. Fonseca, I. Cabrita, R. Benedetto, R. Schreiber, and K. Kunzelmann. 2017. CFTR supports cell death through ROS-dependent activation of TMEM16F (anoctamin 6). *Pflügers Arch. - Eur. J. Physiol.*

Simpson, J.C., B. Joggerst, V. Laketa, F. Verissimo, C. Cetin, H. Erfle, M.G. Bexiga, V.R. Singan, J.-K. Hériché, B. Neumann, A. Mateos, J. Blake, S. Bechtel, V. Benes, S. Wiemann, J. Ellenberg, and R. Pepperkok. 2012. Genome-wide RNAi screening identifies human proteins with a regulatory function in the early secretory pathway. *Nat. Cell Biol.* 14:764–774.

Singh, T.J., A. Akatsuka, K.R. Blake, and K.P. Huang. 1983. Phosphorylation of troponin and myosin light chain by cAMP-independent casein kinase-2 from rabbit skeletal muscle. *Arch. Biochem. Biophys.* 220:615–622.

Stanley, P. 2011. Golgi glycosylation. *Cold Spring Harb. Perspect. Biol.* 3:1–13.

Stathopulos, P.B., R. Schindl, M. Fahrner, L. Zheng, G.M. Gasmi-Seabrook, M. Muik, C. Romanin, and M. Ikura. 2013. STIM1/Orai1 coiled-coil interplay in the regulation of store-operated calcium entry. *Nat. Commun.* 4:1–12.

Su, T.T., and P.H. O'Farrell. 1998. Size control: cell proliferation does not equal growth. *Curr. Biol.* 8:687–689.

Thornton, D.J., K. Rousseau, and M.A. McGuckin. 2008. Structure and Function of the Polymeric Mucins in Airways Mucus. *Annu. Rev. Physiol.* 70:459–486.

Tian, Y., P. Kongsuphol, M. Hug, J. Ousingsawat, R. Witzgall, R. Schreiber, and K. Kunzelmann. 2011. Calmodulin-dependent activation of the epithelial calcium-dependent chloride channel TMEM16A. *FASEB J.* 25:1058–1068.

Tian, Y., R. Schreiber, and K. Kunzelmann. 2012. Anoctamins are a family of Ca2+ activated Cl- channels. *J. Cell Sci.* 125:4991–4998.

Treharne, K.J., Z. Xu, J.H. Chen, O.G. Best, D.M. Cassidy, D.C. Gruenert, P. Hegyi, M.A. Gray, D.N. Sheppard, K. Kunzelmann, and A. Mehta. 2009. Inhibition of protein kinase CK2 closes the CFTR Cl channel, but has no effect on the cystic fibrosis mutant Δf508-CFTR. *Cell. Physiol. Biochem.* 24:347–360.

Tremblay, M.G., and T. Moss. 2016. Loss of all 3 Extended Synaptotagmins does not affect normal mouse development, viability or fertility. *Cell Cycle*. 15:2360–2366.

Tsui, L.C. 1992. The spectrum of cystic fibrosis mutations. *Trends Genet.* 8:392–398.

Van Goor, F., S. Hadida, P.D.J. Grootenhuis, B. Burton, D. Cao, T. Neuberger, A. Turnbull, A. Singh, J. Joubran, A. Hazlewood, J. Zhou, J. McCartney, V. Arumugam, C. Decker, J. Yang, C. Young, E.R. Olson, J.J. Wine, R.A. Frizzell, M. Ashlock, and P. Negulescu. 2009. Rescue of CF airway epithelial cell function in vitro by a CFTR potentiator, VX-770. *Proc. Natl. Acad. Sci.* 106:18825–18830.

Van Goor, F., S. Hadida, P.D.J. Grootenhuis, B. Burton, J.H. Stack, K.S. Straley, C.J. Decker, M. Miller, J. McCartney, E.R. Olson, J.J. Wine, R.A. Frizzell, M. Ashlock, and P.A. Negulescu. 2011. Correction of the F508del-CFTR protein processing defect in vitro by the investigational drug VX-809. *Proc. Natl. Acad. Sci.* 108:18843–18848.

Veit, G., F. Bossard, J. Goepp, A.S. Verkman, L.J. V. Galietta, J.W. Hanrahan, and G.L. Lukacs. 2012. Proinflammatory cytokine secretion is suppressed by TMEM16A or CFTR channel activity in human cystic fibrosis bronchial epithelia. *Mol. Biol. Cell*. 23:4188–4202.

Venerando, A., M.A. Pagano, K. Tosoni, F. Meggio, D. Cassidy, M. Stobbart, L.A. Pinna, and A. Mehta. 2011. Understanding protein kinase CK2 mis-regulation upon F508del CFTR expression. *Naunyn. Schmiedebergs. Arch. Pharmacol.* 384:473–488.

Verkman, A.S., Y. Song, and J.R. Thiagarajah. 2003. Role of airway surface liquid and submucosal glands in cystic fibrosis lung disease. *Am. J. Physiol. - Cell Physiol.* 284:2–15.

Vorotnikov, A. V., N.B. Gusev, S. Hua, J.H. Collins, C.S. Redwood, and S.B. Marston. 1993. Identification of casein kinase II as a major endogeneous caldesmon kinase in sheep aorta smooth muscle. *FEBS Lett.* 334:18–22.

Wang, Y.-N., H. Wang, H. Yamaguchi, H.-J. Lee, H.-H. Lee, and M.-C. Hung. 2010. COPI-mediated retrograde trafficking from the Golgi to the ER regulated EGFR nuclear transport. *Biochem. Biophys. Res. Commun.* 399:498–504.

Wanitchakool, P., L. Wolf, G.E. Koehl, L. Sirianant, R. Schreiber, S. Kulkarni, U. Duvvuri, and K. Kunzelmann. 2014. Role of anoctamins in cancer and apoptosis. *Philos. Trans. R. Soc. Lond. B. Biol. Sci.* 369.

Wei, L., A. Vankeerberghen, H. Cuppens, J. Eggermont, J.-J. Cassiman, G. Droogmans, and B. Nilius. 1999. Interaction between calcium-activated chloride channels and the cystic fibrosis transmembrane conductance regulator. *Pflugers Arch. Eur. J. Physiol.* 438:635–641.

Wei, T., and M. Tao. 1993. Human erythrocytes casein kinase II: characterization and phosphorylation of membrane cytskeletal proteins. *Arch. Biochem. Biophys.* 307:206–216.

Whiting, P., Al Maiwenn, L. Burgers, M. Westwood, S. Ryder, M. Hoogendoorn, N. Armstrong, A. Allen, H. Severens, and J. Kleijnen. 2014. Ivacaftor for the treatment of patients with cystic fibrosis and the G551D mutation: A systematic review and cost-effectiveness analysis. *Health Technol. Assess. (Rockv).* 18:1–106.

Whitlock, J.M., and H.C. Hartzell. 2016. A Pore Idea: the ion conduction pathway of TMEM16/ANO proteins is composed partly of lipid. *Pflugers Arch. Eur. J. Physiol.* 468:455–473.

Xiao, Q., K. Yu, P. Perez-Cornejo, Y. Cui, J. Arreola, and H.C. Hartzell. 2011. Voltage- and calcium-dependent gating of TMEM16A/Ano1 chloride channels are physically coupled by the first intracellular loop. *Proc. Natl. Acad. Sci.* 108:8891–8896.

Yang, H., A. Kim, T. David, D. Palmer, T. Jin, J. Tien, F. Huang, T. Cheng, S.R. Coughlin, Y.N. Jan, and L.Y. Jan. 2012. TMEM16F Forms a Ca2+-Activated Cation Channel Required for Lipid Scrambling in Platelets during Blood Coagulation. *Cell*. 73:713–728.

Yang, Y.D., H. Cho, J.Y. Koo, M.H. Tak, Y. Cho, W.-S. Shim, S.P. Park, J. Lee, B. Lee, B.-M. Kim, R. Raouf, Y.K. Shin, and U. Oh. 2008. TMEM16A confers receptor-activated calcium-dependent chloride conductance. *Nature*. 455:1210–1215.

Yoo, J.-S., B.D. Moyer, S. Bannykh, H.-M. Yoo, J.R. Riordan, and W.E. Balch. 2002. Non-conventional trafficking of the cystic fibrosis transmembrane conductance regulator through the early secretory pathway. *J. Biol. Chem.* 277:11401–11409.

Yu, H., Y. Liu, D.R. Gulbranson, A. Paine, S.S. Rathore, and J. Shen. 2016. Extended synaptotagmins are Ca2+-dependent lipid transfer proteins at membrane contact sites. *Proc. Natl. Acad. Sci. U. S. A.* 113:4362–7.

Zeitlin, P.L., L. Lu, J. Rhim, G. Cutting, G. Stetten, K.A. Kieffer, R. Craig, and W.B. Guggino. 1991. A cystic fibrosis bronchial epithelial cell line: immortalization by adeno-12-SV40 infection. *Am. J. Respir. Cell Mol. Biol.* 4:313–319.

Zenhom, M., A. Hyder, I. Kraus-Stojanowic, A. Auinger, T. Roeder, and J. Schrezenmeir. 2011. PPARγ-dependent peptidoglycan recognition protein 3 (PGlyRP3) expression regulates proinflammatory cytokines by microbial and dietary fatty acids. *Immunobiology*. 216:715–724.

Zenhom, M., A. Hyder, M. De Vrese, K.J. Heller, T. Roeder, and J. Schrezenmeir. 2012. Peptidoglycan recognition protein 3 (PglyRP3) has an anti-inflammatory role in intestinal epithelial cells. *Immunobiology*. 217:412–419.